Mathematical Modelling of Drug Delivery in Tissue Cells by Electroporation

NILAY MONDAL

DEPARTMENT OF MATHEMATICS
INDIAN INSTITUTE OF TECHNOLOGY GUWAHATI
GUWAHATI 781039, INDIA

May, 2022

Mathematical Modelling of Drug Delivery in Tissue Cells by Electroporation

A thesis submitted
in partial fulfillment of the requirements
for the degree of

Doctor of Philosophy

by

Nilay Mondal
(Roll No. 156123021)

Department of Mathematics
Indian Institute of Technology Guwahati
Guwahati 781039, India
May, 2022

Dedicated

To

My Grandmother

Anandamayi De (Dida)

And

My Parents

Nepal Mondal (Baba)
&
Shasthi Mondal (Maa)

Declaration

I do hereby declare that this thesis entitled **Mathematical Modelling of Drug Delivery in Tissue Cells by Electroporation** is a presentation of my original research work done under the supervision of **Dr. Durga Charan Dalal**, Professor, Department of Mathematics, Indian Institute of Technology Guwahati for the award of the degree of Doctor of Philosophy and this work has not been submitted elsewhere for a degree.

May, 2022

Nilay Mondal
Roll No. 156123021
Department of Mathematics
Indian Institute of Technology Guwahati

Certificate

It is to certify that the work contained in this thesis entitled **Mathematical Modelling of Drug Delivery in Tissue Cells by Electroporation** has been carried out by **Nilay Mondal**, a student in the Department of Mathematics, Indian Institute of Technology Guwahati, under my supervision for the award of the degree of Doctor of Philosophy and this work has not been submitted elsewhere for a degree.

May, 2022

Dr. Durga Charan Dalal
Professor
Department of Mathematics
Indian Institute of Technology Guwahati

Acknowledgements

The path to complete my thesis work is not smooth without some special persons and their constant support. I would like to acknowledge their contribution throughout my journey at IITG.

First and foremost, I would like to express my gratitude towards my supervisor, Prof. D. C. Dalal for his immense support, guidance and inspiration throughout my research tenure. My deepest appreciation is extended to him for his patience, understanding and constant believe in me. His vast knowledge, abundant experience and useful critiques helped me to overcome the obstacles of my research work. His mental support have encouraged me all the time in research and daily life. He continuously motivated me to do better research that made it possible to complete my thesis work.

I would like to offer my sincere thanks to my doctoral committee members, Prof. S. N. Bora, Prof. N. Srinivasan and Prof. B. Deka for their valuable advice, support, and encouragement throughout this work. I am deeply grateful to the Head, Department of Mathematics, IIT Guwahati for providing me the necessary facilities to carry out my research. My sincere thanks also goes to all the faculty members of the Department of Mathematics for their help and cooperation. I would like to thank all the staff members of the Department of Mathematics for their assistance and support in various ways during my research period.

I would also like to thank Prof. Wanda K. Neu from Duke University for her helpful suggestions and insightful comments. I am grateful to the Ministry of Human Resource Development, Government of India, for providing the financial support during my research period. I sincerely acknowledge Indian Institute of Technology Guwahati for providing the wonderful educational environment and all kinds of support.

I am extremely indebted to my parents and Archana Masi for their love, concern, care, encouragement and blessing in my life. My heartful thanks to Shilpi (Babu) for being a special person in my life. I am grateful to her for providing me moral support, encouragement and staying beside me all the time. I would like to thank Mama (Narugopal De), Mamima (Anima De), Boro Masi, Kalpana Masi, Ujjyala Masi, Bandana Masi, Chhoto Masi, Kaku (Sanju Biswas), Kakimoni (Madhabi Biswas), Lucky Di and Baby (Suraj) for their support, love, care and blessing to me. I am thankful to my younger brother (Malay), sister in law (Sathi), and all my cousins Mampi, Subha, Priyanka, Rahul, Sourav, Shyamal, Beauty, Nila, Shrabani, Koushik, Dipu Da, Bhola, Bikash Da and Mou Didi.

I would like to thank my seniors, friends and colleagues Hiru Da, Swarup Da, Koyel Di, Debu Da, Madhu Da, Sonjoy Da, Tamal Da, Jogen Da, Nandita Di, Sabyasachi, Abhijit, Shantiram, Rupak, Bandita, Ayan, Shamik, Shyam, Kuldeep, Mrityunjay, Avijit,

Buddha, Puspendu, Rupchand, Gopinath, Tanay, Matap, Golui, Sandip, Sagar, Mijanur, Anirudda and Abhijit Shit for their encouragement, support and entertainments during my research life and for all the cherished times spent together in lab, hostel and social settings. Special thanks goes to my close school friends Anup, Soumitra, Abhishek, and Dipjyoti for being a part of some wonderful moments of my life.

Last but not least, I would like to thank everyone who contributed to the completion of the thesis, and I apologize for not being able to mention them all individually.

May, 2022

(Nilay Mondal)
Department of Mathematics
Indian Institute of Technology Guwahati

ABSTRACT

Electroporation method is a useful tool for delivering drugs into various diseased tissues in the human body. As a result of an applied electric field, drug particles enter the intracellular compartment through the temporarily permeabilized cell membrane. Consequently, electroporation method allows better penetration of drug into the diseased tissue and improves treatment clinically. Electroporation based drug delivery is a topic of interest since twentieth century. In order to help the clinical experiments for smooth drug delivery, mathematical models are needed. In this field, researchers continue to improve and develop theoretical and experimental models. In this thesis, mathematical models are developed to demonstrate how to deliver drugs into the diseased cells using tissue electroporation. A detailed study is carried out on reversible electroporation, thermal effects resulting from pulse application, and on drug elimination and metabolism. The thesis addresses five problems.

The present dissertation starts with a mathematical model of single cell electroporation for delivering drug into the cell. The model is able to capture non-homogeneous drug transport in the cell due to non-uniform cell membrane permeabilization. Several numerical experiments are conducted to understand the effects of electric field and drug permeability on drug uptake into the cell. Through investigation, the appropriate electric field and drug permeability are identified that lead to sufficient drug uptake into the cell. Using this model, experimentalists can gain information before conducting any experiment, and it can reduce the number of actual experiments that might have been conducted otherwise.

The second work contributes an improved mathematical model for drug delivery into the electroporated tissue that deals with both reversibly and irreversibly electroporated cells. This mathematical formulation is expressed through a set of differential equations, which are solved analytically, and numerically, according to their complexities, with a pertinent set of initial and boundary conditions. The time-dependent mass transfer coefficient as a function of pore density is used to find the drug concentrations throughout

reversibly and irreversibly electroporated cells as well as in the extracellular space. The effects of permeability of drug, electric field, and pulse period on drug concentrations in extracellular and intracellular regions are discussed. The threshold value of an electric field ($E > 10$ V mm^{-1}) to initiate drug uptake is identified in this study. Special emphasis is also given on two cases of electroporation, drug dynamics during ongoing electroporation and drug dynamics after the electric pulse period is over. This model could be useful to various clinical experiments for drug delivery in targeted tissues by controlling the model parameters depending on the tissue conditions.

The next work focuses on the development of a mathematical model of drug delivery based on reversible tissue electroporation in order to treat all of the cells at the targeted site. In addition, the thermal effects on the tissue, which is an outcome of Joule heating, are also considered. This model introduces a time-dependent mass transfer coefficient that is significant to drug transport. Multiple pulses with low voltage are applied so that sufficient drugs can reach the targeted cells. The changes in drug concentration with different parameters (e.g., diffusion coefficient, drug permeability, pulse length, and pulse number) are analyzed. The model optimizes the electroporation parameters for the required drug uptake into the cells with no thermal damage. This model can be used in clinical experiments to predict the drug uptake into the infected cells by controlling the model parameters according to the nature of infections.

The subsequent work provides a mathematical model of reversible tissue electroporation for injecting drug into the diseased cells. The model emphasizes the tissue boundary where the drug is injected as a point source. Drug loss from the tissue boundaries through extracellular space and its reaction on drug transport are examined. The effects of electric field on tissue conductivity is studied. Multiple pulses are applied to deliver a sufficient amount of drug into the targeted cells. This model obtains a mass transfer coefficient in terms of pore fraction coefficient and drug permeability. It controls the drug transport from extracellular to intracellular space. The drug penetration throughout the tissue is captured due to the application of different pulses. The advocated model is able to perform homogeneous drug transport into the cells, as a result the affected tissue can be treated completely. This model may be applied to optimize clinical experiments by avoiding the lengthy and costly in vivo and in vitro experiments.

The final work concentrates on the process of drug metabolism in the cells in our modified model. Reversible electroporation and membrane resealing are considered in this model. The main objective is to examine the combined effects of drug loss across tissue boundaries and drug metabolism within cells. A detailed analysis of the effects of metabolism parameters on cellular drug uptake is presented. The model is able to calculate the amount of drug metabolites in cells at the end of drug transport.

NOMENCLATURE

Symbol

A	Magnetic vector potential
A_P	Total pore area of a cell
C	Concentration
C_0, C_1, C_2	Initial drug concentration
C_E	Concentration in extracellular space
C_I	Concentration in intracellular space
C_{IRE}	Concentration in irreversible electroporated cell
C_{RE}	Concentration in reversible electroporated cell
C_m	Membrane capacitance
c	Specific heat
d	Constant in Dirac-delta function
D	Diffusion coefficient
D_E	Extracellular diffusion coefficient
D_I	Intracelluar diffusion coefficient
d_m	Cell membrane thickness
E	Electric field
E_1	Reversal potential
E_f	Fitting parameter for mass transfer coefficient
E_{rev}	Threshold value for reversible electroporation
E_{irrev}	Threshold value for irreversible electroporation
f_p	Pore surface fraction ratio
g_1	Membrane conductance
H	Width of the rectangle
h	Heat transfer coefficient
i_{ep}	Current in a single pore
J	Current density

K_B	Boltzmann constant
k	Thermal conductivity
L	Length of the rectangle/square
N	Pore density
N_0	Equilibrium pore density
N_P	Total number of pores
n_d	Number of dose
$\hat{n}$	Unit vector
M_1	Number of grid along x axis
M_2	Number of grid along y axis
m	Effective electrophoretic mobility
P	Drug permeability
PN	Pulse number
Q	Total mass flux
q	Electroporation constant
q_0	Elementary charge
q_a	Advection mass flux
q_d	Diffusive mass flux
R	Tissue radius
R_P	Pore radius
r	Variable in spherical coordinates
r_c	Cell radius
S	Cell surface
S'	Source or sink
S_M	Source term for drug metabolism
SF	Survival fraction
T	Temperature
T_b	Normal body temperature
T_{ep}	Temperature at t_{ep}
t	Time
tep	Pulse length
t_M	Time for mass transfer
t_p	Time after most recent pulse is applied
u	Velocity
V	Cell Volume
V_0	Volume of a cube surrounding a cell
V_{ep}	Characteristic voltage
V_m	Transmembrane potential
v_m	Non-dimensional transmembrane potential
x, y	Variables
z	Valence

Greek letters

α	Pore creation rate coefficient
β	Rate of mass loss at the boundary
γ_1, γ_2	Electrical conductivity parameter
ϵ	Porosity
ϵ_0	Vacuum permittivity
ϵ_1	Relative permittivity
μ, μ_R	Mass transfer coefficient
μ_{IRE}	Mass transfer coefficient of the irreversibly electroporated cells
μ_{RE}	Mass transfer coefficient of the reversibly electroporated cells
ϕ	Electric potential
ϕ_0	Potential on negative electrode
ϕ_L	Potential on positive electrode
ϕ_e	Extracellular potential
ϕ_i	Intracellular potential
ρ	Density of the tissue
ρ'	Volume charge density
θ	Variable in spherical coordinates
σ	Electrical conductivity
σ_e	Extracellular electrical conductivity
σ_i	Intracellular electrical conductivity
$\sigma_{\max}$	Maximum electrical conductivity
$\sigma_{\min}$	Minimum electrical conductivity
τ	Resealing time constant
δ	Dirac delta function
Ψ	Angle between the direction of electric field and the normal to the cell membrane
Ω	Tissue domain

Abbreviations

DDS	Drug delivery systems
EPR	Enhanced permeation and retention
ECS	Extracellular space
FDM	Finite difference method
FTCS	Forward time centered space
ICS	Intracellular space
IRE	Irreversible electroporation
MTC	Mass transfer coefficient

PIM	Permeable interface method
RE	reversible electroporation
SC	Stratum corneum
SCE	Single cell electroporation

LIST OF FIGURES

LIST OF TABLES

भारतीय प्रौद्योगिकी संस्थान गुवाहाटी
Indian Institute of Technology Guwahati

CONTENTS

भारतीय प्रौद्योगिकी संस्थान गुवाहाटी
Indian Institute of Technology Guwahati

CHAPTER 1

INTRODUCTION

1.1 Background

Disease is an irregular health condition that is not caused by the impact of a physical injury. There are many causes of disease like individual susceptibility, severity, exposure, age and predisposing factors. Diseases are often known as abnormal medical conditions due to external factors, such as pathogens or internal dysfunctions. There are four main types of disease: infectious, deficiency, hereditary, which includes genetic and non-genetic disease, and physiological disease.

A drug is a chemical substance of known structure. A pharmaceutical drug is called medicine that is used to treat, cure, prevent disease to promote well-being. Pharmaceutical drugs are often classified into different classes: groups of related drugs with similar chemical structures, the same mechanism of action, the same mode of action, and used to treat the same disease.

The objective of drug therapy is to correct the imbalances that have occurred in the body system due to the bad health conditions or disease. Drug delivery is the process of delivering a therapeutic substance or pharmaceutical compound to its target site through various approaches, formulations, manufacturing techniques, storage systems, and technologies. In drug delivery, different experiments, carriers, and medical devices are used to alter a drug's pharmacokinetics and specificity. Several studies have been conducted to improve the safety of patient who is under medications. The concept of drug delivery is heavily dependent upon dosage form and route of administration. The route by which a drug enters the body is called the route of administration. There are several routes of administration, including oral, injection, sublingual, topical, transdermal, inhaled, rectal, etc. Drug delivery encloses a variety of devices and methods to deliver a drug with different dosage forms using the same route. However, drugs can be delivered in various ways

through each route.

Drug delivery has various approaches like, local drug delivery, targeted drug delivery, sustained drug delivery, modulated drug delivery, etc. Transdermal drug delivery is a new process in medical science to inject drug or vaccine through the outermost layer (Stratum corneum) of the skin. It offers several advantages, including avoidance of erratic absorption, absence of gastric irritation, painlessness, non-invasiveness, as well as improvement in patient compliance. Several methods are developed over the last few years to enhance the drug delivery. Some of these methods are sonophoresis, iontophoresis, microneedles and electroporation.

Nowadays, 'Electroporation' technique is widely used to deliver drug to different parts of human body. Electroporation is a very useful technique in this branch. It generally uses electric pulses to transport molecule into the cell through the cell membrane. Short time high voltage electric pulses are used for electro-chemotherapy or cancer treatment. In electroporation, when a pulse is applied on a cell, pore area as well as the number of pore keep increasing until discharged. In this area of research, several experimental and theoretical studies are made over the last decade. Mathematical modeling of this kind is of great importance in terms of applications in medical and pharmaceutical sciences. In this thesis, we have proposed some mathematical models for drug delivery using electroporation.

1.2 Basic Definitions and Useful Equations

1.2.1 Cell and Tissue

The human body is composed of small structural and functional units called cells. A cell consists of three parts: the cell membrane, the nucleus, and the cytoplasm between them. Genetic material (DNA) resides in the nucleus of a cell. The nucleus is responsible for both the basic structure and the function of the cell.

A tissue is a biological organizational unit between cells and an organ. Each tissue is composed of cells with similar structures and functions that work together. Multiple tissues are grouped together to form an organ. The body consists of four primary types of tissues: epithelial, connective, muscular, and nervous.

In microscopic view, the tissue is a composition of two distinct regions (see Fig.1.1):

(i) the extracellular space (ECS) which is outerside of the cells, containing the extracellular matrix structure and the interstitial fluid [80],

(ii) the intracellular space (ICS) that represents the sum of all the discrete volumes that are encompassed by the individual cell walls. The intracellular space is the target of cellular drug delivery.

The extracellular and the intracellular spaces are separated by the cell membrane,

which restricts the mass transfer (or cellular drug uptake) from the extracellular to intracellular space. ECS is a continuous media, so drugs are free to diffuse throughout it. As soon as drugs try to enter the ICS, they are restricted from freely diffusing through the cell membrane.

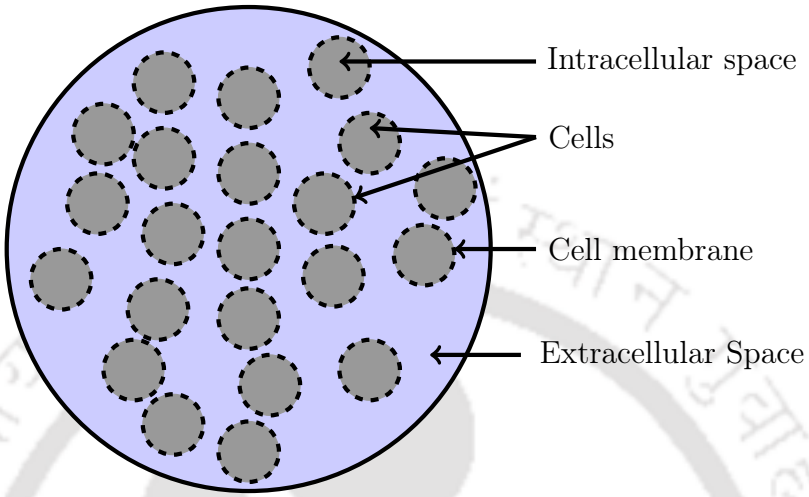

Figure 1.1: A schematic diagram of a biological tissue.

1.2.2 Electroporation

Electroporation is a phenomenon in which cell membrane can be temporarily destabilized due to the application of high intensity electric pulses. A schematic diagram of cell electroporation is shown in Fig. 1.2. During the destabilization period, nanometer-sized pores are formed and the cell membrane becomes highly permeable to exogenous molecules present in the surrounding media. In this transitory permeabilized period, cell membrane allows chemicals, drugs, or DNA to enter into the cell. Consequently, electroporation can be treated as a powerful microinjection method that is used to deliver various pharmaceutical compounds directly into specific target cells (diseased cells) of the human body. When chemotherapeutic agents are transported, it is known as electrochemotherapy, and when DNA is transported, it is known as gene electrotransfer.

Mathematical Equations

Let us consider a cell as a sphere whose surface is S with volume V. If a electric field is applied to the cell, the cell membrane deforms mechanically due to fast polarization. When an electric field is applied to some material, a current flows in that material. The principle of conservation of charge says that the total current that flows through the cell

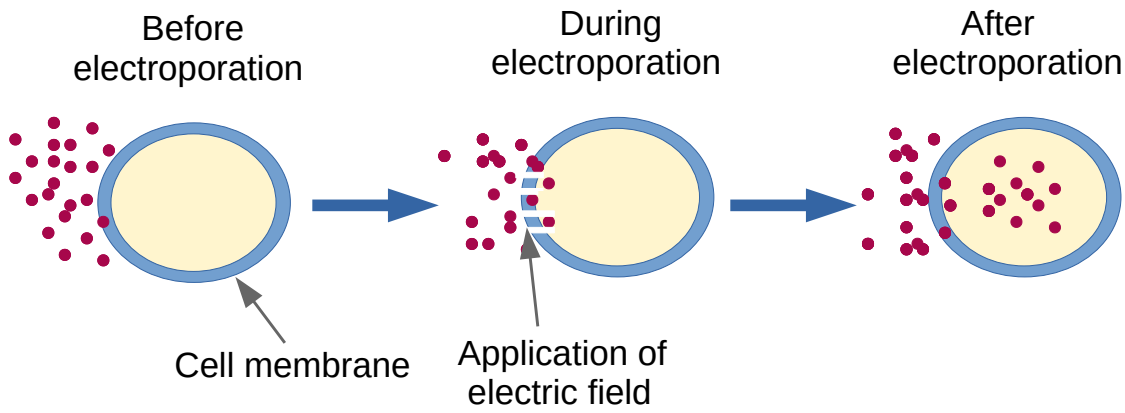

Figure 1.2: A simple diagram of cell electroporation.

of volume V is equal to the net flow charges within V, which is symbolically expressed by

$$\int_S \vec{J} \cdot d\vec{S} = -\frac{\partial}{\partial t} \int_V \rho' dV, \tag{1.1}$$

where J is the current density and ρ' is the volume charge density. By divergence theorem, we have

$$\int_V \vec{\nabla} \cdot \vec{J} dV = -\int_V \frac{\partial \rho'}{\partial t} dV \tag{1.2}$$

$$\implies \int_V \left[\vec{\nabla} \cdot \vec{J} + \frac{\partial \rho'}{\partial t} \right] dV = 0. \tag{1.3}$$

Since V is arbitrary volume, the Eq. (1.3) is true for all V. Therefore, the simplified form of the principle of conservation of charge, i.e., the equation of continuity, is as follows

$$\vec{\nabla} \cdot \vec{J} + \frac{\partial \rho'}{\partial t} = 0. \tag{1.4}$$

For the steady state condition: $\frac{\partial \rho'}{\partial t} = 0$ i.e., no charges are produced over the cell membrane during pulses. So, Eq. (1.4) becomes

$$\vec{\nabla} \cdot \vec{J} = 0. \tag{1.5}$$

Ohm's law states that "the current density is directly proportional to the electric field". So, a relation between current density and applied electric field is

$$\vec{J} = \sigma \vec{E}, \tag{1.6}$$

where σ is the proportionality constant, which is called conductivity of the cell. We know that electric field is the gradient of electric potential i.e., $\vec{E} = \vec{\nabla}\phi$. Hence, Eq. (1.5) can be rewritten as

$$\vec{\nabla} \cdot \left(\sigma \vec{\nabla}\phi\right) = 0. \tag{1.7}$$

The potential distribution in the tissue domain that is induced by the electroporation is calculated by the Eq. (1.7) and the general expression of this equation becomes,

$$\vec{\nabla} \cdot ((\sigma + \varepsilon_0\varepsilon_1)\vec{\nabla}\phi) = 0, \tag{1.8}$$

where ϕ is the electric potential, σ is the tissue electrical conductivity, ε_1 is the relative permittivity and ε_0 is vacuum permittivity. The boundary conditions are defined at the electrodes on which generally potential is applied. As the cells (or tissue) are electroporated, the electrical conductivity of Eq. (1.8) is expected to increase.

The magnitude of electric field (E) [68, 77] is the magnitude of the gradient of the electric potential, which is given by the relation

$$E = |\vec{\nabla}\phi|. \tag{1.9}$$

Membrane permeabilization, pore formation and mass transport depend on some parameters like, pulse strength (strength of the applied electric field), pulse length and time gap between the pulses. The important parameters are explained below:

- **Electrode** is an electrical conductor that makes electrical contact with a nonmetallic component of a circuit. It is also known as anode or cathode in electrochemical cells.
- **Electric field** is the field, which is induced in the targeted region (tissue or cell) by the electrodes. Two electrodes (Cathode: +, Anode: -) with different potential are basically used to generate electric field.
- **Pulse strength** is the magnitude of the induced electric field.
- **Pulse length or pulse duration** is the time of the applied electric field during electroporation. This time can be called pulse time or on time of the electroporation.
- **Time gap between two pulses** is the rest time between two consecutive pulses. Pharmaceutical compounds (like, drug) can be transported through the permeabilized cell membrane in this duration.

Depending on the field strength and pulse duration, electroporation process can be categorized as reversible and irreversible electroporation.

Reversible electroporation

Electroporation is called reversible when the applied electric field to a target cell is below a certain value (threshold value) of that cell. Reversible electroporation (RE) leads to temporary permeabilization of cell membrane with the survival of the treated cells. In reversible electroporation, the cells are able to repair their phospholipid bilayer as the applied current is below the cell's threshold. Reversible electroporation method is typically used in the treatments involving drug delivery, gene transplants, or deliver other molecules (that would not normally penetrate the cell membrane) into the cell. Since, all tissues have different threshold electric fields, it is essential to make careful calculations before any treatment to ensure safety and efficacy.

Irreversible electroporation

Sometimes, electroporation guides to cell death due to permanent permeabilization of the cell membrane when the applied electric field is high enough. This results in consequent loss of cell homeostasis and the process is termed as irreversible electroporation (IRE).

Membrane resealing

Membrane resealing is a physiological process in which the cell membrane closes its pores (which were open during electroporation) once the pulse period ends. Pore creation occurs in microseconds, while membrane resealing occurs in minutes. After the termination of electroporation, the pore area of the membrane decreases over time due to membrane resealing, and mass transport through the membrane gets slower.

Reversibly and irreversibly electroporated cells

The electroporated cells are classified based on the pulse application into two types: reversibly and irreversibly. A cell that has been reversibly electroporated survives the process, and after the pulse period is over, the cell membranes return to their original states. On the other hand, irreversibly electroporated cells cannot survive electroporation, and pores cannot be resealed.

Applications of Electroporation

Electroporation is vastly applied in medical science, such as gene therapy, electro chemotherapy, DNA vaccination, tissue ablation and drug delivery. A picture of an electroporation machine and an example for its application are given in Figs. 1.3 and 1.4. Electroporation has wide applications in both *in vitro* and *in vivo*. Electroporation is used to deliver drug for the treatment of patient with malignant tumour. Skin, liver, tumours and muscles are

the body tissues, which are mainly targeted through *in vivo* electroporation [86]. Currently, skin electroporation procedure is appealing enough to be used as a lesser invasive choice due to its potential for instigating robust adaptive immune reactions. A flow chart for some primary applications of electroporation is given by Fig. 1.5.

Figure 1.3: Electroporation machine [40].

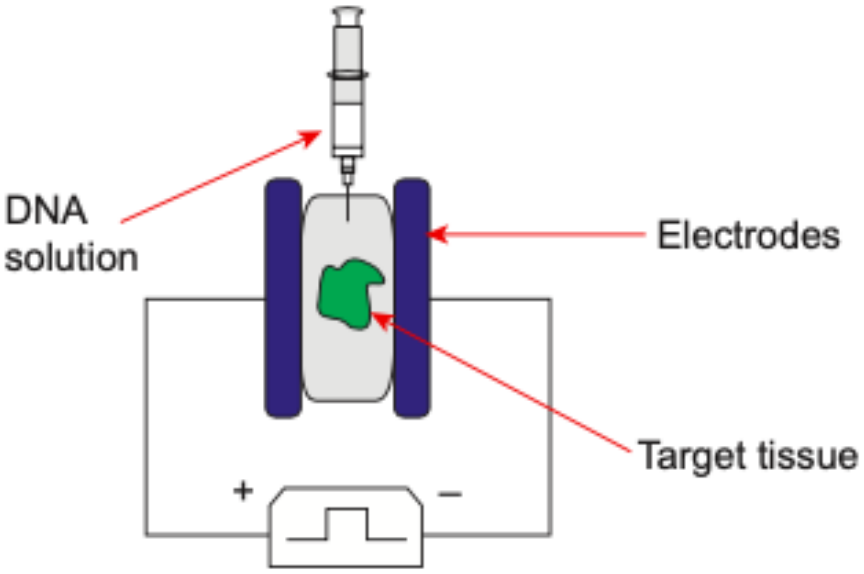

Figure 1.4: Electroporation of a target tissue to inject DNA [44].

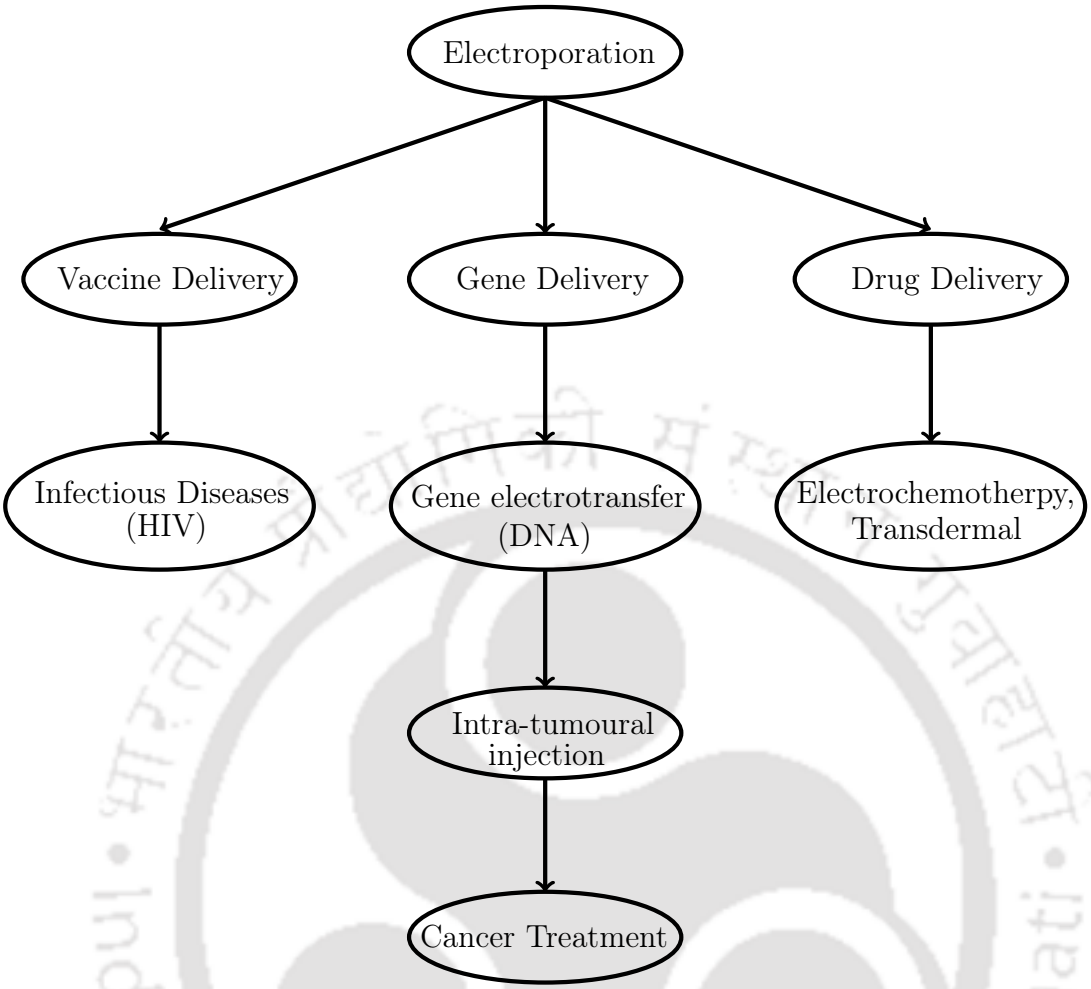

Figure 1.5: Flow chart for application of electroporation.

Advantages of Electroporation

- *Versatility:* The electroporation can be applied equally to all cell types and at all the stages of the cell cycle [29].
- *Efficiency:* Electroporation's efficiency depends on the electrical properties of the cells. A large number of cells can be targeted together for transferring drug, gene or DNA.
- *Small Scale:* Compared to other methods, electroporation requires a smaller amount of DNA.
- *Noninvasive and non-chemical:* Electroporation is a non-invasive, non-chemical method that does not seem to alter the biological structure or function of the target cells [11].
- *In Vivo:* This procedure may be applicable to the target tissue of the human body.

Disadvantages of Electroporation

- *Cell Death (Irreversible Cell):* When high voltage pulses are applied, some pores in cell membranes become too large and may not reseal after discharge, resulting in cell death.

- *Nonspecific Transport:* During electroporation, the delivery of drugs or genes into cells is relatively non-specific.

1.2.3 General Transport Equation

For any control volume, the law of conservation of mass states that the mass of the system must remain constant over time, since mass cannot change, therefore quantity cannot be added or subtracted. Hence, the conservation equation for a scalar quantity is mathematically defined as,

$$\frac{\partial C}{\partial t} = -\vec{\nabla} \cdot \vec{Q} + S, \tag{1.10}$$

where C is the concentration of the scalar, t is the time, $\vec{Q}$ is the total flux of the scalar through the boundaries of the control volume and S is the source or sink term inside.

The total flux $\vec{q}$ is equal to the sum of advective mass flux ($\vec{q_a}$) and diffusive mass flux ($\vec{q_d}$). Scalar advection is a function of the velocity and scalar concentration, caused by fluid particles moving across boundary layers. Therefore, the advective flux can be expressed as,

$$\vec{q_a} = \vec{u}C, \tag{1.11}$$

where $\vec{u}$ is velocity relative to its coordinates. Fick's Law states that the diffusive mass flux of a species is caused by random molecular motions. The Fick's law of diffusion is defined as,

$$\vec{q_d} = -D\vec{\nabla}C, \tag{1.12}$$

where D is the molecular diffusion coefficient and $\vec{\nabla}C$ is the gradient of the scalar concentration.

Using Eqs. (1.11) and (1.12), the mass transport equation (1.10) becomes,

$$\frac{\partial C}{\partial t} + \vec{\nabla} \cdot (\vec{u}C) = \vec{\nabla} \cdot (D\vec{\nabla}C) + S. \tag{1.13}$$

Diffusion Phenomena in the Tissue

The tissue medium is assumed to be homogeneous and cells are arbitrarily distributed throughout the tissue domain. Mass (drug, other chemical compounds) transport can occur through the extracellular fluid. The drug particles get transported into the intracellular compartment from the extracellular one through the pore of the cell membrane.

In this thesis, the effects of partitioning, absorption, and clearance are not considered. The Fickian diffusion model and the corresponding transport equation 1.13 are used to describe the mass transport in the tissue, as no chemical mixture or multi-phase flow is considered in the models, and a single chemical compound (drug) is chosen to deliver into the cells through single-component diffusion (molecular diffusion). The similar model of diffusion has already been used by many researchers to study electroporation based drug delivery problems [1,38,56]. Knudsen diffusion may occur in the process of drug transport through the nano-sized pore. Knudsen diffusivity normally depends on the pore radius, species molar mass, and temperature in Knudsen diffusion. The models proposed in this thesis do not contain any variable diffusion parameter. The diffusion coefficients (in extracellular and intracellular spaces) are assumed to be constant throughout the thesis. The suitable values of the diffusion coefficient are taken from the existing literature [1,2,38,56].

1.2.4 Nernst - Planck Equation

The Nernst-Planck equation is a conservation of mass equation. It describes the relationship between an electrical field and an ionic concentration gradient for the flux of chemical species. The equation is a extended version of Fick's law of diffusion that includes the case where the diffusing particles can move with the fluid due to electrostatic forces.

If the flux of ions ($\vec{q}$) is affected by electrostatic forces with an electric field $E = -\vec{\nabla}\phi - \frac{\partial \vec{A}}{\partial t}$, then using Fick's law of diffusion for this case, we have

$$\vec{q} = -\left[D\vec{\nabla}C - \vec{u}C + \frac{D\,z\,q_0}{K_B T}C\left(\vec{\nabla}\phi + \frac{\partial \vec{A}}{\partial t}\right)\right].$$

Therefore, the Nernst-Planck equation becomes

$$\frac{\partial C}{\partial t} = \vec{\nabla}\cdot\left[D\vec{\nabla}C - \vec{u}C + \frac{D\,z\,q_0}{K_B T}C\left(\vec{\nabla}\phi + \frac{\partial \vec{A}}{\partial t}\right)\right], \tag{1.14}$$

where t: Time, D: Diffusivity of the chemical species, C: Concentration of the species, z: Valence of ionic species, q_0: Elementary Charge, K_B: Boltzmann constant, T: Temperature, u: Velocity of the fluid, ϕ: Electric potential and A: Magnetic vector potential.

If we consider that the fluid is at rest and no magnetic vector potential acts, then equation (1.14)) becomes

$$\frac{\partial C}{\partial t} = \vec{\nabla}\cdot\left[D\vec{\nabla}C + mC\vec{\nabla}\phi\right]. \tag{1.15}$$

This equation is called modified Nernst-Planck equation, where $m = \frac{Dzq_0}{K_B T}$ is the effective electrophoretic mobility.

In this thesis, electrical fields are used during electroporation for cell membrane permeabilization and pore formation. As a result, the mass transfer rate in the membrane increases, and the mass transfer coefficient as a function of pore density is obtained. Effects of the electrical field on the drug particles (ionization or electrical double layer) are not considered here. Electromigration transport caused by an electric field is not considered in the mass transport equations. So, the exact Nernst-Planck equation is not used in the proposed models as charged chemical species are not considered. Mass transport equations involve the terms for diffusion and reaction processes only.

1.3 Literature Survey

1.3.1 General Drug Delivery Technologies

Controlled drug delivery technology has been improved over more than 60 years. Many controlled release formulations have been developed in drug delivery systems (DDS) to help patients and maximize drug efficacy. In 1952, Smith and French introduced the controlled release formulation for the first time for the delivery of dexedrine (C_9NH_{13}) [39, 53]. Based on this idea, the basic concept of controlled drug delivery was established until the end of the 1970s, and different drug release mechanisms including dissolution, diffusion, osmosis, and ion exchange were invented.

Currently, nanotechnology based targeted drug delivery helps to overcome many of the difficulties faced so far. A term called nanoparticle was first introduced in 1976 in the field of drug delivery [50] and many scientists attempted to find novel methods of drug delivery using nanoparticles [42]. Since the late 1990s, the nanoparticle technology has been widely used for improved drug delivery to target tumours. In 1986, Matsumura and Maeda discovered EPR (enhanced permeation and retention) enhancement, which represents the most important mechanism used by nanocarriers and macromolecules in targeting cancer. The EPR effect has been described in details in rodent models [52]. It is the basis for the clinical evaluation in DDS using nanosized anticancer drugs. However, many scientists have questioned the effectiveness of EPR for treating human tumours due to its high failure rate and emphasized the need for improvement [64]. Some physical methods, such as hyperthermia or ultrasound-induced cavitation have been developed recently to improve drug penetration into tumour cells [37, 55].

Some other drug delivery methods are computer-assisted drug delivery, transdermal drug delivery etc. Skin electroporation with transdermal transport theory is discussed in the next section.

1.3.2 Transdermal Drug Delivery

Stratum corneum (SC) is a thin (10 - 50 μm) outermost layer of the epidermis. It is the most transport resistive component of the skin. As early as 1924, H. Rein hypothesized that the principal resistance to transdermal transport is in a layer joining the SC to the epidermis. Blank [6] verified this by conducting stripping experiment in which SC is removed from the skin surface. The electrical resistance of the SC is between 5 and 25 kV cm^{-2} and the electrical breakdown potential is approximately 75 - 100 V [78]. This high resistance poses a major obstacle for successful transdermal drug delivery.

The SC is made up of 15 - 20 layers of dead flat cells, known as corneocytes, which are connected by a lipid bilayer structure in a crystalline-gel phase. In the SC, diffusion transport occurs primarily through the lamellar lipid structure [8]. Researchers are always looking for ways to apply transdermal drug delivery in clinical practice. Transdermal drug delivery offers several advantages, including the scopes of avoiding first-pass effects and gastric irritation as well as painlessness and non-invasiveness. Through the resistive layer, skin electroporation greatly enhances the success of transdermal delivery. In skin electroporation, the skin is exposed to a series of intense electric pulses that alter the structure of the SC by creating microscopic aqueous pores within the lipid filled spaces [70]. This modification of the SC structure allows greater molecular transport and drastically reduces the skin's electrical resistance [71].

Two types of pulses: short and long are generally used in electroporation. Nanometer-sized pores are formed within the individual lipids when a short pulse (less than 100 μs) is used [90]. Smith et al. [79] developed this process by electroporation of single lipid bilayer. Single lipid bilayer electroporation should be contrasted with skin electroporation. The SC can't be made by a single bilayer because it is constructed of a lipid-corneocyte matrix where lipids are arranged in a lamellar network. In the short pulse system, the drug molecules pass through the electropores in each bilayer of the SC. Small drugs can only be transmitted transdermally by short pulse electroporation through small pores created in the skin. Long duration pulse (100 μs - 100 ms) creates two important effects. One is electrophoresis in which the electric field provides electrophoretic forces that drive the large charged molecule through the layers of the SC [24]. The second important effect is Joule heating, which results in localized temperature rise that contributes to the increased permeability of the SC by lipid chain melting [2, 82] .

In 2014, Becker et al. [3] proposed a model involving the Joule effects. They also calculated the drug concentration in all the layers of the skin separately. According to their model, the governing equations are

$$\frac{\partial C}{\partial t} = \vec{\nabla} \cdot \left[D_i \vec{\nabla} C + m_i C \vec{\nabla} \phi \right], \tag{1.16}$$

$$\rho_i c_i \frac{\partial T}{\partial t} = \vec{\nabla} \cdot \left(k_i \vec{\nabla} T \right) + Q_J \left(z, r, t \right). \tag{1.17}$$

Equation (1.16)) comes from the modified Nernst-Planck equation 1.15 and equation (1.17)) describes the transient distribution of thermal energy within each layer of the system. Here, C is the dimensionless solute concentration, m is the effective electrophoretic mobility, D is the diffusion coefficient, ρ is the density, c is the specific heat, k is the thermal conductivity and i refers to one of the layers of the skin. Q_J denotes the source of heat generated by Joule heating due to pulse application.

1.3.3 Electroporation of Tissue and Cells

One of the major difficulties in biotherapy and cancer chemotherapy is the paucity of potent drug and gene delivery. To deliver drug in the intracellular space, cell membrane acts as a barrier and allows restrictive diffusion of drug molecules. Large size particles can not pass through the normal membrane. In order to get rid of such hindrances, different physical approaches are proposed and developed gradually. Physical delivery systems include electroporation, micro-injection, laser, ultrasound and many more [7]. Electroporation or electropermeabilization is used to increase the cell membrane permeability by many researchers [20, 22, 26, 47, 49]. Electroporation is a biophysical phenomenon resulting in the formation of aqueous pores in the cell membrane made up of lipid bilayer. Electroporation is performed by applying an external electric field of sufficient strength [26, 49, 57, 60]. In electroporation, transmembrane potential increases with the application of electric field and once the transmembrane potential exceeds it's critical value, the cell membrane gets permeabilized [47, 66]. The transitory and permeabilized state of cell membranes can be utilized to transport a variety of different molecules, such as ions, drugs, dyes, antibodies, oligonucleotides, RNA and DNA, to name a few, into the intracellular domain. Also, electroporation is widely used in biomedicine, biotechnology, food science and technology, and environmental science [25, 26, 47].

On the basis of some conducted experimental and theoretical studies (in 1960s and 1970s) with respect to bilayer membranes, Neumann et al. [63] were the first to publish a work on gene transfer based on cell destabilization through electroporation in 1982. This destabilization is occurred due to increment in the transmembrane potential and the experiment was done in a custom-built electroporation chamber. In 1989, Neumann et al. [62] introduced a model to calculate the transmembrane potential V_m of a spherical cell in a uniform electrical field. As an application of electroporation, the first clinical investigation was performed in 1993 to enhance the drug (chemotherapeutic agent in particular) uptake in tumours, as reported by Belehradek et al. [4]. The Neumann's model was used and developed later by several other researchers [21,23,48] to build a relationship between experimental and theoretical overviews with respect to tissue electroporation. In

the recent past, electroporation equipment has been refined in such a way that the electric pulse amplitude and pulse length can be independently controlled.

The electrical breakdown in the cell membrane is an important phenomenon in tissue electroporation. Several theoretical and experimental studies [16–18, 89] have been done by many researchers (Coster, Zimmermann and their group) during 1970-1980. From the experimental studies on the cells of 'Valonia utricularis' [16–18], it is observed that the electrical breakdown occurs when the transmembrane potential reaches a critical voltage. Researchers have also discovered that a reversible electrical breakdown occurs in the cell membrane for a voltage difference between the electrodes around 0.5-0.85 V [14–16]. This voltage difference generally depends on the membrane temperature during electroporation [18].

Usually, two types of electroporation pulses are prevalent, short and long. From experimental studies, it is observed that the application of a high voltage electric field for short duration (1 μs - 100 μs) increases pore density within the cell membrane [65, 81, 85]. Nanometer-sized pores are created within individual lipids through the application of short pulses [90]. For single cell electroporation (SCE), an inhomogeneous low voltage electric pulse is applied around cell surface to avoid cell death. SCE is used by some researchers [5, 46, 84] to deliver drugs, DNA, RNA, nucleic acid into the cell membrane in both *in vivo* and *in vitro* applications. Bulk electroporation is generally conducted to electroporate the whole tissue or a group of cells using a homogeneous long duration (100 μs - 100 ms) electric pulse. Single lipid bilayer electroporation differs from skin electroporation because the stratum corneum (SC) is made of a lamellar network of about 100 lipid bilayers instead of a single lipid bilayer. Therefore, skin electroporation needs long duration pulse since only smaller sized drug particles are able to get transdermally transported during short pulse electroporation. Long duration pulse initiates two significant upshots in the form of electrophoresis and Joule heating. Joule heating leads to localized temperature rise that has an influence on increased permeability of cell membrane through lipid chain melting [2, 79].

Depending on the field strength and pulse duration, electroporation process can be categorized as reversible and irreversible electroporation. In reversible electroporation, the electric field is applied under a certain range so that the membrane is temporarily permeabilized and recover the original state spontaneously after removal of electric field [31]. Once the pulse period is over, the cell membrane starts closing its pores, which are opened due to application of external electric field, is called membrane resealing [20, 38]. The resealing effect of cell membrane was discovered during the late 1970s [32, 45]. It has been observed that the time duration in pore creation is of the order of microsecond whereas membrane resealing happens in the minute time scale [65, 66]. The reversibly electroporated cell undergoes the treatment, and once the pulse period is over, the cell membrane reseals. In irreversible electroporation, the high electric field is applied

that leads to the permanent pore generation in the cell membrane [19]. The irreversible electroporation may lead to the loss in cell homeostasis that can cause cell death [74]. However, irreversibly electroporated cell can not sustain the treatment and pores do not reseal [43]. Reversible electroporation has been used to deliver drug into tumour cells through the process of electrochemotherapy [27, 58], gene delivery [73] and transdermal drug delivery [25, 90]. On the other hand, irreversible electroporation is generally used in cancer treatment [19, 74].

It has not been comprehended clearly about this uncommon way of cell death. A noteworthy theoretical study on the basis of empirical data was conducted by Saulis in 1997 [76]. The issue of irreversible permeabilization is an engrossing topic for investigation. It is now a known fact that due to the usage of strong electric pulses, irreversible permeabilization happens. However, the information regarding the loss of intracellular components as a result of extensive permeabilization is insufficient. Gehl et al. [33] in 1999 reported that cell death due to electroporation was more in *in vitro* than that in *in vivo*. It is reasonable to take into consideration that increment of permeability, resealing of pores and cell death seem to regulate the drug uptake in reversibly electroporated cells. Researchers endeavoured to develop mathematical models on the basis of the aforementioned factors.

The efficacy of drug transport in the tissues, as an outcome of electroporation, depends on several electrical parameters, physical and biochemical properties of the tissue, and drug's physicochemical characterization. Electropermeabilization depends on pulse strength, pulse duration, and the number of pulses [13]. Some tissue properties, such as conductivity, size, shape and distribution of cells also play a significant role in drug transport phenomena [65, 72]. Experimental findings reveal that the number of pulses and their durations are responsible for drug transport across the permeabilized membrane [75]. In SCE, short duration of a high electric field is used to permeabilize a specific portion of the cell [72, 85]. However, in bulk electroporation, long-duration electric pulses are generally conducted to electroporate the tissue [25, 38, 90].

The followings are some important theoretical models proposed and developed which are relevant to this thesis.

- In 2007, Krassowska and Filev [49] proposed a mathematical model of electroporation in a spherical cell. This model calculates pore density, transmembrane potential and distribution of pore radii as a function of time and space on the cell surface. The changes of pore with time is determined by the following differential equation

$$\frac{dN}{dt} = \alpha \exp\left(\frac{V_m}{V_{ep}}\right)^2 \left[1 - \frac{N}{N_0 \exp\left(q\left(\frac{V_m}{V_{ep}}\right)^2\right)}\right], \tag{1.18}$$

where N is the pore density, t is the time, α the pore creation rate coefficient, V_m the transmembrane potential, V_{ep} the characteristic voltage of electroporation, N_0 the equilibrium pore density for the membrane area at $V_m = 0$ and q is an electroporation constant.

- In 2008, Granot and Rubinsky [38] presented a mathematical model of drug delivery in tissue cells with reversible electroporation. They obtained the concentration distribution over the extracellular space from the following differential equation

$$\frac{\partial C_E}{\partial t} = \vec{\nabla} \cdot \left(D_{eff} \vec{\nabla} C_E \right) - P \left(\frac{A_P}{V_0} \right) C_E, \tag{1.19}$$

where C_E is the extracellular drug concentration, D_{eff} is the effective diffusion coefficient that is determined experimentally or approximated theoretically [41], P is the permeability of drug, $V_0 = 8r_c^3$ is the volume of a cube surrounding a cell and A_P is the total area of the pores per cell.

- In 2012, Corovič et al. [13] conducted an *in-vivo* experiment on muscle electroporation and also developed a mathematical model for this. They discussed the conductivity of skin and muscle changes due to the application of voltage.

- In 2014, the Miklavčič group [56] was the first to establish a relation between electroporation and the increment in resulted permeability that affected macroscopic transport and cellular uptake of drug. The article theoretically described the mass transport coefficient signifying the characteristics of electropores and drug. The effects of irreversible electroporation were not taken into account in their work and the study considered a uniform electric field.

- In 2016, Boyd and Becker [9] modified the model to implement tissue electroporation, where they categorized tissue into two parts: extracellular space and intracellular space. Pore resealing was considered in their study though there was no emphatic differentiation between transient transport behaviour of reversibly electroporated cells and that of irreversibly electroporated cells. The concentration of the drug in the extracellular space (C_E) and the intracellular space (C_I) are governed by

$$\frac{\partial C_E}{\partial t} = \vec{\nabla} \cdot \left(D_{eff} \vec{\nabla} C_E \right) - \left(\frac{1-\varepsilon}{\varepsilon} \right) \cdot \mu_R \cdot (C_E - C_I), \tag{1.20}$$

$$\frac{\partial C_I}{\partial t} = \mu_R \cdot (C_E - C_I), \tag{1.21}$$

where μ_R is the mass transfer coefficient and ε is the porosity.

- Recently, in 2017, Argus et al. [1] presented a three equations model of drug delivery, where both reversible and irreversible electroporations were taken into account. According to their model, the coupled concentration equations are given by

$$\frac{\partial C_E}{\partial t} = \vec{\nabla} \cdot \left(D_{eff} \vec{\nabla} C_E \right) - \left(\frac{1-\varepsilon}{\varepsilon} \right) \times \left[\mu_{RE} \cdot \exp\left(-\frac{t_p}{\tau} \right) \cdot SF \cdot (C_E - C_{RE}) + \mu_{IRE} \cdot (1 - SF) \cdot (C_E - C_{IRE}) \right], \tag{1.22}$$

$$\frac{\partial C_{RE}}{\partial t} = \mu_{RE} \cdot \exp(-\frac{t_p}{\tau}) \cdot (C_E - C_{RE}), \tag{1.23}$$

$$\frac{\partial C_{IRE}}{\partial t} = \mu_{IRE} \cdot (C_E - C_{IRE}), \tag{1.24}$$

where C_{RE} and C_{IRE} are the drug concentrations in the reversible and irreversible electroporated cells respectively, μ_{RE} and μ_{IRE} are the mass transport coefficients of the reversibly and irreversibly electroporated cells respectively, SF is the survival fraction of cells, τ is the resealing time constant [28], and t_p is the time after most recent pulse is applied.

1.3.4 Thermal Effects Due to Electroporation

The membrane structure of a cell have electrical resistivity even if the lipid layers of the membrane are thin. The cell membranes act as capacitors with high resistance [30]. Moreover, when the tissue gets exposed to an external electric field, the cell membranes become charged up. Elevated current density due to tissue electroporation guides to Joule heating, which is significant especially when longer electric pulses are applied. The Joule heating may not be biologically significant when electric pulses are applied for short duration, but in order to investigate the underlying mechanisms behind electro-chemotherapy, the role played by elevated temperature is important. Furthermore, the study of temperature variation is essential because it helps in the formation of stable permeable structures and hence plays a crucial role in electrically mediated molecular transport [69]. Also, the increment in temperature in cells plays a significant role in the dielectric breakdown of cell membrane. It has been experimentally observed that the potential difference between electrodes for dielectric breakdown decreases as the temperature of the cell membrane increases [18].

1.4 Objectives

The main objectives of the thesis work are as follows:

- ★ To present some mathematical models of drug delivery into the biological tissue through electroporation.
- ★ To deal with both reversible and irreversible electroporation.
- ★ To observe drug dynamics in the tissue during and after electroporation process.
- ★ To study the thermal effects in the tissue due to the application of electric pulses.
- ★ To discuss the importance of the electroporation parameters (electric field, pulse duration, time gap between pulses) and the drug permeability in drug transport into the cell.
- ★ To focus on the effects of drug loss at the tissue boundary and drug metabolism of the cell.

1.5 Motivation and thesis contribution

During the past few decades, most of the available literature on electroporation-based drug delivery focused on the membrane permeability and cell survival rate in both reversible and irreversible electroporation. Scientists are constantly trying to improve how electroporation increases membrane permeability and mass transfer so that sufficient amount of drug enters into the target cells. It is necessary to develop mathematical models for the delivery of drugs to diseased tissues (e.g., tumour cells) by reversible electroporation. In the pharmaceutical industry or clinical technology, models help to predict how drugs will be used at a particular site. In this field of research, it is necessary to thoroughly investigate the effects of electric field, drug permeability, temperature changes in the tissue, drug loss at tissue boundaries, and drug metabolism.

The present thesis is to provide some improved mathematical models for drug delivery concerning the above facts. The contributions of the current thesis are summarized below.

- ♣ In the first problem, a mathematical model is proposed to study the transport of drugs into a single cell by electroporation. This model captures the non-uniformity of membrane permeability, since pore formation rates differ across the membrane. The spatial changes of cellular drug uptake have been examined. A set of mathematical differential equations with appropriate initial and boundary conditions governs the biological processes. In order to deal with the drug transport across the cell membrane, the permeable interface method (PIM) is incorporated. To determine

the appropriate voltage for sufficient drug uptake into the target cell, a variety of experiments are conducted using various electric fields.

- The second problem deals with the mathematical modelling of drug delivery into the targeted cells by tissue electroporation. The model considers reversible, irreversible electroporation and membrane resealing effects. The drug transport through extracellular to intracellular region of the tissue is analyzed in details. This study investigates two cases of mass transport: (i) mass transfer during electroporation, and (ii) mass transfer after the termination of electroporation. This work examines the effects of membrane pore density on cellular drug uptake. The pore density is involved in terms of mass transfer coefficient that controls total mass exchange in the cell membrane. The role of the applied electric field to initiate the drug uptake into the cells is also investigated.

- In the third problem, only reversible electroporation is considered for treatment of an entire infected tissue by delivering drugs as medicine. Therefore, in order to avoid cell death and permanent membrane permeabilization, low voltage pulses are applied repeatedly. In this study, the major objective is to analyze the drug transport processes in extracellular and intracellular domains of the targeted tissues when the drugs are administered from one side. The temperature changes in the tissue due to electroporation are also examined.

- Fourth problem considers bulk electroporation on tissue in a mathematical model for drug delivery. In order to achieve a sufficient amount of drug in the targeted cells, some multiple pulses are applied in electroporation. Dirac-delta function is used to represent point source drug as initial drug distribution at the tissue boundary. A thorough investigation of the effects of drug loss from tissue boundary is conducted. On this account, mass transport equations are solved with flux boundary conditions.

- In the last problem, the previous work is extended with inclusion of drug metabolism phenomena in the cell. When drugs are absorbed by the cells, some portion of drug is metabolized, and so the intracellular concentration of drug decreases over time. In this study, we analyze some parameters of metabolism that play a significant role in reducing drug concentration once it reaches the intracellular space.

1.6 Organization of the work

The thesis is arranged in the following manner.

- In Chapter 1, a brief introduction, basic definitions and literature review are provided.
- In Chapter 2, a model of single cell electroporation to deliver drug into the cell is presented.
- In Chapter 3, drug dynamics in an electroporated tissue considering both reversible and irreversible electroporation is studied.
- In Chapter 4, the thermal effects in the tissue with reversible electroporation to deliver drug into the targeted cells is discussed.
- Chapter 5 deals with the point source drug and the drug loss from the tissue boundary in study of reversible electroporation with repeated pulse to inject drug into the diseased tissue.
- Chapter 6 emphasizes on the effects of drug metabolism in the cell after injecting mass into the cell.
- In Chapter 7, conclusions of the thesis work and future scopes are presented.

CHAPTER 2

DRUG DELIVERY INTO A SINGLE CELL BY ELECTROPORATION

In this chapter, we have solved proposed a simple mathematical model to study drug transport in a single cell by electroporation. In the model, microscopic mass transport behavior is analyzed from extracellular space to the cell via permeabilized cell membrane.

2.1 Introduction

One of the major challenges in drug delivery is to deliver a sufficient amount of drug (as a medicine) into the targeted cells. Drug molecules are not allowed to enter into cells because the cell membrane acts as a barrier. Different physical approaches are proposed and developed with time to eliminate these obstacles [7]. Electroporation is a method to deliver drugs to diseased cells when there is an obstruction of cell membrane in their path [20, 47]. Electric pulses of a high enough intensity are employed to overcome the obstruction. Membrane permeabilization and aqueous pores are formed in lipid bilayers during electroporation. Cell membrane can be exploited in their transitory and permeabilized states to transport drugs into the intracellular domain . This destabilization is occurred due to increment in the transmembrane potential [63]. In 1989, Neumann et al. [62] introduced a model to calculate the transmembrane potential V_m of a spherical cell in a uniform electrical field. DeBrurin and Krassowka also developed a model [22] in 1999 to calculate numerically the transmembrane potential of spherical cells in an electrical field. In 2007, Krassowska and Filev [49] proposed a mathematical model of single cell electroporation that discussed pore density, transmembrane potential, and the distribution of pore radius. Goldberg et al. [36] used the pore creation model [49] and proposed a multiphysics model for ion transport. In their model, they presented a mass transport equation using the Nernst-Planck equation for transporting different species into the cells.

A recent study by Goldberg et al. [35] uses the previous model to examine the effects of electrical pulses on the transport of cisplatin across the plasma membrane.

This work proposes a mathematical model to study drug transport into a cell by the application of electroporation. In this model, one of the concerns is the non-uniformity of membrane permeability, as pore formation rates differ in different places in the cell membrane. Spatial changes in cellular drug uptake are analyzed at different times. Multiple pulses of a certain electric field are used in electroporation in order to long time permeabilization of the cell membrane. Various electrode arrangements are tested to determine the locations of maximum pore formation and analyze how mass is transported through those locations. The biological processes are represented by governing differential equations with appropriate initial and boundary conditions. Numerical methods are adopted to solve the model equations. The permeable interface method (PIM) is employed to deal with the mass transport across the cell membrane. Different experiments for various electric fields (E = 15, 25 and 40 V mm^{-1}) are conducted. Suitable electric field is determined according to the type of drug that enters the cell. In addition, a comparison on the results for different values of drug permeability is made to select appropriate class of drug that can be injected into the cell of desired amount. The model is validated with the existing experimental works.

2.2 Model Formulation

This study investigates the drug transport through the electro-permeabilized cell membrane. A square domain (Ω) of edge length L is considered, and a single-cell is assumed to be placed at the center of Ω. Structurally, the domain can be viewed as two parts: extracellular space and intracellular space. The spaces are separated by the cell membrane, which is selective permeable and controls the mass exchange between the extracellular and intracellular domains. The schematic diagram is shown in the Fig. 2.1. In order to electroporate the cell membrane, two electrodes with potential values ϕ_0 and ϕ_L are placed along the vertical lines at A and B, respectively (as shown in Fig. 2.2). A uniform electric field E is induced in the region directed from positive to negative electrode. The transmembrane potential (V_m) increases due to the induced electric field. On increasing V_m, cell membrane is destabilized and nanometer-sized pores are generated in the cell membrane as a result of pulse application. Pulses are applied repeatedly for a short duration (1 ms) with maintaining a fixed temporal gap between two pulses. It is assumed that the mass transfer takes place only when the pulse is off. The drug transport from extracellular to the intracellular domain occurs in the resealing period of the cell membrane. The maximum number of pores are created near the poles $\Psi = 0, \pi$, in the setup as shown in Fig. 2.2, as transmembrane potentials are maximum at those locations; whereas, no

new pores are formed at $\Psi = \frac{\pi}{2}, \frac{3\pi}{2}$ as almost negligible transmembrane potential induced at those particular locations.

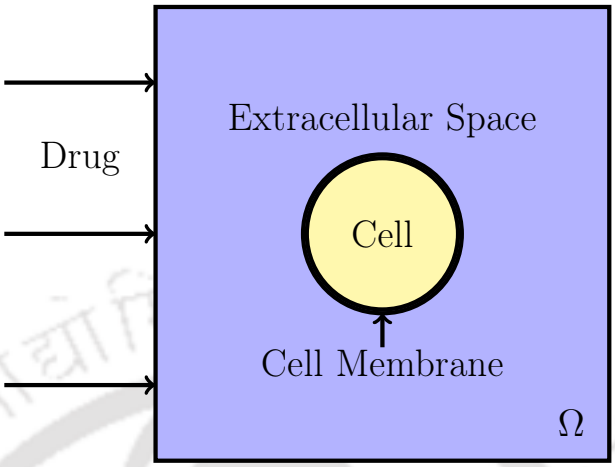

Figure 2.1: A schematic diagram of injecting drug into a biological tissue.

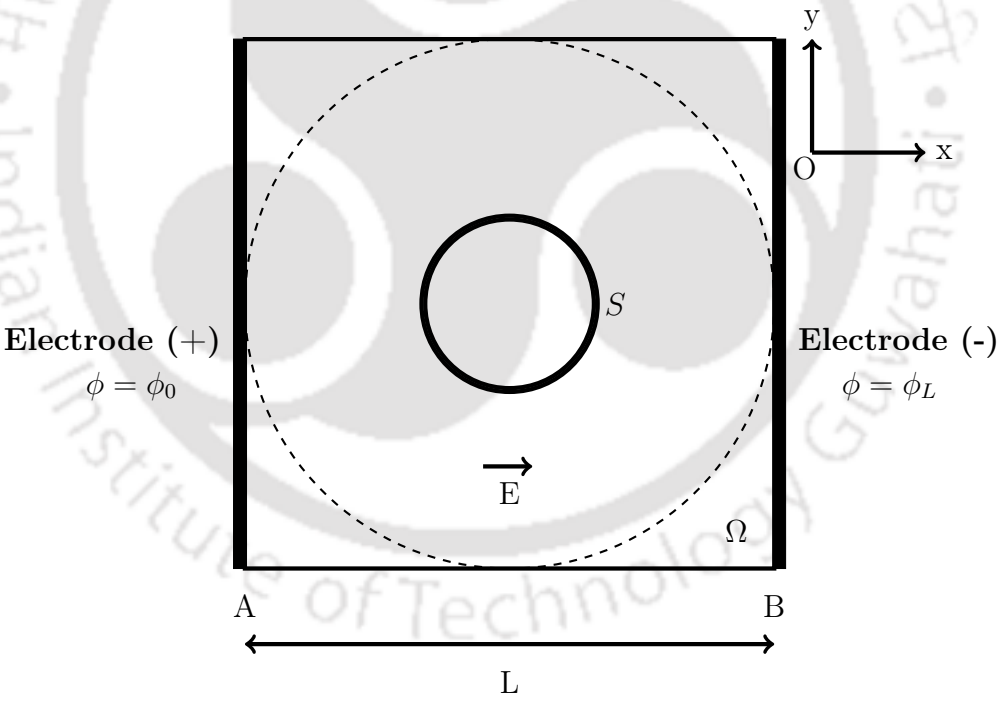

Figure 2.2: Schematic representation of a single cell electroporation.

A uniform electric field and non-uniform electric potential has been developed on the arrangement of two parallel electrodes. The potential (ϕ) distribution inside the domain is obtained by solving the Laplace equation given as [9, 13, 77],

$$\nabla^2 \phi = 0. \tag{2.1}$$

The uniform electric field (E) throughout the domain Ω is obtained by taking the magnitude of potential gradient expressed as,

$$E = |\vec{\nabla}\phi|. \tag{2.2}$$

2.2.1 Transmembrane potential and pore calculations

In this model, we consider a single-cell electroporation in which the spherical cell with radius r_c is immersed in an extracellular space of spherical shape with radius $3r_c$. A uniform electric field is induced from the boundary of the extracellular space to destabilize the cell membrane. The physical structure of the model is schematically portrayed by Fig. 2.3.

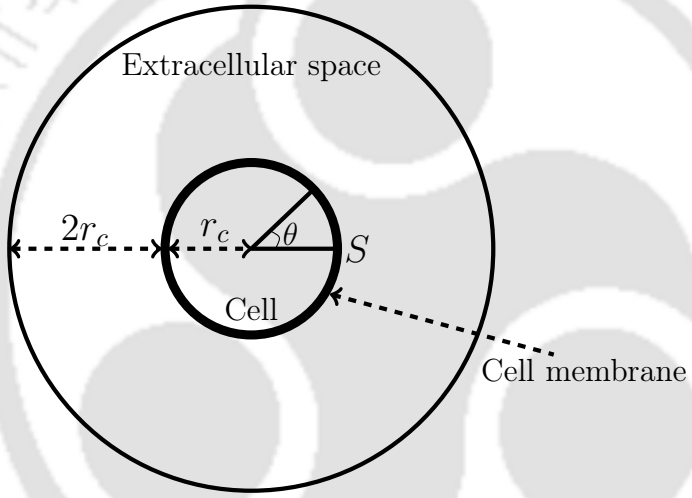

Figure 2.3: Schematic diagram of a spherical cell with radius r_c immersed in extracellular space of thickness $2r_c$.

The transmembrane potential V_m on the cell membrane due to the application of electric field is the difference of potentials in intracellular and extracellular domains. As both the domains are source-free, the potentials are calculated using the Laplace equations as [22],

$$\nabla^2\Phi_i = 0 \quad \text{in intracellular space,} \tag{2.3}$$
$$\nabla^2\Phi_e = 0 \quad \text{in extracellular space,} \tag{2.4}$$

where Φ_i and Φ_e are the intracellular and extracellular potentials. The uniform external field E is assumed at the outer boundary and the boundary condition on Φ_e can be defined as,

$$\Phi_e = -3r_cE\cos\theta. \tag{2.5}$$

The current density across the cell membrane (S) is given by

$$-\hat{n}\cdot(\sigma_i\nabla\Phi_i) = -\hat{n}\cdot(\sigma_e\nabla\Phi_e) = C_m\frac{\partial V_m}{\partial t} + g_1\left(V_m - E_1\right) + Ni_{ep}, \tag{2.6}$$

where $\hat{n}$ is the unit vector normal to the membrane surface; σ_i and σ_e are the intracellular and extracellular conductivities, respectively; C_m is the specific membrane capacitance; g_1 is the specific membrane conductance; t is the time; and E_1 the reversal potential of the ionic current. The transmembrane potential is defined as $V_m = \Phi_i - \Phi_e$ on S. The current (i_{ep}) in a single pore is obtained as [21],

$$i_{ep} = \frac{\pi r_m^2\sigma v_m RT}{Fh}\frac{e^{v_m-1}}{\frac{w_0e^{(w_0-nv_m)}-nv_m}{w_0-nv_m}e^{v_m} - \frac{w_0e^{(w_0+nv_m)}+nv_m}{w_0+nv_m}}, \tag{2.7}$$

where $v_m = V_m\left(\frac{F}{RT}\right)$ is the non-dimensional transmembrane potential. The detailed explanation of the equation 2.7 is given in the model [21].

The pore density $N(t,\theta)$ given by Krassowka and Filev [49] is as follows,

$$\frac{dN}{dt} = \alpha A\left[1 - \frac{N}{N_0}A^{-q}\right], \tag{2.8}$$

where $A = \exp\left[\left(\frac{V_m}{V_{ep}}\right)^2\right]$, t the time, α the pore creation rate coefficient, V_m the transmembrane potential, V_{ep} the characteristic voltage of electroporation, N_0 the equilibrium pore density for the membrane area at $V_m = 0$ and q is an electroporation constant.

The total number of pores (N_P) in Δ_θ of the cell membrane is obtained after the application of an electric pulse as,

$$N_P(\theta) = \oint_{\Delta_\theta} N(t_{ep})\,d\theta, \tag{2.9}$$

where Δ_θ is the local area at θ and t_{ep} is pulse duration.

2.2.2 Pore resealing and mass transfer coefficient

The pore area decreases with time after electroporation due to the membrane resealing effect, which can be expressed as,

$$A_P(\theta,t) = \pi R_P^2\cdot N_P(\theta)\exp\left(-\frac{t}{\tau}\right), \tag{2.10}$$

where τ is the resealing time and R_P is the pore radius.

The mass transfer coefficient depends on the pore density and time. The mathematical

formulation of the mass transfer coefficient (μ) is given as follows,

$$\mu(\theta, t) = \frac{A_P(\theta, t)}{\Delta_\theta} P, \tag{2.11}$$

where P is the permeability of drug particles across the cell membrane.

2.2.3 Drug transport phenomenon in the tissue

The drug concentrations in extracellular space and in the reversibly electroporated cell are obtained by the mass transport equations,

$$\frac{\partial C_E}{\partial t} = \nabla \cdot (D_E \nabla C_E), \tag{2.12}$$

$$\frac{\partial C_I}{\partial t} = \nabla \cdot (D_I \nabla C_I), \tag{2.13}$$

with the initial and boundary conditions

$$C_E(x, y, 0) = \begin{cases} C_0, & x = 0, \\ 0, & \text{otherwise}, \end{cases} \tag{2.14}$$

$$C_{RE}(x, y, 0) = 0, \tag{2.15}$$

$$\frac{\partial C_E}{\partial \eta} = 0. \tag{2.16}$$

Here, the subscripts E and I denote the variables from extracellular and intracellular spaces, respectively. C is the drug concentration and D is the drug diffusivity. C_0 denotes input initial drug concentration. η is an outward normal vector to the tissue surface.

Interface conditions

The cell membrane is selective permeable and the permeability depends on the drug properties. The improved permeability of cell membrane in terms of μ is incorporated in the drug transport as,

$$D_E \nabla C_E = D_I \nabla C_I = \mu(\theta, t)(C_E - C_I)\eta. \tag{2.17}$$

2.3 Method of Solution

The equations (2.3) - (2.11) are solved numerically to calculate pore density and MTC. The mass transport equations (2.12) - (2.17) are solved using the permeable interface method (PIM) proposed by Yadav and Dalal [88]. The PIM can be described briefly as

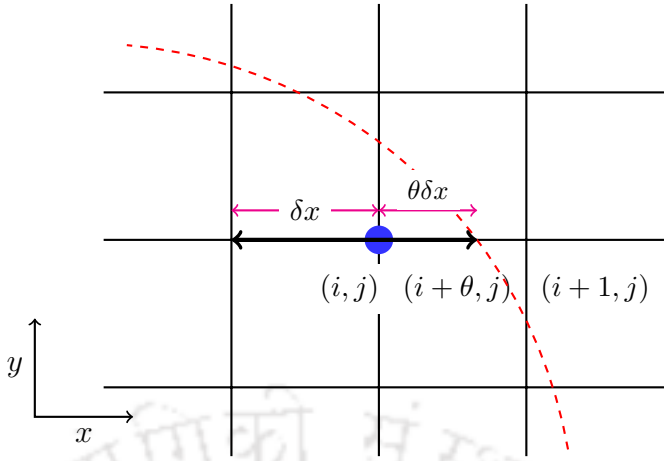

Figure 2.4: Discretization near the interface.

follows. The set of governing equations are solved using finite difference methods. The domain is discretized using the Cartesian mesh, say the grid point is denoted by (i, j), where i is an index in the x-direction while j is in the y-direction. The central-difference scheme used to discretize the Eq. (2.13) is as follows:

$$\left(\delta_x \left(D\delta_x C\right)\right)_{i,j} + \left(\delta_y \left(D\delta_y C\right)\right)_{i,j} = 0, \tag{2.18}$$

where

$$\left(\delta_x \left(D\delta_x C\right)\right)_{i,j} = \left\{ \frac{D_{i+1/2,j}C_{i+1,j} - (D_{i+1/2,j} + D_{i-1/2,j})C_{i,j} + D_{i-1/2,j}C_{i-1,j}}{(\delta x)^2} \right\}$$

and

$$\left(\delta_y \left(D\delta_y C\right)\right)_{i,j} = \left\{ \frac{D_{i,j+1/2}C_{i,j+1} - (D_{i,j+1/2} + D_{i,j-1/2})C_{i,j} + D_{i,j-1/2}C_{i,j-1}}{(\delta y)^2} \right\}.$$

Here, the subscript $(i + 1/2, j)$ denotes the position $(x_i + \delta x/2, y_j)$ with step-size δx in the x-direction. Other indices are defined in similar manner.

However, on the grid points near the interface (as depicted in Fig. 2.4), central-difference scheme can not be used directly. For this, the following scheme [88] is used,

$$\left(\delta_x \left(D\delta_x C\right)\right)_i = \left\{ D_{i+\theta/2} \frac{C^-_{i+\theta} - C_i}{x_{i+\theta} - x_i} - D_{i-1/2} \frac{C_i - C_{i-1}}{x_i - x_{i-1}} \right\} \Bigg/ \left(\frac{x_{i+\theta} - x_{i-1}}{2} \right), \tag{2.19}$$

where $x_{i+\theta} = x_i + \theta\delta x$ for some $0 < \theta < 1$. $C^-_{i+\theta}$ is the limiting concentration at the point $x_{i+\theta}$ approaching from the left side (Fig. 2.4).

The limiting concentrations at the interface are obtained using linear interpolation from the left and right sides, respectively, which also satisfy the interface conditions (Eq.

2.17) [88]. The resulted system of equations is solved using the BiCGSTAB algorithm without preconditioning with maximum allowable error between two consecutive iterative solutions falls below 10^{-15}.

Table 2.1: The details of the parameters values used in the simulations.

Sym	Value	Definition	Source
r_c	50 μm	Cell radius	[49]
α	10^9 m^{-2} s	Pore creation coefficient	[49]
V_{ep}	0.258 V	Characteristic voltage	[49]
N_0	1.5×10^9 m^{-2}	Equilibrium pore density	[49]
q	2.46	Electroporation constant	[38]
D_E	10^{-3} mm^{-2} s^{-1}	Extracellular diffusion coefficient	
D_I	10^{-4} mm^{-2} s^{-1}	Intracellular diffusion coefficient	
R_P	0.8 nm	Pore radius	[38]
P	$(0.1 - 1)$ mm s^{-1}	Permeability of drug	[38]
E	$(15 - 40)$ V mm^{-1}	Electrical field	
C_0	1 M	Initial drug concentration	
L	3 mm	Edge length of the square	Fig. 2.2
ϕ_0	25 V	Potential at A	Fig. 2.2
ϕ_L	0 V	Potential at B	Fig. 2.2
t_{ep}	1 ms	Pulse length (ON TIME)	
t_M	50 s, 100 s	Time for mass transfer (OFF TIME)	
PN	20	Pulse number	

2.4 Results and Discussion

In this section, the effects of electroporation on drug transport in single-cell are analyzed through numerical experiments. The key parameters, such as drug permeability, electric field and pulse number are explored. In the model experiment, repeated pulses with a fixed voltage are applied to make the cell membrane permeabilized and retained this state for a longer period of time. Time gaps between every two consecutive pulses (50 s or 100 s) are maintained for drug transport into the cell. In order to incorporate the physiological situation, the parameters are taken from the literature as listed in the Table 2.1. The results are obtained on a mesh size 250×250 after ensuring grid independence outcomes.

2.4.1 Validation

The results obtained from the model are validated with that of an existing article of Miyauchi et al. [59] and presented in Fig. 2.5. For this comparison, a square domain is considered with a cell placed at the center of it as shown in Fig. 2.5a. $P = 0$ is chosen,

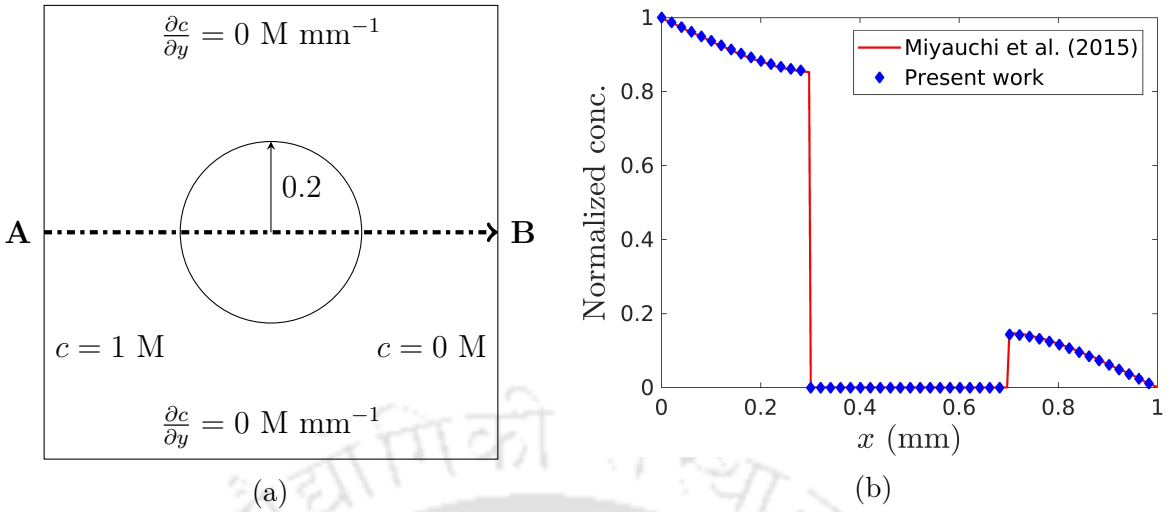

Figure 2.5: (a) Computational domain and (b) comparison of present results with the results of Miyauchi et al. [59] along the line **AB**.

so no drug uptake is expected. The concentration distributions along the line **AB** are displayed in Fig. 2.5b. It can be seen that the results are in good agreement.

2.4.2 Drug distribution versus time

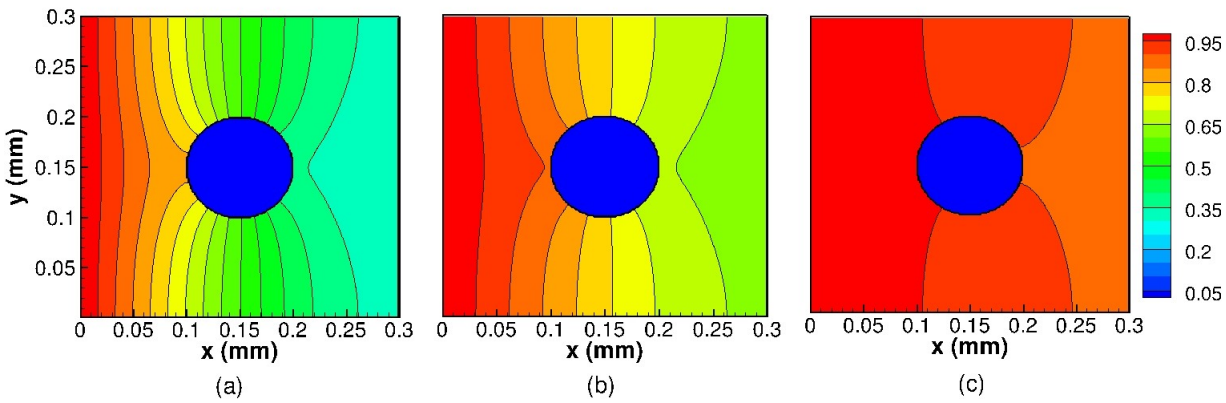

Figure 2.6: Contour plots of drug penetration at various times (a) $t = 250$ s, (b) $t = 500$ s and (c) $t = 1000$ s for $P = 0.1$ mm s^{-1} and $E = 15$ V mm^{-1}.

Fig. 2.6 shows the contour plots of drug transport into the intracellular space from the extracellular region through the permeabilized cell membrane. It shows drug concentrations for different time durations, as $t = 250$ s, 500 s, and for 1000 s. The drug uptake into the cell is almost nill due to the application of significantly low voltage (15 V mm^{-1}) pulses. The reason is that when low voltage pulses are applied to the tissue, fewer pores are created in the cell membrane, and as a result, the resultant membrane permeability becomes less.

In order to improve membrane permeability, it is necessary to increase field strength (i.e., $E > 15$ V mm^{-1}) of the applied pulses in the experiments. Since a high voltage pulse enhances pore area and its number in the cell membrane (see Eq. (2.8)), this gives rise to increase in mass transfer rate. The mass transfer rate may also increase for some drugs (basically small sized pharmaceutical molecules) that are highly permeable to the target cell membrane. This is due to μ is directly proportional to drug permeability P, which is expressed in Eq. (2.11). So, several experiments are conducted to analyze the roles of the field strength of the applied pulses and drug permeability. Detailed discussions about the effects of significant parameters on cellular drug uptake are presented below.

2.4.3 Effects of electric field on drug penetration

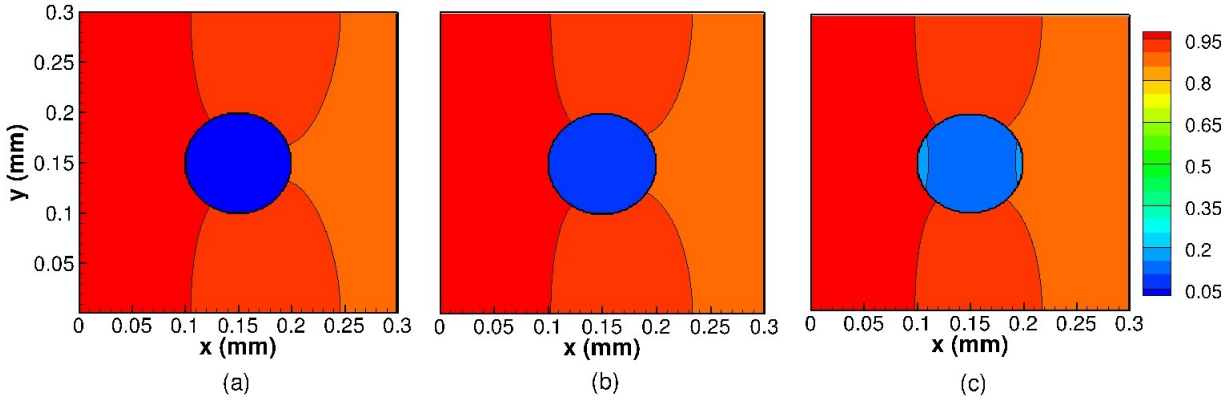

Figure 2.7: Effects of electric field (a) $E = 15$ V mm^{-1}, (b) $E = 25$ V mm^{-1} and (c) $E = 40$ V mm^{-1} ($P = 0.1$ mm s^{-1}, $t = 1000$ s).

The experiments are on the application of 20 pulses of 1 ms with three different electric fields as, $E = 15$, 25 and 40 V mm^{-1}. Fig. 2.7 shows the effects of electric field on drug uptake. From first two graphs (Figs. 2.7a, 2.7b), it is noticed that the cell intakes less amount of drugs due to insufficient permeabilization of the cell membrane with low voltage pulses ($E = 15$, 25 V mm^{-1}). So, $E = 15$, 25 V mm^{-1} are not suitable voltages for introducing sufficient drug uptake into the cell. Another experiment for $E = 40$ V mm^{-1} with same value of the drug permeability ($P = 0.1$ mm s^{-1}) is conducted to observe the effects of high electric pulse on mass transport and the results are shown in Fig. 2.7c. A significant improvement in drug uptake is noticed; thus, sufficiently strong electric field is required in order to permeabilize the cell membrane appropriately. As indicated in Fig. 2.7c, drugs enter the cell through both routes ($\theta = 0$, π), where maximum pores are created.

Fig. 2.8 shows the concentrations, plotted against the time, obtained from some selected points inside the cell. The selected points are $(0.11, 0.15)$, $(0.15, 0.15)$ and

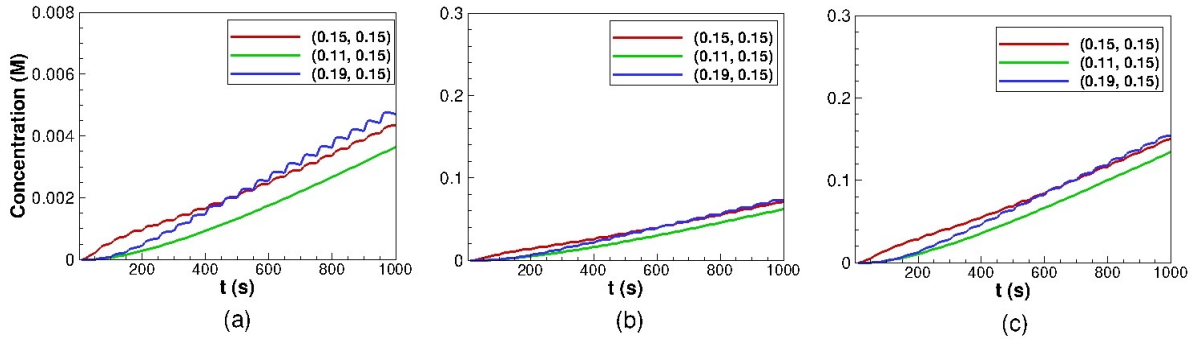

Figure 2.8: Concentration vs time inside the intracellular space for (a) $E = 15$ V mm^{-1}, (b) $E = 25$ V mm^{-1} and (c) $E = 40$ V mm^{-1} ($P = 0.1$ mm s^{-1}).

$(0.19, 0.15)$. Clearly, one can observe that the drug concentration increases with time owing to the drug uptake. Effects of several pulses can be seen. On a given pulse, drug uptake initially improves and then gets saturated due to the resealing effect, and subsequent application of another shot of pulse creates faster uptake. Clearly, the intracellular concentration increases with increasing E. The maximum intracellular concentration is achieved for $E = 40$ V mm^{-1}.

2.4.4 Drug distribution versus x

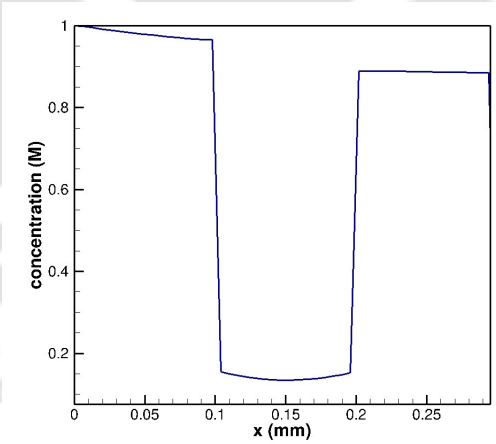

Figure 2.9: Concentration across a cross-section of domain at $y = 0.15$ for $P = 0.1$ mm s^{-1} and $E = 40$ V mm^{-1}.

Fig. 2.9 illustrates the amount of drugs reached at every point along the line $y = 0.15$ in the tissue domain. The result is obtained at the end of the process in which 20 pulses of 1 ms and a 50 s time gap between two pulses are taken. The figure shows that the extracellular concentration of the drug is much higher than the intracellular concentration. The use of a high electric field and the application of more pulses repeatedly improve drug uptake into the cell. Therefore, our goal is to choose the electroporation parameters based

on both the nature of the drugs as well as the quantity of drugs that needs to be introduced into the cell.

2.4.5 Effects of drug permeability on drug penetration

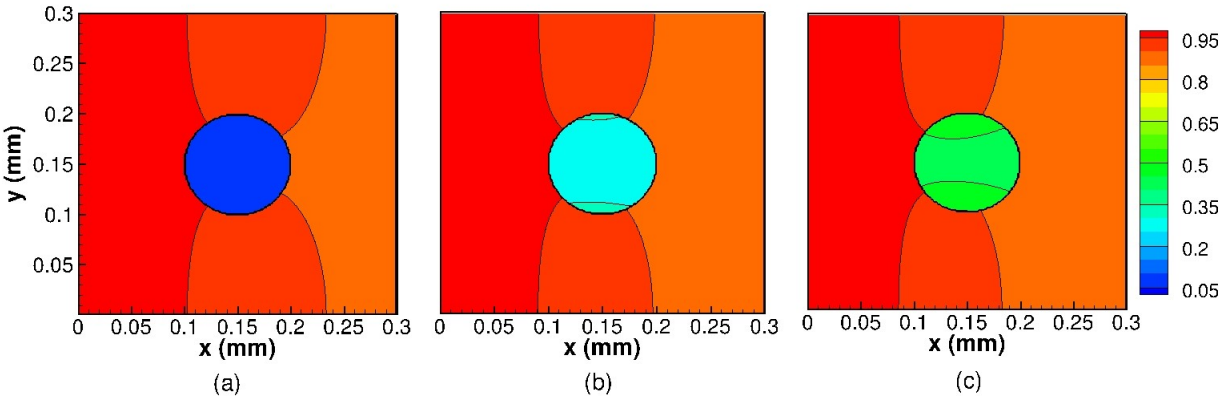

Figure 2.10: Effects of drug permeability (a) $P = 0.1$ mm s^{-1}, (b) $P = 0.5$ mm s^{-1} and (c) $P = 1$ mm s^{-1} ($E = 25$ V mm^{-1}, $t = 1000$ s).

In order to observe the effects of drug permeability across the cell membrane on drug transport into the cell, numerical experiments are conducted with different permeability values for the voltage $E = 25$ V mm^{-1}. The results provided in Fig. 2.10 explain that the drug uptake increases with the increase in P as mass transfer rate increases with P. However, diffusion of the drug into the extracellular space is same at $t = 1000$, while its mass transfer from the extracellular to intracellular region differs. This shows that the drugs having higher permeability are required when low voltage field is used. It is evident from Figs. 2.10b and 2.10c that a large amount of drug (> 0.2 M) has entered the cell, which may fulfill the requirement for treating the target cell. Thus, the drugs with permeability greater than 0.005 can be chosen to inject it into the cell for $E = 25$ V mm^{-1}.

2.4.6 Final set up of E and P

Fig. 2.11 is presented to see the drug penetration into the targeted region at different times of mass transport for the application of the pulses with suitable voltage ($E = 25$ V mm^{-1}) and for the appropriate choice of drug with permeability $P = 0.5$ mm s^{-1}. In Fig. 2.11a, it is noticed that drugs start entering into the cell within the time of 250 s from the left side when a sufficient drug is diffused at the location near the cell. This is due to the fact that a proper mass transfer rate occurs as increased values of both parameters electric field and drug permeability are considered. On increasing time, the drug spreads out in extracellular space and enters into the cell. Up to the end of the process ($t = 1000$

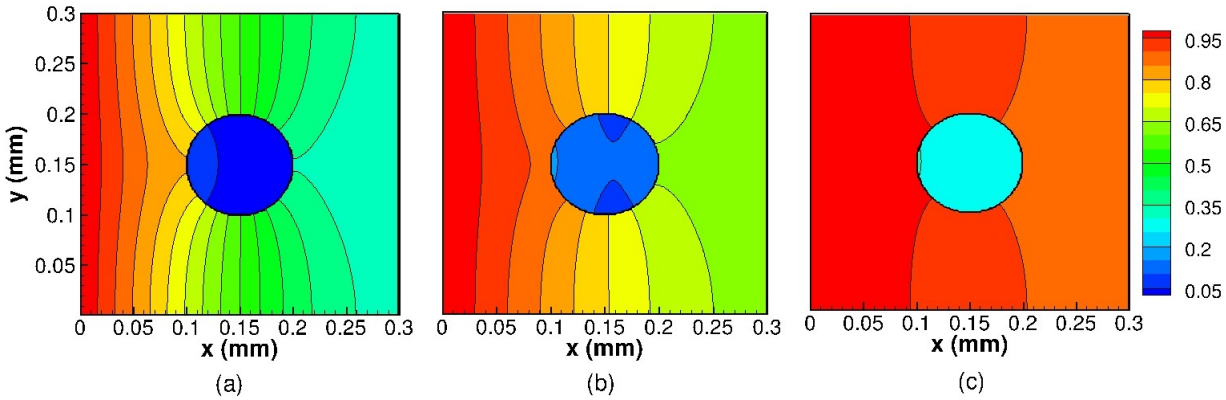

Figure 2.11: Contour plots of drug penetration at various times (a) $t = 250$ s, (b) $t = 500$ s and (c) $t = 1000$ s for $P = 0.5$ mm s^{-1} and $E = 25$ V mm^{-1}.

s), the drug uptake into the cell increases continuously over time, that is observed by Figs. 2.11b and 2.11c. Fig. 2.11b illustrates an important point: drugs enter the cell through pores in the right side at $\theta = \pi$ when some amount of drugs reaches to the ECS near $\theta = \pi$. At the end of the process of drug delivery, the cell contains a certain amount (≈ 0.25 M) of drugs by continuous mass introducing through both the paths (left and right) in the cell, which is shown in Fig. 2.11c.

Comparison between two sets of parameter choice

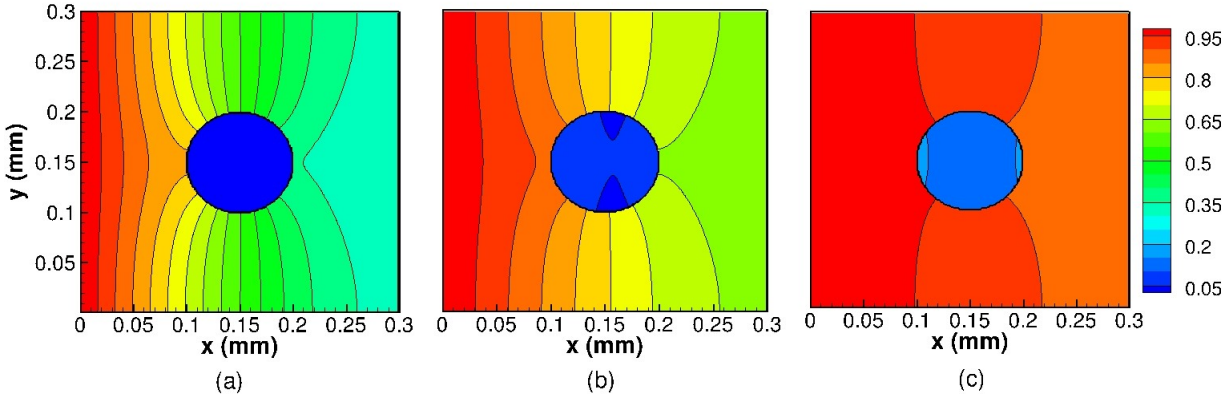

Figure 2.12: Contour plots of drug penetration at various times (a) $t = 250$ s, (b) $t = 500$ s and (c) $t = 1000$ s for $P = 0.1$ mm s^{-1} and $E = 40$ V mm^{-1}.

It can be seen from the Fig. 2.12 that the cellular drug uptake at the end ($t = 1000$ s) is almost equivalent to the cellular drug uptake for $E = 25$ V mm^{-1} and $P = 0.5$ mm s^{-1} (see Fig. 2.11). If we notice Fig. 2.11c and Fig. 2.12c), the amount of the final drug uptake is lie in the range (0.2 - 0.3 M) for both the cases. Therefore, those parameters, such as ($E = 20$ V mm^{-1}, $P = 0.5$ mm s^{-1}) and ($E = 40$ V mm^{-1}, $P = 0.1$ mm s^{-1}) can

be taken into consideration in clinical experiments for the treatment of a cancer cell by sufficient drug absorption.

2.4.7 Effects of number of pulses

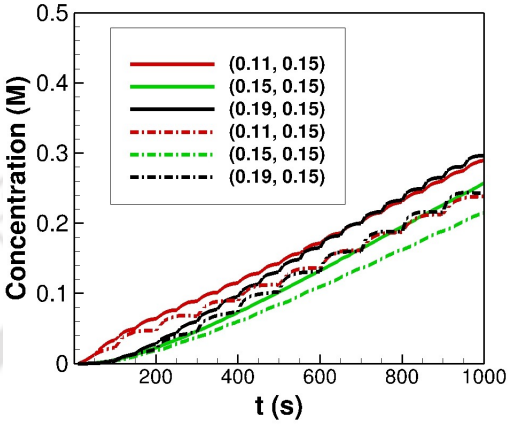

Figure 2.13: Effects of number of pulse shots on drug uptake ($E = 25$ V mm^{-1}, $P = 0.5$ mm s^{-1}). Solid lines '–' show for 50 s pulse gap while dashed lines '- -' represent 100 s pulse gap.

In order to study the effects of pulse shots on drug uptake, numerical experiments are performed in two ways; one, where a pulse is given after each 50 s while in other, a pulse is given after each 100 s. In the latter case, the time between two consecutive pulses is large, and consequently, for a given simulation time period the number of pulses is lesser. Concentration versus time on some intracellular points are plotted in Fig. 2.13. The drug concentration increases over time for the application of pulses (PN: 20 if pulse gap is 50 s and 10 if pulse gap is 100 s). However, drug uptake improves on increasing number of pulses. It is due to the resealing effects that will be pronounced if the time gap is more between two consecutive pulse shots.

2.4.8 Arrangement of electrodes

In order to understand the effects of arrangement of electrodes, the experiments are conducted by setting electrodes on the top and bottom of the cell. In this case, the higher pore density is obtained at the top and bottom of the cell, i.e., for $\theta = \frac{\pi}{2}$ and $\frac{3\pi}{2}$. Fig. 2.14 shows drug distributions for different drug permeability values. In the extracellular region, drug distribution patterns are the same as obtained in earlier cases. However, drug uptake happens from the top and bottom parts of the cell, where pore density is high owing to the particular arrangement of electrodes.

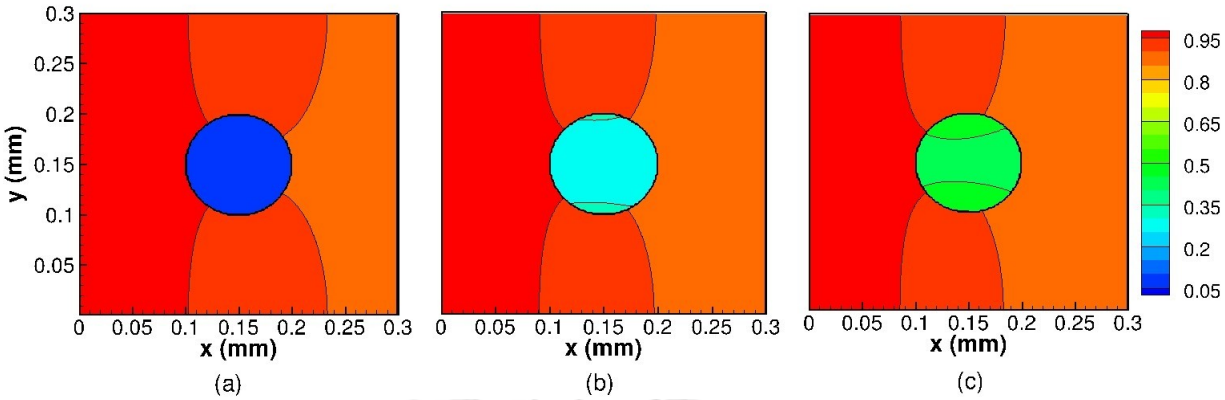

Figure 2.14: Drug distribution for the case where electrodes are placed at the top and bottom sides for (a) $P = 0.1$ mm s^{-1}, (b) $P = 0.5$ mm s^{-1} and (c) $P = 1$ mm s^{-1} ($E = 25$ V mm^{-1}).

2.5 Conclusions

In this chapter, drug transport in a single-cell model has been studied. The effects of electroporation on drug uptake into the single-cell is explored. The transport across the cell membrane is incorporated using the permeable interface method available in the literature. A better generalized model is analyzed in comparison to the literature studies where the models are limited to the spherical coordinates.

Numerical experiments are conducted with electric fields $E = 15$, 25 and 40 V mm^{-1} and for different drug permeabilities. The drug uptake into the cell is almost negligible on application of significantly low voltage ($E = 15$ V mm^{-1}) pulses. This is due to a fewer number of pores that have been generated with low voltage. As a result, the membrane does not get permeabilized enough. For $E = 40$ V mm^{-1}, a significant improvement in drug uptake is noticed. A stronger electric field is required to properly permeabilize the cell membrane, allowing a desired amount of drug to enter the cell. Based on the experiments with this model, it is learnt that the suitable electric field is 25 V mm^{-1} or more, and appropriate drugs whose permeability is at least 0.5 mm s^{-1} for injecting a desired quantity of drugs into the target cell. Thus, in real life practice, one may choose two different parameter values, such as ($E = 25$, $P = 0.5$) and ($E = 40$, $P = 0.1$) for delivering pharmaceutical compounds into the target zone.

The drug uptake is initiated as soon as a pulse is completed. The drug uptake increases if the pulse is applied repeatedly. Once it gets saturated with time due to the resealing effect, another shot of pulse is required to restore mass transport. Multiple pulses are needed to achieve a desired level of drug absorption into the cell. The maximum drug uptake occurs through the poles at $\theta = 0, \pi$ on setting electrodes on the left and right sides. The mass transfer rate increases with the increase in cell membrane permeability. Drug uptake is improved for high permeable drugs and by increasing number of pulses.

CHAPTER 3

DRUG DYNAMICS IN AN ELECTROPORATED TISSUE

In the previous chapter, we solve a model to study drug penetration into the target cell by single cell electroporation. In this chapter, we look into a tissue that contains several cells. The model focuses the transport of drugs into the whole targeted tissue at the macroscopic level.

3.1 Introduction

Mathematical models are gradually taking the center stage in the research arena of the drug delivery through electroporation. In macroscopic drug transport, Granot and Rubinsky [38] proposed a mathematical model of drug delivery in tissue cells with reversible electroporation. The authors used the model of single cell electroporation proposed by Krassowska and Filev [49] and described that the mass transfer rate in the cells is increased with pore creation due to electroporation. In a slightly different way, some current models [1, 9, 56] are developed to implement tissue electroporation for drug delivery. These models consider the effects of tissue conductivity to increase cellular permeability. Pore resealing process and the transient transport behavior of reversibly and irreversibly electroporated cells are also described in these models.

The present study deals with the mathematical modelling of tissue electroporation to introduce drug into the targeted cells. In this model, a uniform electric field is applied to electroporate the tissue; reversible as well as irreversible electroporation is considered, and membrane resealing effects are also taken into account. The principal purpose of this model is to have a detailed analysis of the drug transport through extracellular as well as intracellular region of the biological tissue. A time-variant mass transfer coefficient is considered to be dependent on membrane pore density as the increment of pores during electroporation enhances the drug transport into the cells. In this study, mass transfer

during electroporation and after the termination of electroporation are investigated. The physical phenomena are demonstrated through a system of coupled differential equations along with appropriate initial and boundary conditions. Based on the mathematical complexities, some of the equations are solved analytically, and rest are solved numerically. The numerical scheme is validated by comparing the numerical results with analytical solutions. The effects of various significant parameters, such as field strength, pulse duration and drug permeability on transport phenomena, are discussed. Sensitivity analysis of some important parameters that play significant roles in cellular drug uptake is performed with graphical representations. A comparative study of the proposed model with the existing ones [9, 38, 56] is also made in order to show the potency and authenticity of the advocated model.

3.2 Problem Formulation

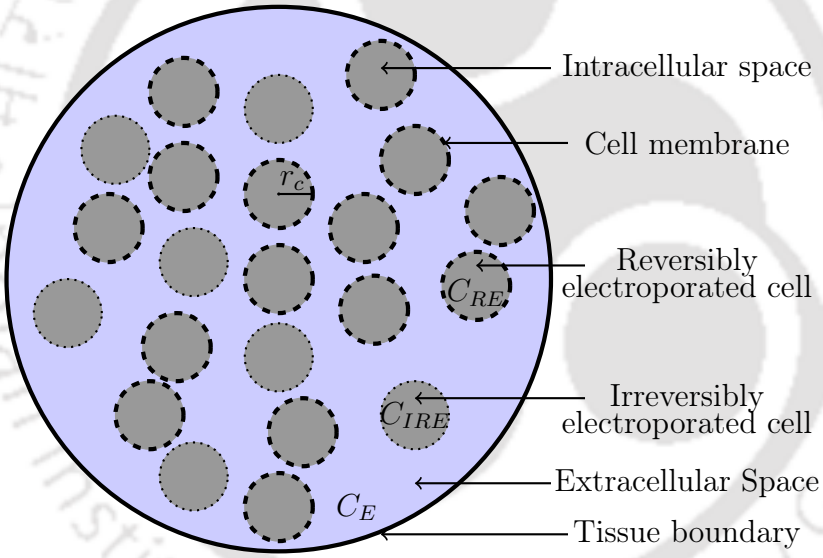

Figure 3.1: A schematic diagram of a biological tissue. Here, C_E: drug concentration in extracellular space; C_{RE}, C_{IRE}: drug concentrations in reversibly, irreversibly electroporated cells; r_c: cell radius.

In this work, a biological tissue is considered. The tissue is assumed to be spherical having radius R. From a macroscopic viewpoint, the tissue region may be categorically divided into two parts: extracellular space and intracellular space. The extracellular space is defined as the tissue region outside the cellular domain. The extracellular one is generally assumed to be outside the cell membrane, occupied by interstitial fluid and extracellular matrix. Intracellular space is a compartment within individual cell, separated from the extracellular space by cell membrane. The cell membranes control the mass transfer of molecules, proteins, drugs etc., between extracellular and intracellular domains.

The cell membrane contains millions of nanometre-sized pores through which drugs or some specific molecules may not be able to permeate. The complete structure of the biological tissue comprising of cells and porous cell membranes is schematically portrayed through Fig. 3.1.

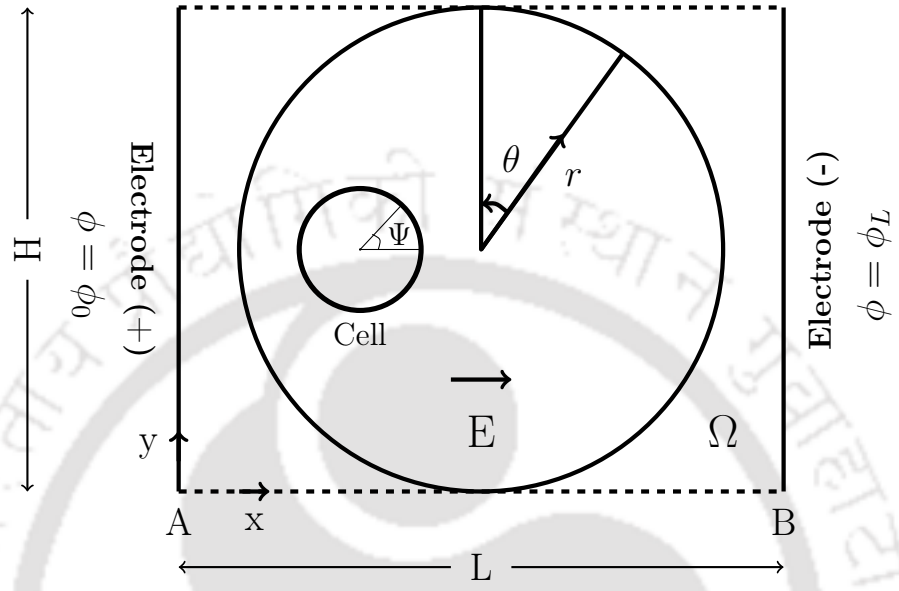

Figure 3.2: A schematic representation of bulk electroporation on a spherical tissue. Here L, H: length, width of the rectangular region Ω; ϕ_0, ϕ_L: electric potentials on the electrodes at A, B; E: induced electric field directed from left to right; r, θ: variables in spherical coordinates; ψ: angle between the direction of electric field and the normal to the cell membrane.

The fundamental aspect of tissue electroporation is that the cell membrane gets destabilized once electric pulses are applied [26, 49]. Generally, electric pulses are used in two different approaches. Either a single pulse is applied continuously over a stipulated time period, or multiple pulses are applied for a time (pulse period) with some time gap between two pulses [26,35]. During electroporation, cell membranes are permeabilized when the induced transmembrane potential exceeds its threshold value. In order to generate an electric field, two electrodes with different potential values ϕ_0, ϕ_L are placed at A and B respectively (as shown in Fig. 3.2). A large number of hydrophilic transient pores are formed due to electroporation so that the mass transport is expedited. In the present study, it is assumed that the pores are uniformly distributed in each cell surface, and the pore radius is considered to be constant for all cells embedded within the tissue. With the commencement of destabilization of the cell membrane, drug particles slowly move from the extracellular to the intracellular region. The number of pores per unit area on the cell surface increases in addition to the rise in the individual pore size, thus allowing enhanced drug uptake into the intracellular domain.

3.3 Model Development

The biological tissue is usually represented as a conductive medium. Electroporation leads to augmentation of medium conductivity [66, 77]. The potential distribution, due to electroporation pulse induction, is obtained from the solution of Laplace equation. In order to mathematically model the electric field allied with electroporation, the Laplace equation is used [9] as follows,

$$\vec{\nabla} \cdot (\sigma \vec{\nabla} \phi) = 0, \tag{3.1}$$

where ϕ is the electrical potential, σ represents the tissue electrical conductivity and it is considered as constant. The boundary conditions are defined as $\phi = \phi_0$ on the electrode at A ($x = 0$) and $\phi = \phi_L$ on the electrode at B ($x = L$) (as shown in Fig. 3.2). Measure of the electric field (E) is the magnitude of the gradient of the potential and is defined as $E = |\vec{\nabla}\phi|$.

The total number of pores (N_P) per cell surface (S) after the application of electric pulse is defined as

$$N_P(t) = \oint_S N(t)\, dS. \tag{3.2}$$

During electroporation, the pore density N in the cell membrane is evaluated by the equation, proposed in the model on single cell electroporation by Krassowka and Filev [49], which is as follows.

$$\frac{dN}{dt} = \alpha A \left[1 - \frac{N}{N_0} A^{-q}\right], \tag{3.3}$$

where $A = \exp\left[\left(\frac{V_m}{V_{ep}}\right)^2\right]$, t is the time, α is the pore creation rate coefficient, V_m is the transmembrane potential, V_{ep} is the characteristic voltage of electroporation, N_0 is the equilibrium pore density for the membrane area at $V_m = 0$ and q is an electroporation constant. The Eq. (3.3) is derived from the two facts: (i) the pore creation rate depends on transmembrane potential exponentially and it agrees well with the experimental findings [34], (ii) Eq. (3.3) is a stochastic description of pore creation and evolution, which is formulated from the Smoluchowki equation by Neu and Krassowska [61].

The transmembrane potential V_m, of a spherical cell in a uniform electrical field E was developed by DeBrurin and Krassowka [22] and is defined as,

$$V_m = 1.5E \times r_c \cos\Psi, \tag{3.4}$$

where r_c denotes the radius of the cell and Ψ is the angle between the direction of electric field and normal to the cell membrane at the position in which V_m is calculated.

In this model, the magnitude of the electric field is taken a value between 10 and 15

V mm^{-1}. Since, the transmembrane potential reaches its peak at the poles $\Psi = 0$ and π, the maximum number of pores are created at those particular poles. Moreover, the transmembrane potential is almost null at $\Psi = \frac{\pi}{2}$ and $\frac{3\pi}{2}$ and therefore, no new pores are formed at those locations. The total area of pores (A_P) in the cell surface is calculated by the product of number of pores per cell and individual pore area, and is represented mathematically as,

$$A_P = \pi R_P^2 \cdot N_P, \tag{3.5}$$

where R_P is the radius of a typical pore in the electroporated cell membrane. As already mentioned, Argus et al. [1] presented a mathematical model for tissue electroporation considering both reversible and irreversible electroporation. In their work, two different mass transfer coefficients were considered for reversibly and irreversibly electroporated cells in the mass transport equations. In the present study, a more generalized mass transfer coefficient, which is considered to be dependent on the total number of pores, is used. The mathematical formulation of the mass transfer coefficient (μ), which is applicable to both reversibly and irreversibly electroporated cells, is given as follows,

$$\mu(t) = \left(\frac{\pi R_P^2}{V_0}\right) \cdot N_P(t) \cdot P, \tag{3.6}$$

where V_0 is the volume of a cube that just contains a cell and P is the permeability of drug particles across the cell membrane.

In this investigation, the following two cases are studied:

3.3.1 Case 1: Mass transfer during ongoing electroporation

In the present case, it is assumed that the drug is injected prior to the initiation of the electroporation process. Furthermore, it is considered that a uniform electric field is applied continuously for a particular time duration so that the drug particles get transported into the intracellular compartment from the extracellular one, once the cell membrane starts destabilizing. The electric pulses are applied continuously on the tissue throughout the process of drug diffusion from the extracellular to intracellular domain. The electric pulses are halted on the completion of the drug diffusion phenomenon. Hence, no resealing effect is observed during this molecular diffusion since the time duration required for resealing effect is not achieved by the membrane pores of reversibly electroporated cells. Thus, the increased pore area obtained from the Eq. (3.5) remains constant with time. For the present case, the mass transfer coefficient is considered to be the same as given in the Eq. (3.6). The extracellular space can be thought of as the temporary reservoir of the drug, and the present investigation focuses on how the drug is being transported into the reversibly and irreversibly electroporated cells from the extracellular region when the

electroporation process is on. Accordingly, the drug dynamics, during ongoing electroporation, is manifested through the subsequent mathematical formulation [1] as,

$$\frac{\partial C_E}{\partial t} = \vec{\nabla}.\left(D\vec{\nabla}C_E\right) - \left(\frac{1-\varepsilon}{\varepsilon}\right)\mu(t) \times \left[SF\left(C_E - C_{RE}\right) + (1-SF)(C_E - C_{IRE})\right], \quad (3.7)$$

with initial condition: $C_E(r, \theta, 0) = C_0$,
where C_E is the drug concentration in the extracellular space, C_{RE} and C_{IRE} are the drug concentrations in the reversible and irreversible electroporated cells respectively, C_0 is the initial drug concentration in the extracellular domain, D is the effective diffusion coefficient of the drug in the extracellular space, ε is the porosity (i.e., the volumetric ratio between extracellular volume and total volume), and SF is the survival fraction of cells. In Eq (3.7), the left hand side represents the rate of change of drug concentration with time in extracellular space, the first term on the right hand side represents drug diffusion in the extracellular media and the second term (as reaction) represents the total amount of mass transfer at time t from extracellular into intracellular domain with mass transfer coefficient $\mu(t)$ [see Eq. (3.6)].

The governing equations for the drug dynamics in the reversibly and irreversibly electroporated cells can be written as,

$$\frac{\partial C_{RE}}{\partial t} = \mu(t) \cdot (C_E - C_{RE}), \quad (3.8)$$

$$\frac{\partial C_{IRE}}{\partial t} = \mu(t) \cdot (C_E - C_{IRE}), \quad (3.9)$$

with initial conditions:
$C_{RE}(r, \theta, 0) = 0$, $C_{IRE}(r, \theta, 0) = 0$.

Equations (3.8) and (3.9) obtained from the mass balance equation, represent the rate of drug uptake into the reversibly and irreversibly electroporated cells. Since, a uniform electric field is applied during electroporation, the whole tissue is electroporated uniformly. Mass transport from extracellular space into intracellular space occurs through molecular diffusion due to concentration gradient. Since, initially the concentrations in extracellular ($C_E = C_0$) and intracellular ($C_{RE} = 0$, $C_{IRE} = 0$) regions are different, mass transport continues to occur until the concentrations becomes equal (i.e., $C_E = C_{RE} = C_{IRE}$). The concentration variables may be considered as space independent due to uniform electroporation and homogeneous media. Hence, only temporal changes in drug concentrations are emphasized here. On considering $\nabla^2 C_E = 0$ and D as constant, the Eqs. (3.7) - (3.9) are simplified as,

$$\frac{dC_E}{dt} = -\left(\frac{1-\varepsilon}{\varepsilon}\right)\mu(t) \times \left[SF \cdot (C_E - C_{RE}) + (1-SF) \cdot (C_E - C_{IRE})\right], \quad (3.10)$$

$$\frac{dC_{RE}}{dt} = \mu(t) \cdot (C_E - C_{RE}), \tag{3.11}$$

$$\frac{dC_{IRE}}{dt} = \mu(t) \cdot (C_E - C_{IRE}), \tag{3.12}$$

subject to initial conditions:
$C_E(0) = C_0$, $C_{RE}(0) = C_{IRE}(0) = 0$.

3.3.2 Case 2: Mass transfer after the termination of electroporation

In this case, the drug is assumed to be injected into the biological tissue immediately after the electroporation process is stopped. Moreover, it is considered that continuous electroporation is actioned due to the application of a uniform electric field for a specific time span t_{ep}. Before the initiation of electroporation, there is no accumulation of the drug in the extracellular space, whereas drug transport into the intracellular compartment starts immediately after the end of the pulse period. At this juncture, as the reversibly electroporated cell membrane pores get adequate time to reseal, the pore area starts decreasing with time. Hence, the pore area can be mathematically illustrated through an exponentially decreasing function of time [38], which is as follows.

$$A_P = \pi R_P^2 \cdot N_P \cdot \exp\left(-\frac{t}{\tau}\right), \tag{3.13}$$

where τ is the resealing time constant.

In this case, we take $\mu(t_{ep}) = \left(\frac{\pi R_P^2}{V_0}\right) \cdot N_P(t_{ep}) \cdot P$, which represents the mass transfer coefficient and the Eqs. (3.10) - (3.12) are remodelled as Eqs (3.14) - (3.16) respectively,

$$\frac{dC_E}{dt} = -\left(\frac{1-\varepsilon}{\varepsilon}\right)\mu(t_{ep})\times \left[\exp\left(-\frac{t}{\tau}\right) \cdot SF \cdot (C_E - C_{RE}) + (1 - SF) \cdot (C_E - C_{IRE})\right], \tag{3.14}$$

$$\frac{dC_{RE}}{dt} = \mu(t_{ep}) \cdot \exp\left(-\frac{t}{\tau}\right) \cdot (C_E - C_{RE}), \tag{3.15}$$

$$\frac{dC_{IRE}}{dt} = \mu(t_{ep}) \cdot (C_E - C_{IRE}), \tag{3.16}$$

with initial conditions:
$C_E(0) = C_0$, $C_{RE}(0) = C_{IRE}(0) = 0$.

3.4 Methods of Solution

In this model, both analytical and numerical methods are applied to solve the governing equations wherever applicable. The Eq. (3.1) is solved analytically in the rectangular region Ω ($0 \leq x \leq L$, $0 \leq y \leq H$). It is observed from the geometry (Fig. 3.2) that ϕ is independent of y and $\frac{\partial \phi}{\partial y} = 0$. Equations (3.2) and (3.3) are also solved analytically considering $\Psi = 0$ or π. The coupled Eqs. (3.10) - (3.12) are solved analytically and also numerically using the finite difference method. A comparison between analytical and numerical results is conducted to ensure the accuracy of the numerical scheme. This validation is required as the same numerical scheme is used to solve the coupled Eqs. (3.14) - (3.16). For this purpose, Euler explicit method is used with a time step $\Delta t = 10^{-5}$ s. The parameter values used in the present work are provided in Table 3.1. Solutions are obtained for various parameter values, and computations are performed in a computer having an Intel-core i5 processor and 4GB RAM. Plots of numerical solutions are obtained with the help of Matlab R2019a.

Table 3.1: Parameter values used for simulation of the model.

Symbol	Value	Definition	Source
σ	0.241 S m^{-1}	Tissue electrical conductivity	[1]
r_c	25 μm	Cell radius	[56]
α	10^9 m^{-2} s^{-1}	Pore creation coefficient	[49]
V_{ep}	0.258 V	Characteristic voltage	[49]
N_0	1.5×10^9 m^{-2}	Equilibrium pore density	[49]
q	2.46	Electroporation constant	[38]
R_P	0.8 nm	Pore radius	[38]
ε	0.18	Porosity (volumetric ratio)	[1, 56]
P	5×10^{-3} mm s^{-1}	Permeability of drug	[38]
SF	0.8	Survival fraction of cells	[1]
τ	100 s	Resealing time constant	[1]
E	14 V mm^{-1}	Electrical field	
C_0	10^{-6} mol L^{-1} = 10^{-6} M	Initial drug concentration	
t_{ep}	20 s	Pulse length	
L	2.5 mm	Length of the rectangle	Fig. 3.2
H	2 mm	Width of the rectangle	Fig. 3.2
R	1 mm	Radius of the tissue	Fig. 3.2
ϕ_0	35 V	Potential at A	Fig. 3.2
ϕ_L	0 V	Potential at B	Fig. 3.2
f_p	1.4×10^{-5}	Pore surface fraction ratio	[56, 67]
d_m	5×10^{-9} m	Cell membrane thickness	[56]

3.4.1 Analytical solutions

We have solved the model completely by analytical method for the case 1 and the solutions are given below.

The potential function $\phi(x)$ is obtained from Eq. (3.1) with the specified boundary conditions as

$$\phi(x) = \frac{(\phi_L - \phi_0)}{L} x + \phi_0. \tag{3.17}$$

The uniform electric field in the whole region Ω is

$$E = \frac{(\phi_0 - \phi_L)}{L}. \tag{3.18}$$

Solving the Eq. (3.3) with initial condition $N(0) = 0$, the pore density $N(t)$ is

$$N(t) = N_0 A^q \left[1 - \exp\left(-\frac{\alpha t}{N_0 \cdot A^{q-1}}\right)\right]. \tag{3.19}$$

The total number of pores on a cell surface (S) is obtained from the Eq. (3.2) as

$$N_P(t) = 4\pi r_c^2 \cdot N(t). \tag{3.20}$$

Using Eqs. (3.11) and (3.12) in Eq. (3.10), it becomes

$$\frac{dC_E}{dt} = -\left(\frac{1-\varepsilon}{\varepsilon}\right) \times \left[SF \cdot \frac{dC_{RE}}{dt} + (1 - SF) \cdot \frac{dC_{IRE}}{dt}\right]. \tag{3.21}$$

Now, integrating the Eq. (3.21) and using the initial conditions, C_E can be expressed as,

$$C_E = C_0 - \left(\frac{1-\varepsilon}{\varepsilon}\right) \times \left[SF \cdot C_{RE} + (1 - SF) \cdot C_{IRE}\right]. \tag{3.22}$$

From Eqs. (3.11) and (3.12), we have

$$\frac{d}{dt}(C_{RE} - C_{IRE}) = -\mu(t) \cdot (C_{RE} - C_{IRE}). \tag{3.23}$$

Integrating the Eq. (3.23) and using the initial conditions, a relation between C_{RE} and C_{IRE} can be obtained as,

$$C_{RE} = C_{IRE}. \tag{3.24}$$

By substituting C_E from the Eq. (3.22) into the Eq. (3.11), we have

$$\frac{dC_{RE}}{dt} = \mu(t) \cdot \frac{C_0\varepsilon - C_{RE}}{\varepsilon}. \tag{3.25}$$

Substituting $\mu(t)$ into the above equation, we obtained C_{RE} and C_{IRE} as,

$$C_{IRE}(t) = C_{RE}(t) = C_0\varepsilon \times \left[1 - \exp\left(\frac{k_1}{k_2\varepsilon} \cdot \{1 - k_2 t - \exp(-k_2 t)\}\right)\right], \tag{3.26}$$

where $k_1 = \frac{\pi^2 R_P^2 N_0 P A^q}{2r_c}$ and $k_2 = \frac{\alpha}{N_0 A^{q-1}}$.
Finally, from the Eq. (3.22), C_E can be obtained as,

$$C_E(t) = C_0\left[\varepsilon + (1-\varepsilon) \times \exp\left(\frac{k_1}{k_2\varepsilon} \cdot \{1 - k_2 t - \exp(-k_2 t)\}\right)\right]. \tag{3.27}$$

3.5 Results and Discussion

The objective of the current study is to characterize the drug transport kinetics in biological tissues. This characterization is done through qualitative analysis that can be visualized from Figs. 3.3 - 3.17. The detailed qualitative analysis through the graphical representations reveal the underlying physical and physiological phenomena. Arbitrary choice of parameter values may not lead to the projected objectives of the present study. Hence, extensive literature is consulted, and model parameter values are obtained from the relevant literature and presented in Table 1. In this section, a detailed discussion on the effects of various model parameters, like drug permeability (P), electric field (E) and pulse duration (t_{ep}) is made. Since the drug concentrations in different regions are space independent, the graphs (Figs. 3.5 - 3.17) are plotted for a typical location.

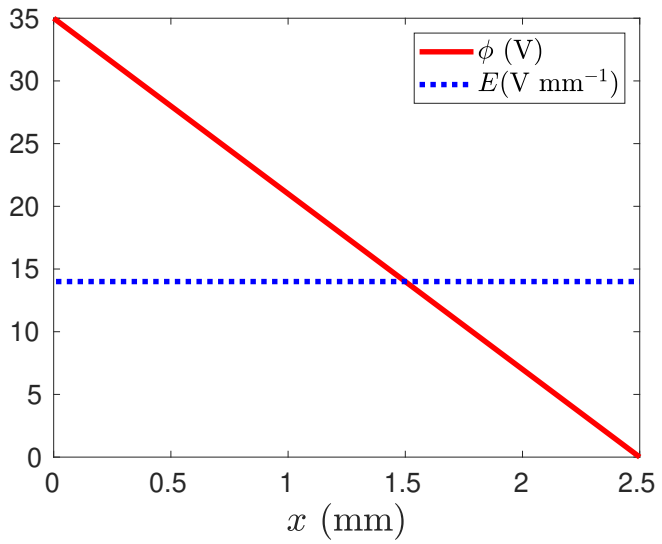

Figure 3.3: Spatial distribution of electrical potential and electric field for $\phi_0 = 35\ V$, $\phi_L = 0\ V$ and $L = 2.5$ mm.

Fig. 3.3 represents the space variant potential (ϕ) distribution as a result of induced

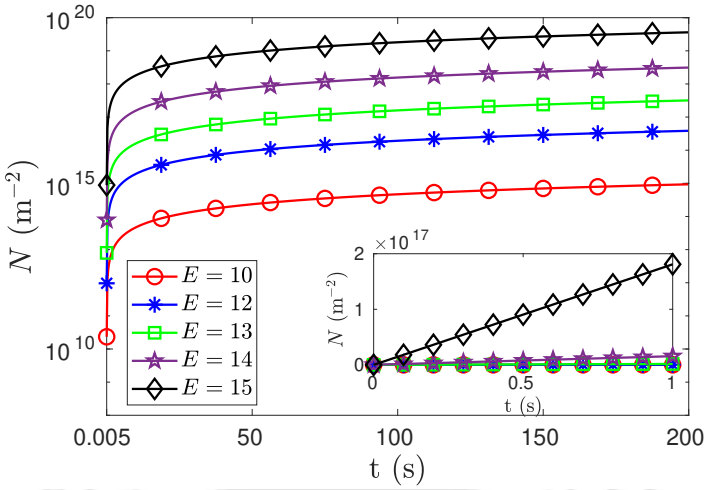

Figure 3.4: The change of pore density N (m^{-2}) with time t for different electrical fields E (V mm^{-1}). This is a semilog plot for better understanding of the changes of N. The normal plot is shown in the inset for initial 1 s.

electric field. It gives an overview about how the potential and electric fields are distributed throughout the tissue area. It shows that ϕ changes linearly with x, whereas the electric field E does not change with x.

Fig. 3.4 shows the semilog plot for N against t to accommodate the wide range of variations in N. As initially ($t = 0$), the pore density is zero ($N = 0$), so $\log N$ is not defined at the initial time. In order to avoid this, we have plotted from $t = 0.005$ instead of $t = 0$. However, to verify the initial condition, we have shown the actual plots for the initial time, in the inset. This figure depicts the time variant pore density (N) change with the application of different electric fields. It may be observed from the figure that with the increasing electric field, the pore density increases. This is a very usual phenomena as the electroporation itself is dependent on the above mentioned electrical parameters.

3.5.1 Validation of the results

In order to validate the numerical scheme of this model, a comparison between numerical and analytical solutions of drug concentrations in extracellular and intracellular regions is done as shown in the Fig. 3.5. From the figure, it is seen that both the profiles of analytical and numerical results agree perfectly for each of the cases of C_E and C_{RE}. This computational scheme is used to solve the Eqs. (3.14) - (3.16).

3.5.2 Mass transfer during electroporation

In this section, it is considered that the drug is transported from the extracellular space into the intracellular space when the electroporation process is under way. It may be kept

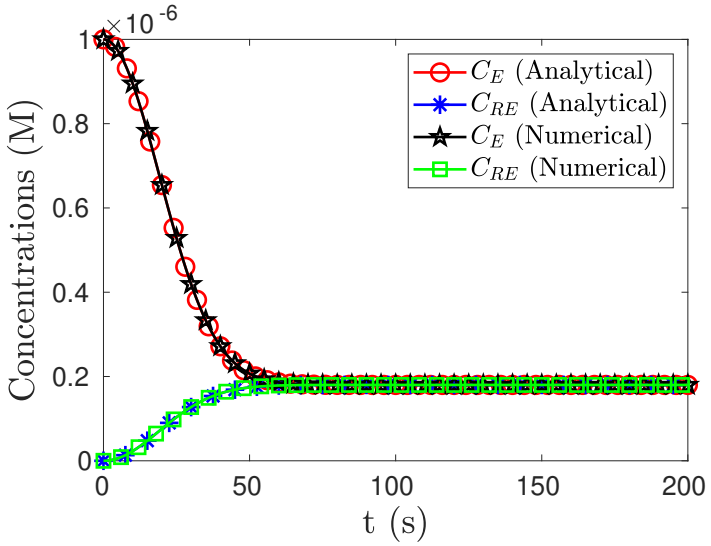

Figure 3.5: A comparison between the analytical and numerical results of drug concentrations C_E and C_{RE} (or C_{IRE}) for the case 1 (Mass transfer during ongoing electroporation) is shown. Here, analytical results corresponding to the Eqs. (3.26), (3.27) and numerical results of the Eqs. (3.10) - (3.12) for $P = 0.0005$ mm s^{-1}, $E = 14$ V mm^{-1} are plotted.

in mind that the resealing effect is not significant in this phase, as discussed earlier.

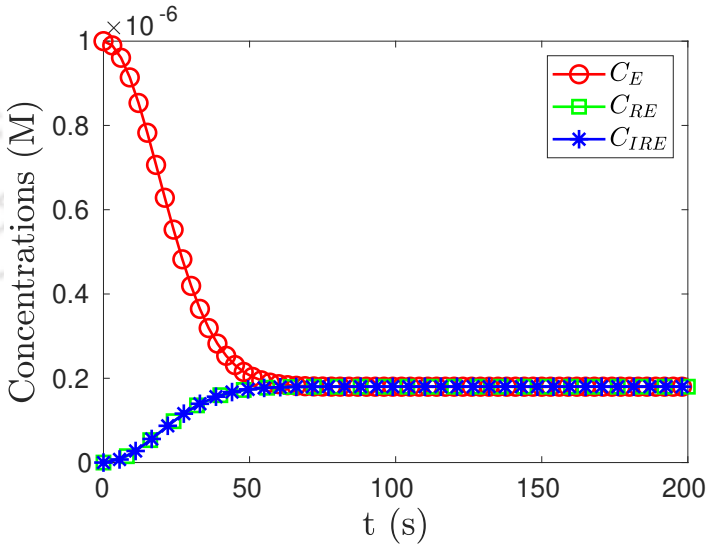

Figure 3.6: Time variant drug concentration profiles of C_E, C_{RE} and C_{IRE} for $P = 0.0005$ mm s^{-1} and $E = 14$ V mm^{-1}.

Fig. 3.6 represents the time variant concentration profiles of drug concentrations in extracellular space, reversibly and irreversibly electroporated cells, respectively. In the present scenario, electroporation and resultant mass transfer, i.e., drug transport in particular, take place simultaneously and there is no time for resealing effect. These events can be clearly visualized from Fig. 3.6. As the drug has its maximum concentration in the

extracellular space, concentration declines from its peak value once the drug starts entering into the intracellular space. On the other hand, the drug concentrations in reversibly and irreversibly electroporated cells increase from their initial zero concentrations due to drug uptake. Moreover, due to insignificant resealing effect, the reversibly and irreversibly electroporated cells behave similarly, and hence their corresponding contours overlap, which is evident from the figure itself. In the mathematical formulation, the physiological processes starting form electroporation upto drug uptake by the cells are considered. As no drug clearance or drug degradation is modeled, the residual drug accumulates in the extracellular space due to the absence of drug clearance. The maximum limit of drug uptake is attained by the cells before drug degradation, or drug clearance starts.

Effects of drug permeability on drug concentrations

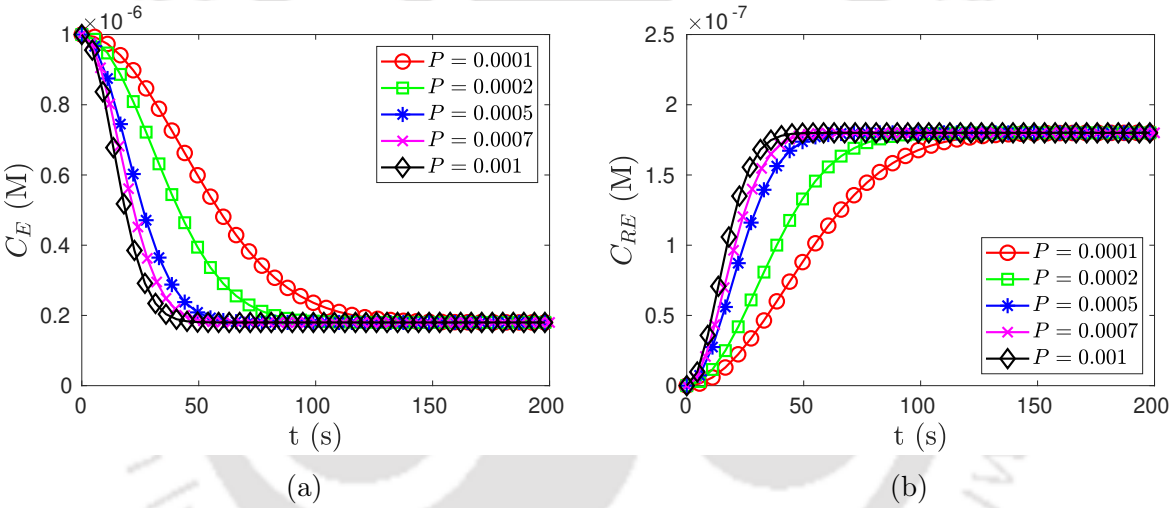

Figure 3.7: Time variant drug concentration profiles of (a) C_E and (b) C_{RE} (or C_{IRE}) for different P (mm s^{-1}) and $E = 14$ V mm^{-1}. The drug concentrations (C_{RE}, C_{IRE}) are exactly same as there is no resealing effect.

Fig. 3.7 illustrates the time variant drug concentration profiles in the extracellular space (Fig. 3.7a) and reversibly (or irreversibly) electroporated cells (Fig. 3.7b) for different drug permeability. The mass transfer coefficient is directly proportional to the drug permeability (see Eq. 3.10), hence increment in P leads to increment in μ which results in faster decline of drug concentration in the extracellular space from its peak value. On the other hand, in Fig. 3.7b, the contours for increased permeability attain their respective peaks in a shorter time duration in comparison with other contours of reduced permeability. After a certain time (approximately 120 s), the contours with different permeability get merged with each other because a saturation condition is attained by the cells where drug uptake reaches its maximum limit.

Effects of electric field on drug concentrations

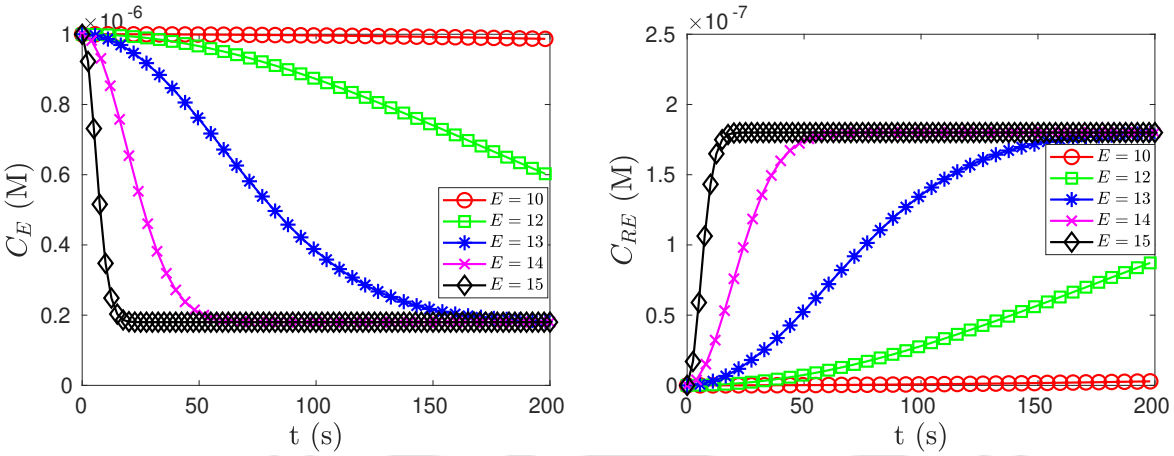

Figure 3.8: Time variant drug concentration profiles of (a) C_E and (b) C_{RE} (or C_{IRE}) for different E (V mm^{-1}) and $P = 0.0005$ mm s^{-1}. The drug concentrations (C_{RE}, C_{IRE}) are analogous to each other as there is no resealing effect and same mass transfer rate in reversibly and irreversibly electroporated cells.

Fig. 3.8 presents the time variant drug concentration profiles in the extracellular region (Fig. 3.8a) and reversibly (or irreversibly) electroporated cells (Fig. 3.8b) for different magnitudes of the electrical field (E). For a low electric field $E = 10$ V mm^{-1}, it is clearly observed from Fig. 3.8a that the drug concentration (C_E) remains unaltered with time. But with the increase in strength of the electric field, the concentration profiles gradually decline from their maximum values. Initiation of drug uptake into the intracellular region depends on μ. And μ depends on the number of pores N_P along with pore radius R_P (see Eq. (3.6)). For a low electric field ($E \leq 10$ V mm^{-1}), N_P is very small so as μ. The drug uptake is almost zero for $E \leq 10$ V mm^{-1} and it gets initiated when $E > 10$ V mm^{-1}. So, it is observed that electric field $E > 10$ V mm^{-1} is necessary for the initiation of cell destabilization. Hence, it is calculated in this study that a threshold value ($E > 10$ V mm^{-1}) of the electric field is needed to initiate drug uptake into the cells. However, this threshold value may depends on types of drug particles and diseased sites. As time elapses, C_E profiles for higher electric fields decline faster before being merged in comparison with that for lower electric fields. This happens as new pores are formed after the commencement of electroporation. The pore radii are widened with ascending electric field values to allow more drug particles to permeate through the cell membranes. Since, the pore density increases with the electrical field, the contours for higher electrical field attain their zenith rapidly due to the faster drug uptake in the cells (Fig. 3.8b).

3.5.3 Mass transfer after the termination of electroporation

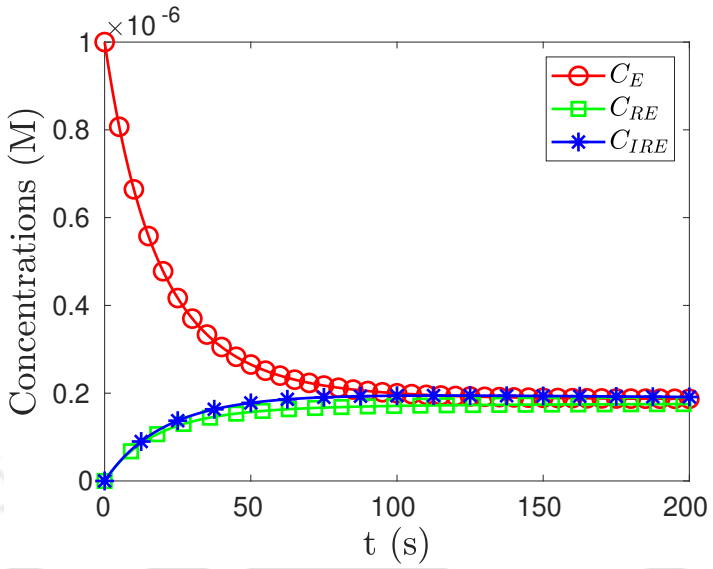

Figure 3.9: Time variant drug concentration profiles of C_E, C_{RE} and C_{IRE} for $P = 0.0005$ mm s^{-1}, E=14 V mm^{-1} and $t_{ep} = 20$ s.

In this section, it is assumed that mass transfer in the form of drug transport initiates immediately after the completion of the electroporation process. The following graphical portrayals represent various facets of the underlying phenomena when the particular condition mentioned in the Section 3.3.2 is taken into consideration.

In the case of post electroporation drug transport, Fig. 3.9 represents the time variant drug concentration profiles in the extracellular space, reversibly and irreversibly electroporated cells. From the figure, it may be observed that the C_E plots gradually decline due to drug diffusion into the intracellular region, whereas the drug concentrations C_{RE} and C_{IRE} increase slowly with time due to drug uptake in the cells. Unlike Fig. 3.6, it can be visualized in Fig. 3.9 that the drug concentration in reversibly electroporated cells is less than the drug concentration in irreversibly electroporated cells. This type of trend could be due to the pore resealing effect that reduces the drug uptake in reversibly electroporated cells after a specific time.

Effects of drug permeability on drug concentrations

Fig. 3.10 demonstrates the time-dependent drug concentration profiles in the extracellular space, reversibly and irreversibly electroporated cells, for different values of drug permeability. Fig. 3.10a shows that the concentration graphs for lower permeability take a prolonged time to decay compared to that with higher permeability because increased drug permeability increases the cellular drug uptake. Fig. 3.10b shows that with the increase in drug permeability, the drug uptake consistently enhances. However, one point is

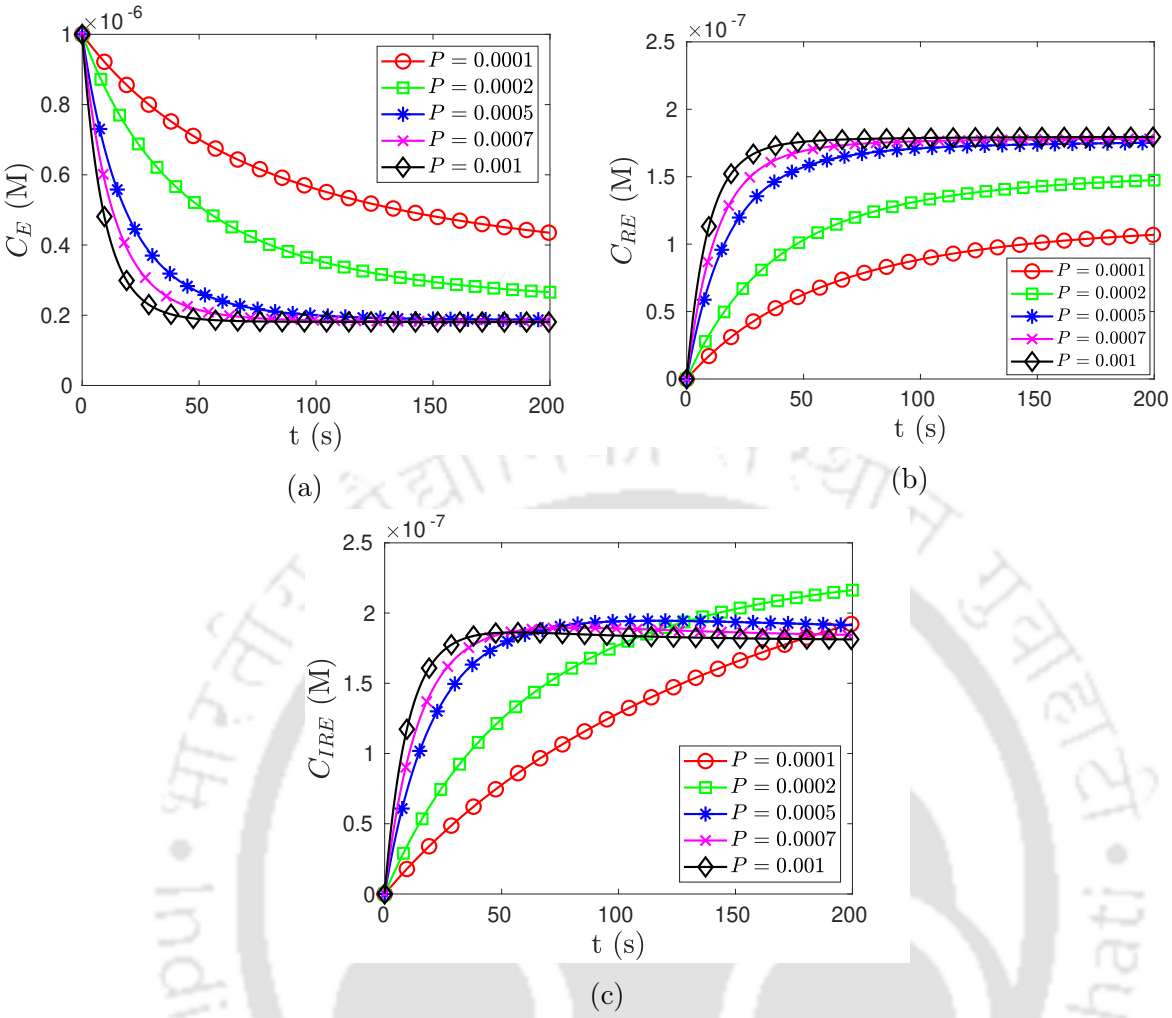

Figure 3.10: Time variant drug concentration profiles of (a) C_E, (b) C_{RE} and (c) C_{IRE} for different P (mm s^{-1}), E=14 V mm^{-1} and $t_{ep} = 20$ s.

noticed in the Fig. 3.10c that prior to a particular time, the C_{IRE} profiles behave similarly to that of C_{RE}. After the specific time, the graphs for lower drug permeability increase more than the maximum limit attained by the graphs of higher drug permeability. This is due to the fact that the initiation of resealing effect restricts the drug uptake by reversibly electroporated cells, and as a result, the surplus drug particles enter into the irreversibly electroporated cells.

Effects of electric field on drug concentrations

Fig. 3.11 shows the effects of electrical field in drug concentrations for the case of post pulse drug delivery. Fig. 3.11a is analogous to Fig. 3.8a, hence detailed discussion is omitted for the sake of brevity. In Fig. 3.11b, it seen that the drug uptake by reversibly electroporated cells increases with higher value of electric field. This increment is seen only when the applied electric field is higher than a specific threshold value, otherwise

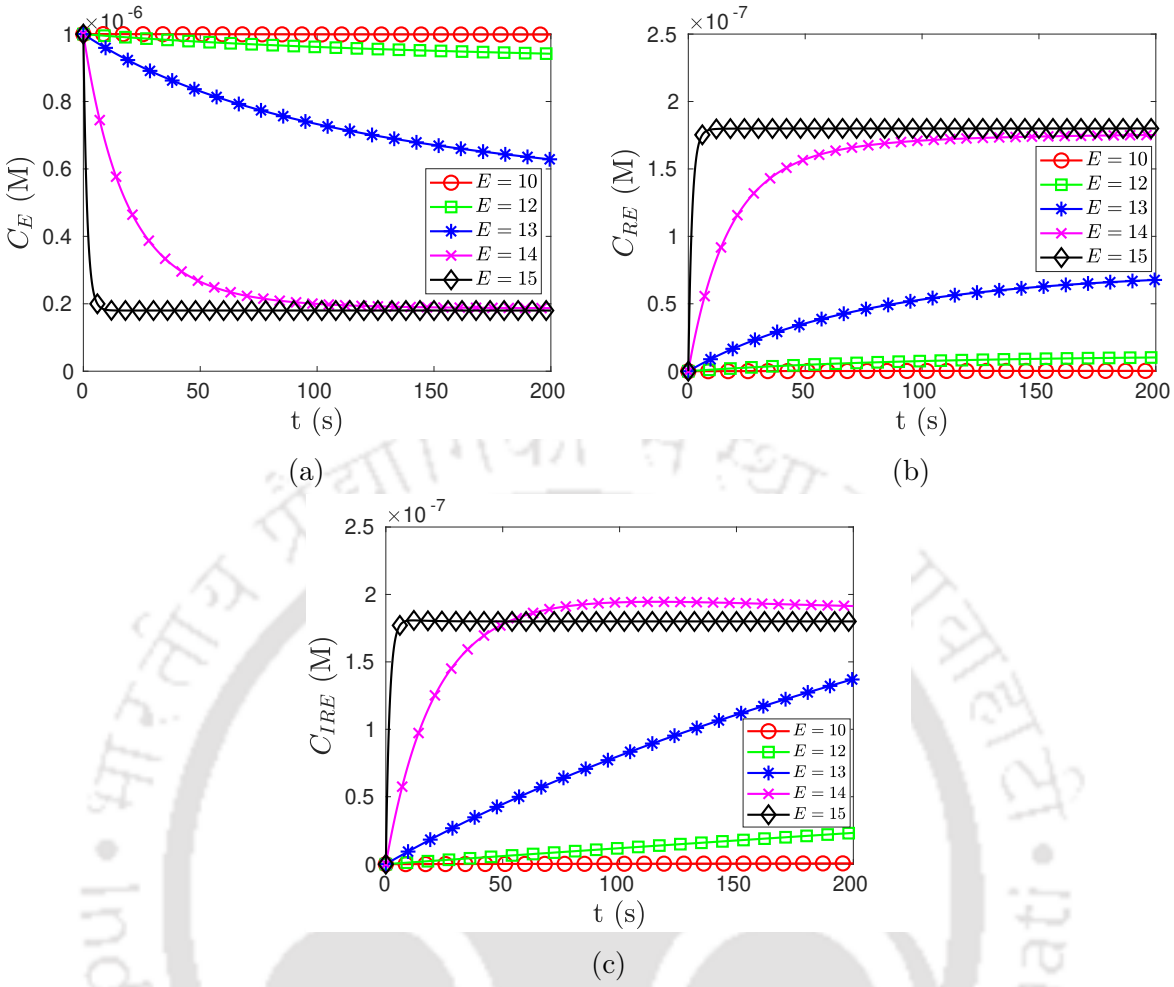

Figure 3.11: Time variant drug concentration profiles of (a) C_E, (b) C_{RE} and (c) C_{IRE} for different E (V mm^{-1}), $P = 0.0005$ mm s^{-1} and $t_{ep} = 20$ s.

electroporation will not be initiated. It can be noticed in Fig. 3.11c that the drug uptake in irreversibly electroporated cells is higher for $E = 14$ V mm^{-1} than that for $E = 15$ V mm^{-1}. This is because surplus drug particles enter the irreversibly electroporated cells as drug uptake by reversibly electroporated cells is less for $E = 14$ V mm^{-1} due to the resealing effect.

Effects of pulse length on drug concentrations

Fig. 3.12 presents the temporal changes of drug concentrations in the extracellular space, reversibly and irreversibly electroporated cells, for different time duration of electroporation. Fig. 3.12a shows that if the time duration increases, the drug uptake gets higher and hence respective concentration C_E declines faster. In both Figs. 3.12b and 3.12c, it is observed that if the time span of electroporation is longer, the drug uptake gets higher. This is due to the fact that the application of a long-time electric pulse creates a large number of pores, and hence permeability of the cell membrane gets increased. It may be

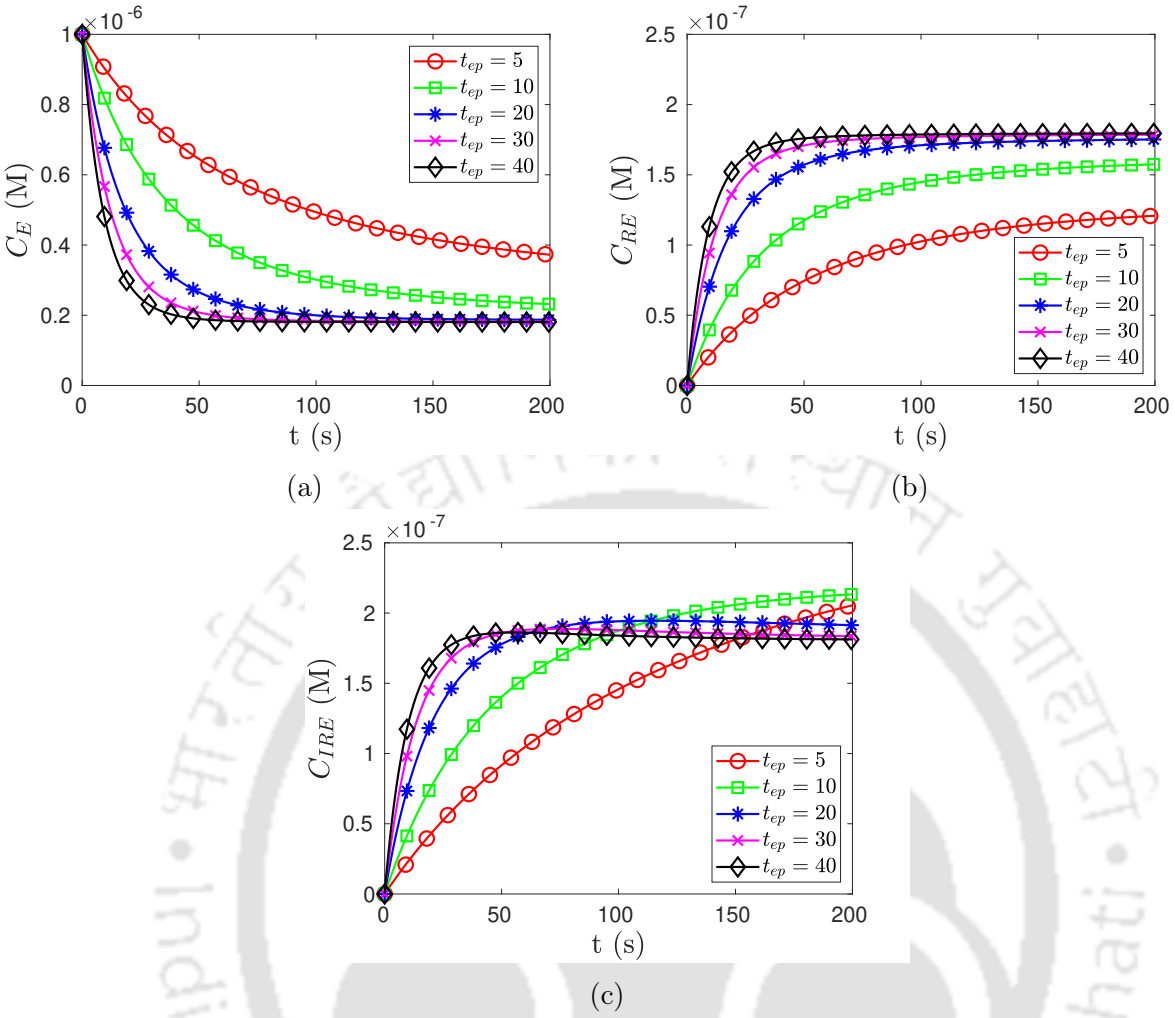

Figure 3.12: Time variant drug concentration profiles of (a) C_E, (b) C_{RE} and (c) C_{IRE} for different t_{ep} (s), $P = 0.0005$ mm s^{-1} and $E = 14$ V mm^{-1}. Here, electroporation is performed for different time duration before the commencement of drug transfer.

observed from Fig. 3.12c that maximum values of the concentration C_{IRE} for the cases $t_{ep} = 5$ s and $t_{ep} = 10$ s are more than that of other cases. The reasons are: these pulse periods are so small that resealing effect starts early enough for the reversibly electroporated cells to engulf the surplus drug particles from the extracellular space; a shorter electric pulse leads to a lesser number of pores formation so that the relative resealing effect will have more impact; the resealing effect has changed the mass transfer rate of reversibly electroporated cells but not of irreversibly electroporated cells.

3.5.4 Comparison

A comparative study is conducted between the results of the present model having variable mass transfer coefficient (case 1, case 2). Besides, an additional case (case 3) is considered in which a mass transfer coefficient, $\mu = \frac{3D \times f_p}{d_m \times r_c}$ is taken from the dual-porosity model of

Kalamiza et al. [56] and is substituted in the Eqs. (3.14) - (3.16) of our model. In the model of [56], the mass transfer coefficient is formulated using pore surface fraction ratio (f_p), which is well described in the literature [67]. Based on that mass transfer coefficient, the corresponding drug concentrations are calculated and represented graphically as case 3 in Fig. 3.13. The figure represents time variant drug concentration profiles of C_E and C_{RE} for both the cases in the present study along with the case 3 where $\mu = 0.0168$ s^{-1} (for particular value of f_p [67]). In case 3, a steady decline in C_E (Fig. 3.13a) and a steady increase in C_{RE} (Fig. 3.13b) are noticed as the constant mass transfer coefficient in case 3 is greater than the mass transfer coefficients in cases 1 and 2. In case 1, where electroporation is under way, C_E declines slowly from its maximum concentration in comparison with that of case 2, where the electroporation process is terminated. The reason is that in case 1, new pores are being formed with time during drug transport, and in case 2, the maximum number of pores are already created before drug transport. It is

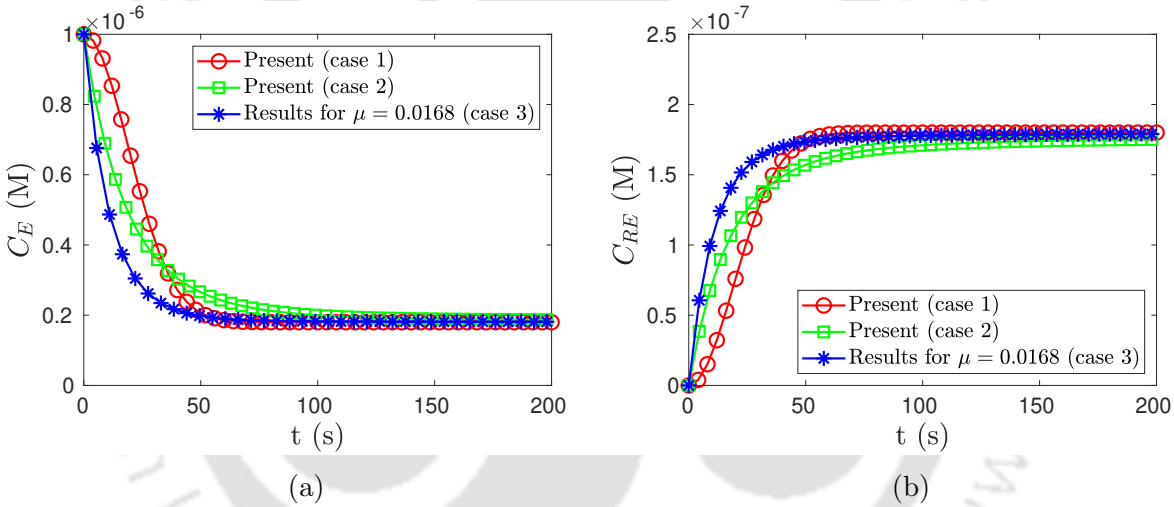

Figure 3.13: A comparison of drug concentration profiles of (a) C_E and (b) C_{RE} for various cases. Here, in case 1 (present), Eqs. (3.10) - (3.12) are solved with $P = 0.0005$ mm s^{-1} and $E = 14$ V mm^{-1}; in case 2 (present), Eqs. (3.14) - (3.16) are solved with $P = 0.0005$ mm s^{-1}, $E = 14$ V mm^{-1} and $t_{ep} = 20$ s; in case 3, Eqs. (3.14) - (3.16) are solved taking mass transfer coefficient ($\mu = 0.0168$ s^{-1}) from the model of Kalamiza et al. [56] with $P = 0.0005$ mm s^{-1}, $E = 14$ V mm^{-1} and $t_{ep} = 20$ s.

observed in Fig. 3.13b that due to continuous increment in membrane pore density, the resultant drug uptake in case 1 overtakes the drug uptake in case 2. Fig. 3.13 reveals an important observation that whatever process (case 1 or case 2) is followed to administer the drug in the intracellular domain, the resultant drug uptake is similar. Experimental research on tissue electroporation with respect to the geometry considered in this study is not available. Hence, there is little scope to validate our theoretical results with those of experimental ones. However, the graphical representations provided here are analogous to those present in the works of Granot and Rubinsky [38], Kalamiza et al. [56] and Boyd

and Becker [9]. This depicts the authenticity of our model.

3.5.5 Sensitivity analysis

In this section, a sensitivity analysis of drug concentrations (C_E, C_{RE}, C_{RE}) with respect to the parameters, such as permeability of drug (P), electric field (E), 'pulse length (t_{ep})' and 'characteristic voltage for electroporation (V_{ep})' is performed and the graphical representation is shown in Figs. 3.14 - Fig. 3.17. This analysis evaluates the sensitivity of the parameters P, E, V_{ep} for case 1 (mass transport during electroporation) and t_{ep} for case 2 (mass transport after termination of electroporation).

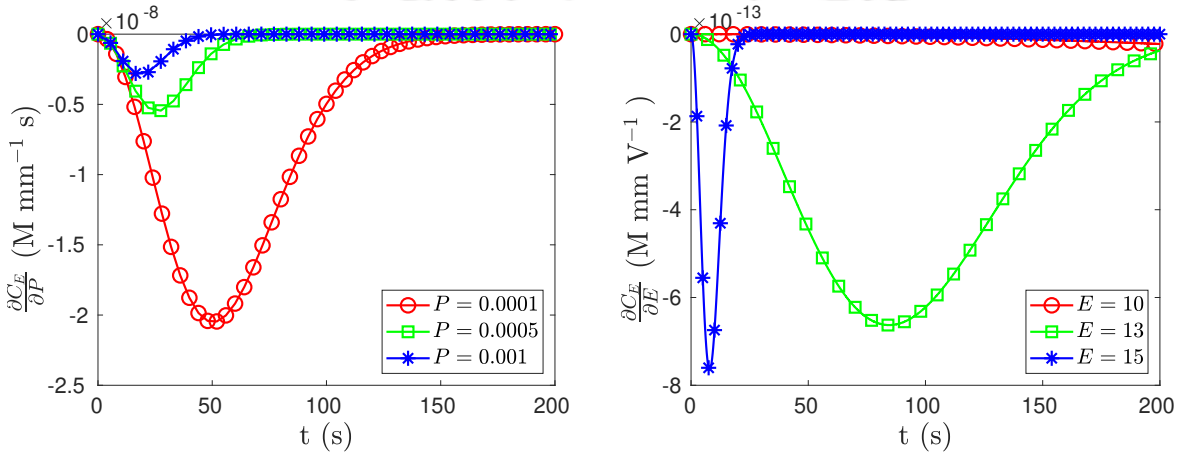

Figure 3.14: Sensitivity of C_E to the parameters (a) P (mm s^{-1}) and (b) E (V mm^{-1}). From the Eq. (3.27), $\frac{\partial C_E}{\partial P}$ at different P and $\frac{\partial C_E}{\partial E}$ at different E are computed and plotted against time.

Fig. 3.14 shows the sensitivity of the drug concentration C_E to the parameters P and E. From Fig. 3.14a, it is observed that deviation in the curve becomes larger with smaller permeability and the deviation approaches to zero near time t = 150 s. Also, deviations in the curves for higher values of permeability are relatively less. It is clear from Fig. 3.14b that the deviation of the E - variant curve for $E = 10$ V mm^{-1} is almost zero over the entire time. Deviation in the curve for $\frac{\partial C_E}{\partial E}$ increases with the increase in E. In Fig. 3.14, one may notice that the rate of change in the concentration (C_E) with respect to both the parameters is negative due to continuous decrease in mass in the extracellular region.

Fig. 3.15 represents the sensitivity of the drug concentration C_{RE} to the parameters P and E. In Fig. 3.15a, the deviation of the curve for smaller permeability is larger than the curves for higher permeabilities. In Fig. 3.15, it is observed that the rate of change in the concentration (C_{RE}) with respect to both the parameters are positive due to continuous mass uptake in both the intracellular regions. The sensitivity of the drug

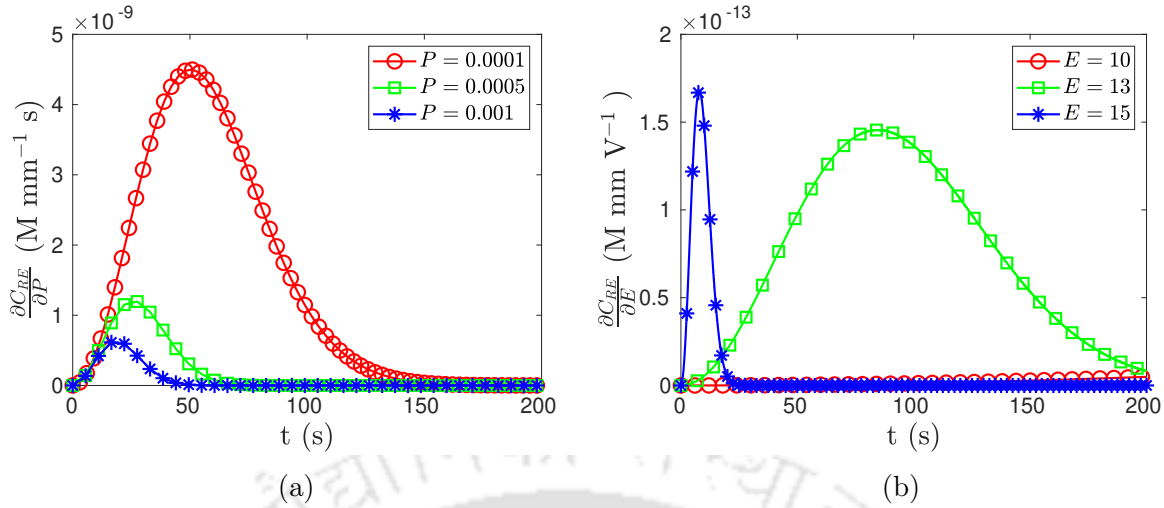

Figure 3.15: Sensitivity of C_{RE} to the parameters (a) P (mm s^{-1}) and (b) E (V mm^{-1}). From the Eq. (3.26), $\frac{\partial C_{RE}}{\partial P}$ at different P and $\frac{\partial C_{RE}}{\partial E}$ at different E are computed and plotted against time.

concentration C_{IRE} is similar to that of C_{RE}. From the above discussion, it is concluded that the drug concentrations (C_E, C_{RE}, C_{IRE}) are more sensitive to P than that to E.

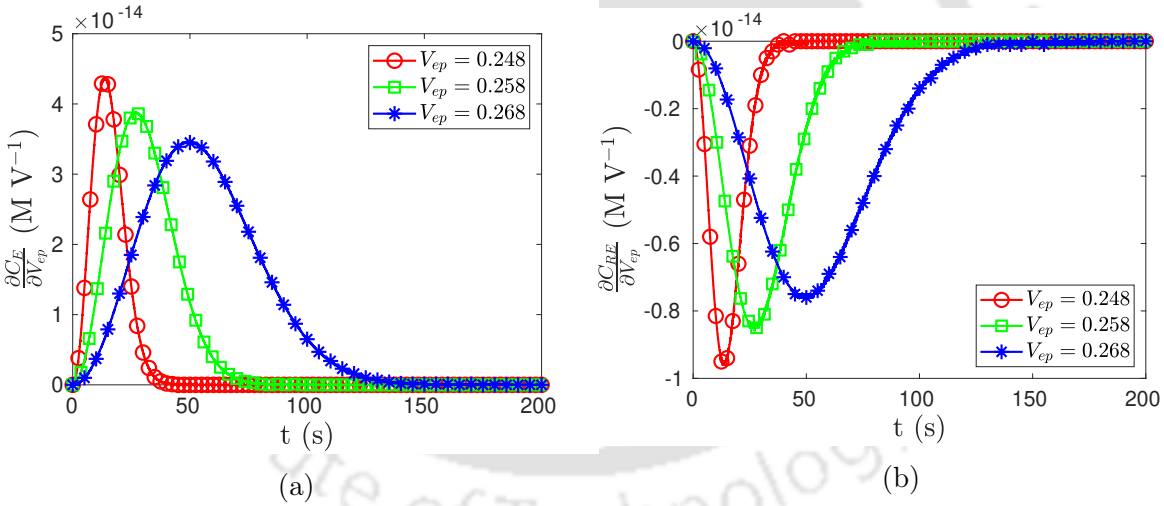

Figure 3.16: Sensitivity of (a) C_E and (b) C_{RE} to the parameter V_{ep} (V).

A sensitivity analysis of drug concentrations (C_E, C_{RE}) to the parameter 'characteristic voltage for electroporation (V_{ep})' is performed and the graphical representation is shown in Fig. 3.16. In both the figure, the variation decreases with the increase of V_{ep} and the maximum variation occurs at around t = 20 s for $V_{ep} = 0.248$ V. The reason is that the MTC that depends on the term $A = \exp\left[\left(\frac{V_m}{V_{ep}}\right)^2\right]$ decreases with V_{ep}.

Fig. 3.17 represent the local sensitivity of C_E and C_{RE} for different values of the parameter 'pulse length (t_{ep})'. It is observed from both the figures that the deviation in

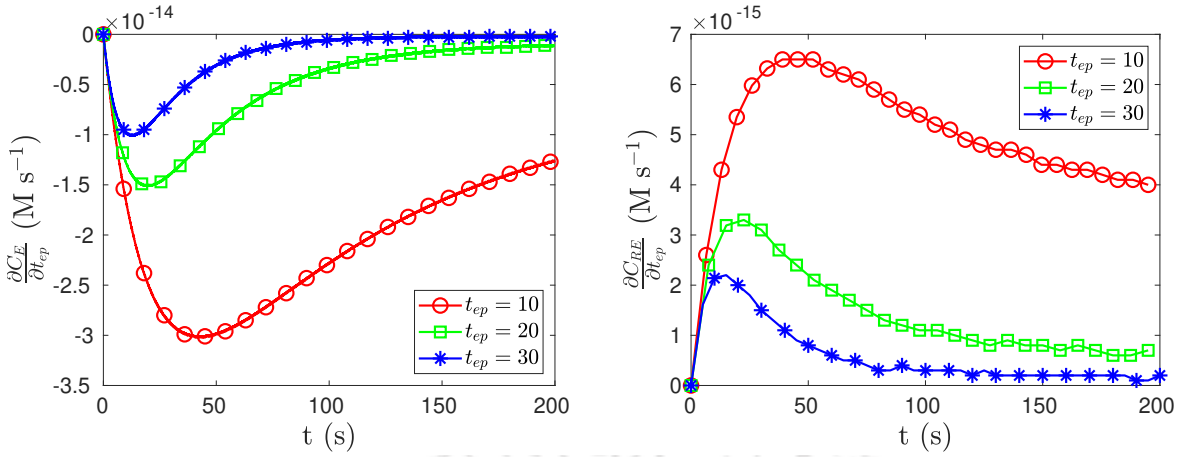

(a) (b)

Figure 3.17: Sensitivity of (a) C_E and (b) C_{RE} to the parameter t_{ep} (s).

the curve for shorter pulse ($t_{ep} = 10$ s) is higher than that for longer pulses ($t_{ep} = 20, 30$ s). The reason for this is that the MTC increases as t_{ep} increases. The trends of the curves in the Fig. 3.17a are reverse to that in the Fig. 3.17b due to continuous decrease of mass in the extracellular space and continuous increase of mass in reversibly electroporated cells.

It is concluded from the above sensitivity analysis that the drug concentrations are most sensitive to the drug permeability (P) and least sensitive to characteristic voltage for electroporation (V_{ep}) compared to other parameters.

3.6 Conclusions

The following observations can be inferred from the outcomes of the present study:

- The propounded model is more realistic as vital physical phenomenon i.e., the possibility of transport of drug during electroporation is incorporated.
- Two types of electroporation approaches to drug delivery, like drug delivery during ongoing electroporation and drug delivery just after the termination of electroporation, are simultaneously investigated. It is found that both the approaches give similar results in drug administration to the cells.
- The mass transfer coefficient generally depends on the pore density. The pore density is a function of time during electroporation. In this model, a time-dependent mass transfer coefficient is studied for the first time (to the best of our knowledge).
- The threshold value of the electric field ($E > 10$ V mm^{-1}) to initiate drug uptake in the intracellular regions is the novel outcome of the study.

- Through the sensitivity analysis, it is observed that the drug concentrations (C_E, C_{RE}, C_{IRE}) are most sensitive to P and least sensitive to V_{ep}.
- The authenticity of the advocated mathematical model is verified through a comparative study.

CHAPTER 4

REVERSIBLE TISSUE ELECTROPORATION AND THERMAL EFFECTS IN DRUG DELIVERY

In chapter 3, we have proposed a mathematical model of tissue electroporation for transporting drugs into cells. The model considers reversible and irreversible electroporation with uniform electric fields and pores resealing. The delivery of drugs during and after electroporation are depicted separately. It is considered that the initial drug source is in the extracellular space throughout the tissue. In the current chapter, we have considered the initial drug source at one of the tissue boundaries in the model. Thermal effects due to electroporation is also discussed.

4.1 Introduction

In the area of electroporation based drug delivery, Granot and Rubinsky [38] proposed a mass transfer model in 2008 to deliver drug into the cells with reversible electroporation. In their study, the pore creation model [49] is used and how the rate of mass transfer to the cells increases with pore density is described. In 2014, Kalamiza et al. [56] established a dual-porosity model focusing on solute diffusion in the biological tissue after electroporation. This is probably the first study that built a relationship between the increment of resultant permeability and the macroscopic drug transport into the cells. The mass transfer coefficient (MTC) that depends on the increased membrane permeability due to the formation of electropores was proposed in the model. The effects of irreversible electroporation is not taken into account. Later in 2016, Boyd and Becker [9] used the previous model to drug delivery using tissue electroporation. In their study, mass transport equations for extracellular and intracellular spaces are provided separately. Pore resealing effects on drug uptake is also studied. Argus et al. [1] modified the last model in 2017 by considering irreversible electroporation into account. The study represents

a three-equation mass transport model to calculate drug concentrations in extracellular space, reversibly and irreversibly electroporated cells.

Only temporal changes of drug concentrations are emphasized but spatial changes of drug concentrations are not considered in the previous chapter.

In the present study, a mathematical model of drug delivery is developed considering bulk electroporation on a tissue. Only reversible electroporation is emphasized in order to cure whole infected tissue by delivering drug as a medicine. On this account, low voltage multiple pulses are used to avoid cell death and permanent permeabilization of the membrane. The principle goal of this study is to analyze the drug transport phenomena in extracellular and intracellular domains of the targeted tissue, when drug is administrated from one side. Temperature changes during and after electroporation are also investigated. Due to the application of repeated pulses in electroporation, a time dependent MTC is considered. The MTC is basically a function of pore density and it plays a significant role to control drug transport from extracellular to intracellular space. Some differential equations along with appropriate initial and boundary conditions are prescribed to represent the governing biological circumstances. Analytical and numerical methods are used to solve the differential equations wherever applicable. In numerical simulation, equations are discretized by finite difference method (FDM). The parameters' dependencies on mass transfer are studied in details. It is possible to introduce sufficient amount of drugs into the targeted cells of a tissue through this model. No cell damage or cell death is noticed due to thermal effect as low voltage pulses are applied. Qualitative comparisons between the present study and the existing theoretical and experimental studies [56, 87, 88] are made in order to authenticate the advocated model. The numerical results of this model can be helpful in the pharmaceutical and medical research.

4.2 Problem Formulation

This study considers a tissue, which is assumed to be cubical having side length L. The tissue domain consists of extracellular and intracellular spaces. Both areas are separated by the porous cell membrane, which controls the mass transport from the extracellular to the intracellular domain. A schematic diagram (shown by Fig. 4.1) is provided to visualize the complete tissue structure as well as the drug injecting process into the tissue. In order to electroporate the whole tissue, two electrodes with different potential values ϕ_0 and ϕ_L are placed along two different boundaries, respectively (as shown in Fig. 4.2). A uniform electric field E is induced in the whole tissue directed from the positive to the negative electrode. Here, bulk electroporation is applied to electroporate all the cells of the tissue using multiple pulses with low voltage. The transmembrane potential (V_m) is increased, and nanometer-sized pores are formed in the cell membrane due to application of electric

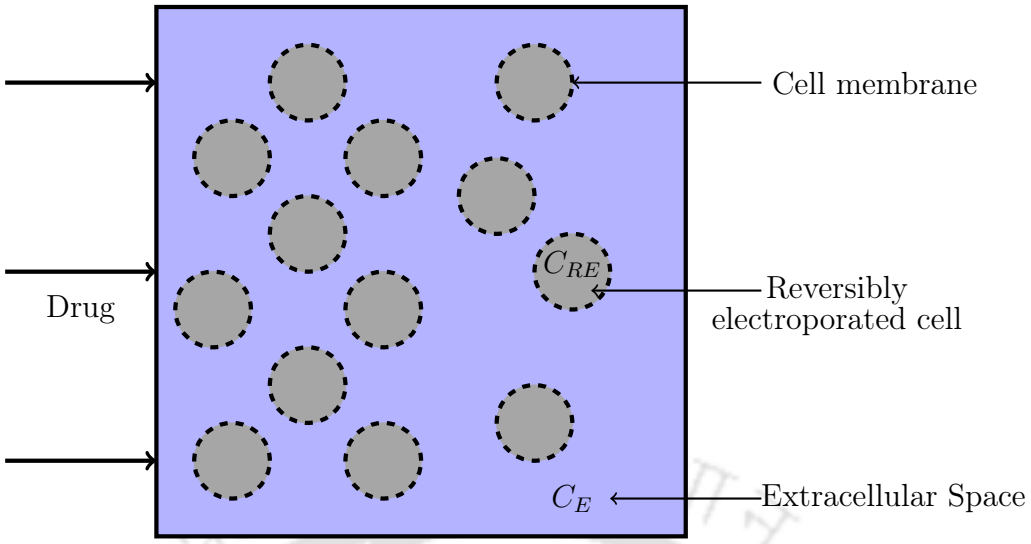

Figure 4.1: A schematic diagram of injecting drug into a biological tissue.

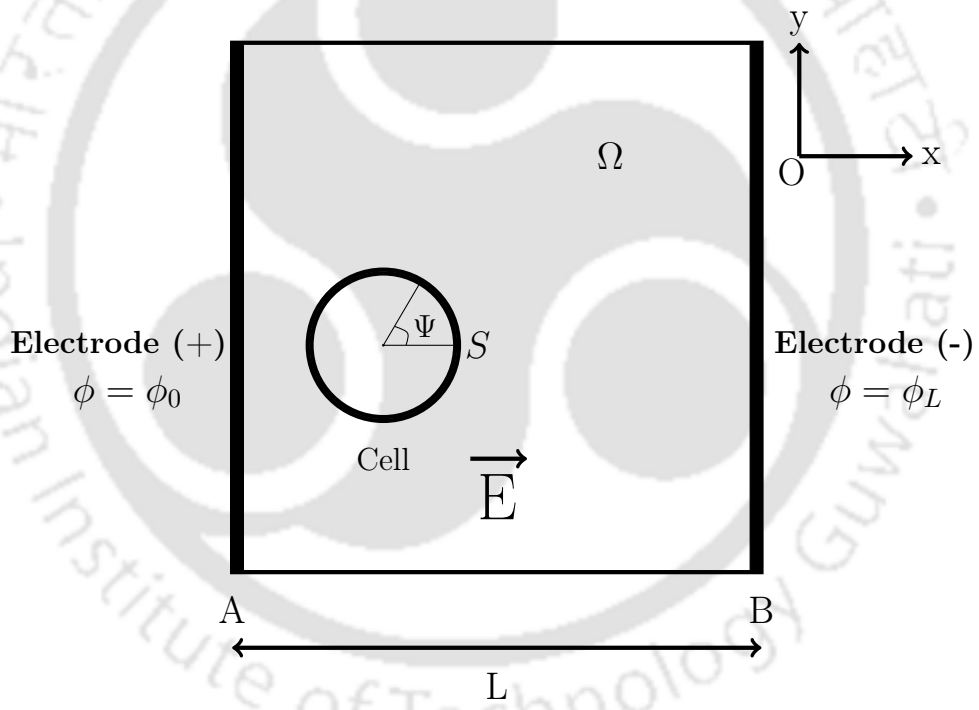

Figure 4.2: A schematic representation of bulk electroporation on a square tissue using two electrodes at A and B.

pulses. It is considered that the strength of the applied electric field does not exceed the value 28 V mm^{-1} to maintain the critical transmembrane potential ($\approxeq$ 1 V). The maximum pores are created at the poles $\Psi = 0, \pi$ as transmembrane potentials are maximum at those locations. No new pores are formed at the poles $\Psi = \frac{\pi}{2}, \frac{3\pi}{2}$ as the transmembrane potential is zero at those poles. All cells in the tissue are electroporated reversibly due to application of low voltage pulses. After electroporation, the cell membrane gets permeabilized and

allows drugs to enter the cell. The resealing process in the electroporated cells happens during the rest time between the pulses, and the drug transport occurs only in this rest time. The drug uptake into cells is affected due to the membrane resealing effect.

4.3 Model Development and Mathematical Equations

Based on the arrangement of two parallel electrodes, a uniform electric field is generated inside the tissue. The potential (ϕ) distribution inside the tissue is obtained by solving the Laplace equation [9, 13, 77]

$$\nabla^2 \phi = 0, \tag{4.1}$$

with boundary conditions: $\phi(x = 0) = \phi_0$ and $\phi(x = L) = \phi_L$.
The uniform electric field (E) in the domain Ω is calculated by the magnitude of the gradient of the potential and mathematically expressed as,

$$E = |\vec{\nabla}\phi| \tag{4.2}$$

The transmembrane potential V_m due to the effect of electric field E is obtained by the relation [22]

$$V_m = 1.5E \times r_c \cos\Psi, \tag{4.3}$$

where r_c is the radius of the cell and Ψ is the angle between the direction of electric field and the normal to the cell membrane at the position where V_m is calculated.

The pore density N in the cell membrane is obtained from the time dependent equation proposed by Krassowka and Filev [49] as,

$$\frac{dN}{dt} = \alpha A \left[1 - \frac{N}{N_0} A^{-q}\right], \tag{4.4}$$

where $A = \exp\left[\left(\frac{V_m}{V_{ep}}\right)^2\right]$, t is the time, α is the pore creation rate coefficient, V_{ep} the characteristic voltage of electroporation, N_0 the equilibrium pore density at $V_m = 0$ and q is an electroporation constant. Initially, it is considered that there is no pore in the membrane i.e., $N(0) = 0$.

The total pore area (A_P) of a single cell is calculated as, $A_P = \pi R_P^2 \cdot N_P$, where R_P is the pore radius and N_P is the total number of pore in a cell membrane. As cells are reversibly electroporated, the cell membrane goes to reseal after electroporation and the pore area starts decreasing with time. The modified pore area can be mathematically

expressed as an exponentially decreasing function of time [38],

$$A_P = \pi R_P^2 \cdot N_P(t_{ep}) \cdot \exp\left(-\frac{t}{\tau}\right), \tag{4.5}$$

where t_{ep} is the pulse duration, and τ is the resealing time constant.

4.3.1 Drug transport phenomenon in the tissue

In this model, the drug is introduced as a medicine at the left boundary of the targeted tissue. It is assumed that the drug is injected before the electroporation process starts. Multiple pulses are applied for a certain time duration (t_{ep}) mentioning a long time gap (t_M) between the pulses. Only in this time gap, mass transfer occurs from extracellular to intracellular compartment. The electric pulses are applied periodically until a sufficient drug reaches into the cells. The mass transfer rate depends on the total pore area of the cell. The pore area is a function of time due to the membrane resealing effect. So, the MTC (μ) is a function of time and it is mathematically defined as,

$$\mu(t) = \left(\frac{4\pi^2 R_P^2 r_c^2}{V_0}\right) P \cdot N(t_{ep}) \cdot \exp\left(-\frac{t}{\tau}\right), \tag{4.6}$$

where V_0 is the volume of a cube containing a cell and P is the permeability of drug particles across the cell membrane.

The drug diffuses from left to right through the extracellular space of the tissue, and when pores are formed, drug enters into the cells. The drug concentrations in the extracellular space and in the electroporated cells are obtained by the mass transport equations and mathematically can be expressed as,

$$\frac{\partial C_E}{\partial t} = \vec{\nabla}.\left(D\vec{\nabla}C_E\right) - \left(\frac{1-\varepsilon}{\varepsilon}\right)\mu(t) \times (C_E - C_{RE}), \tag{4.7}$$

$$\frac{\partial C_{RE}}{\partial t} = \mu(t) \times (C_E - C_{RE}), \tag{4.8}$$

where C_E and C_{RE} are the drug concentrations in the extracellular space and reversibly electroporated cells respectively; D is the effective diffusion coefficient of the drug in the extracellular space; ε is the porosity and it is defined as the volumetric ratio of extracellular volume to the total volume of the tissue. The above equations are solved considering appropriate initial and boundary conditions, which are as follows:

$$\left.\begin{aligned} &C_E(x,y,0) = C_1(x,y), && C_{RE}(x,y,0) = 0, \\ &C_E(0,y,t) = C_2, && \left(\frac{\partial C_E}{\partial x}\right)_{x=L} = 0, \\ &\left(\frac{\partial C_E}{\partial y}\right)_{y=0} = 0, && \left(\frac{\partial C_E}{\partial y}\right)_{y=L} = 0, \end{aligned}\right\} \tag{4.9}$$

where

$$C_1(x,y) = \begin{cases} C_2; & x = 0, \quad 0 \le y \le L, \\ 0; & \text{otherwise} \end{cases}$$

4.3.2 Thermal effects in the tissue

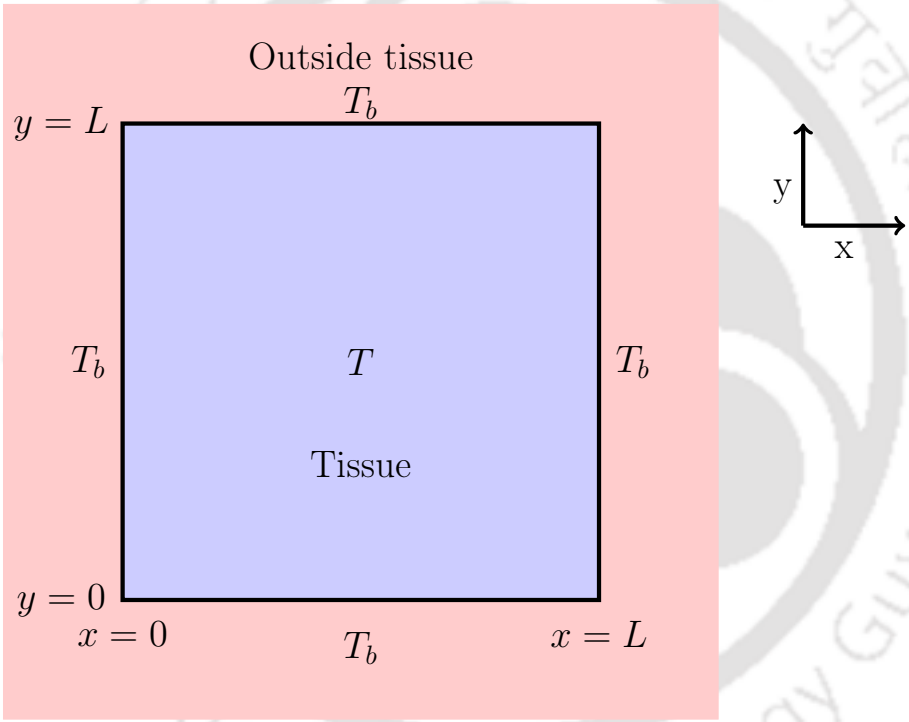

Figure 4.3: A schematic representation of temperature distribution in a tissue due to electroporation.

The membrane structure of a cell has the electrical resistivity even if the lipid layers of the membrane are thin. The cell membranes act as capacitors with high resistance [30]. Moreover, when the tissue gets exposed to an external electric field, the cell membranes become charged up. Elevated current density due to tissue electroporation guides to Joule heating, which is significant especially when longer electric pulses are applied. The Joule heating may not be biologically significant when electric pulses are applied for short duration, but in order to investigate the underlying mechanisms behind electrochemotherapy, the role played by the elevated temperature is important. Furthermore,

the study of temperature variation is essential because it helps in formation of stable permeable structures and hence plays a crucial role in electrically mediated molecular transport [69]. Also, the increment in temperature in cells plays a significant role in the dielectric breakdown of cell membrane. The mathematical formulation of Joule effect is represented through the following equations.

The change in temperature due to ongoing electroporation inside the tissue is obtained by the heat equation [31],

$$\rho c \frac{\partial T}{\partial t} = k\nabla^2 T + Q_J, \tag{4.10}$$

with initial condition: $T(x, y, 0) = T_b$,
and boundary conditions:

$$\begin{aligned} \left(\tfrac{\partial T}{\partial x}\right)_{x=0} &= \tfrac{h}{k}(T - T_b), \quad & \left(\tfrac{\partial T}{\partial x}\right)_{x=L} &= -\tfrac{h}{k}(T - T_b), \\ \left(\tfrac{\partial T}{\partial y}\right)_{y=0} &= \tfrac{h}{k}(T - T_b), \quad & \left(\tfrac{\partial T}{\partial y}\right)_{y=L} &= -\tfrac{h}{k}(T - T_b), \end{aligned}$$

where ρ is the density, c, the specific heat and k is the thermal conductivity of the tissue; T_b ($\leq T$), the body temperature; h, the heat transfer coefficient.
The resistive heating term Q_J refers to the heat source due to Joule heating as a result of applied electric pulse and it can be defined as

$$Q_J = \sigma |\vec{\nabla}\phi|^2, \tag{4.11}$$

where σ is the tissue electrical conductivity.

The temperature is expected to increase continuously with time over the time duration of electroporation and on the termination electric pulse, temperature may decrease with time. The governing temperature equation for this process may be the standard heat equation

$$\rho c \frac{\partial T}{\partial t} = k\nabla^2 T, \tag{4.12}$$

with initial condition: $T(x, y, 0) = T_{ep}$,
and boundary conditions:

$$\begin{aligned} \left(\tfrac{\partial T}{\partial x}\right)_{x=0} &= \tfrac{h}{k}(T - T_b), \quad & \left(\tfrac{\partial T}{\partial x}\right)_{x=L} &= -\tfrac{h}{k}(T - T_b), \\ \left(\tfrac{\partial T}{\partial y}\right)_{y=0} &= \tfrac{h}{k}(T - T_b), \quad & \left(\tfrac{\partial T}{\partial y}\right)_{y=L} &= -\tfrac{h}{k}(T - T_b). \end{aligned}$$

Here, T_{ep} is the temperature of the tissue after application of electric pulse over the time duration t_{ep}.

Table 4.1: The parameter's detail used for simulation of the model:

Symbol	Value	Definition	Source
σ	0.241 S m^{-1}	Tissue electrical conductivity	[1]
r_c	25 μm	Cell radius	[56]
α	10^9 m^{-2} s^{-1}	Pore creation coefficient	[49]
V_{ep}	0.258 V	Characteristic voltage	[49]
N_0	1.5×10^9 m^{-2}	Equilibrium pore density	[49]
q	2.46	Electroporation constant	[38]
D	10^{-4} mm^2 s^{-1}	Effective diffusion coefficient	
R_P	0.8 nm	Pore radius	[38]
ε	0.18	Porosity	[1]
P	5×10^{-4} mm s^{-1}	Permeability of drug	[38]
E	28 V mm^{-1}	Electrical field	
C_2	1 M	Initial drug concentration	
L	1 mm	Length of the square	Fig. 4.2
ϕ_0	28 V	Potential along $x = 0$	Fig. 4.2
ϕ_L	0 V	Potential along $x = L$	Fig. 4.2
ρ	1060 kg m^{-3}	Density of the tissue	[31]
c	3600 J kg^{-1} K^{-1}	Specific heat capacity of the tissue	[31]
k	0.502 W m^{-1} K^{-1}	Thermal conductivity of the tissue	[31]
h	50 W m^{-2} K^{-1}	Heat transfer coefficient of the tissue	[20]
T_b	37 ° C = 310.15 K	Normal body temperature	[31]
t_{ep}	80 ms	Pulse length (ON TIME)	
t_M	600 s	Time for mass transfer (OFF TIME)	
PN	10	Pulse number	

4.4 Method of Solutions

The governing equations are solved analytically wherever possible otherwise, numerical methods are applied to obtain approximate solutions. Since, two electrodes are placed vertically along left and right boundaries with different potentials, a uniform electrical field is induced over the whole tissue region. Due to parallel electrode arrangement (see Fig. 4.2), it may be considered that ϕ is independent of y i.e. $\frac{\partial \phi}{\partial y} = 0$. Eq. (4.1) along with the boundary conditions is solved analytically in a square region Ω ($0 \leq x \leq L$, $0 \leq y \leq L$) and the potential distribution is obtained as,

$$\phi(x) = \frac{(\phi_L - \phi_0)}{L} x + \phi_0. \tag{4.13}$$

Hence, from the Eq. (4.2), a uniform electric field in the tissue region Ω can be obtained as,

$$E = \frac{(\phi_0 - \phi_L)}{L}.$$

Eq. (4.4) is also solved analytically considering $\Psi = 0$ or π and the initial condition $N(0) = 0$. The pore density $N(t)$ is found as,

$$N(t) = N_0 A^q \left[1 - \exp\left(-\frac{\alpha t}{N_0 \cdot A^{q-1}}\right)\right]. \tag{4.14}$$

The Eq. (4.6) gives the MTC as,

$$\mu(t) = \left(\frac{4\pi^2 R_P^2 r_c^2 P N_0 A^q}{V_0}\right) \cdot \left[1 - \exp\left(-\frac{\alpha t}{N_0 \cdot A^{q-1}}\right)\right]. \tag{4.15}$$

The Eqs. (4.7)-(4.12) are solved numerically using finite difference method. In numerical computation, the Eqs. (4.7)-(4.8) are discretized using the forward time centered space (FTCS) scheme. The discretized equations are as follows,

$$\begin{aligned}(C_E)_{i,j}^{n+1} =& a\,(C_E)_{i+1,j}^{n} + a\,(C_E)_{i-1,j}^{n} + b(t)\,(C_E)_{i,j}^{n} \\ &+ c\,(C_E)_{i,j+1}^{n} + c\,(C_E)_{i,j-1}^{n} + d(t)\,(C_{RE})_{i,j}^{n}, \qquad \begin{matrix} i = 1, 2, \cdots, M_1 \\ j = 1, 2, \cdots, M_2 \end{matrix}\end{aligned} \tag{4.16}$$

$$(C_{RE})_{i,j}^{n+1} = (C_{RE})_{i,j}^{n} + \mu(t)\Delta t\left[(C_E)_{i,j}^{n} - (C_{RE})_{i,j}^{n}\right], \qquad \begin{matrix} i = 1, 2, \cdots, M_1 \\ j = 1, 2, \cdots, M_2 \end{matrix} \tag{4.17}$$

where $a = \frac{D\Delta t}{(\Delta x)^2}$, $b(t) = 1 - \left[2D\left(\frac{1}{(\Delta x)^2} + \frac{1}{(\Delta y)^2}\right) + \frac{1-\varepsilon}{\varepsilon}\mu(t)\right]\Delta t$, $c = \frac{D\Delta t}{(\Delta y)^2}$, and $d(t) = \frac{1-\varepsilon}{\varepsilon}\mu(t)\Delta t$. Here, Δt is the time step size, Δx and Δy are the step sizes for space, M_1 and M_2 are the numbers of grid along x-axis and y-axis respectively.
The stability condition used to solve the Eqs. (4.16)-(4.17) is

$$\Delta t < \frac{1}{2} \times \frac{(\Delta x)^2 (\Delta y)^2}{D[(\Delta x)^2 + (\Delta y)^2]}.$$

Here, $M_1 = 101$, $M_2 = 101$, $\Delta x = 0.01$, $\Delta y = 0.01$ and $\Delta t = 0.2$ are chosen for simulation.

The Eqs. (4.10)-(4.12) are also discretized by FTCS scheme and the discretized equations are as follows,

$$T_{i,j}^{n+1} = eT_{i+1,j}^{n} + eT_{i-1,j}^{n} + fT_{i,j}^{n} + gT_{i,j+1}^{n} + gT_{i,j-1}^{n} + lQ_J, \qquad \begin{matrix} i = 1, 2, \cdots, M_1 \\ j = 1, 2, \cdots, M_2 \end{matrix} \tag{4.18}$$

$$T_{i,j}^{n+1} = eT_{i+1,j}^{n} + eT_{i-1,j}^{n} + fT_{i,j}^{n} + gT_{i,j+1}^{n} + gT_{i,j-1}^{n} \qquad \begin{matrix} i = 1, 2, \cdots, M_1 \\ j = 1, 2, \cdots, M_2 \end{matrix} \tag{4.19}$$

where $e = \frac{k\Delta t}{\rho c(\Delta x)^2}$, $f = 1 - \frac{2k}{\rho c}\left[\frac{1}{(\Delta x)^2} + \frac{1}{(\Delta y)^2}\right]\Delta t$, $g = \frac{k\Delta t}{\rho c(\Delta y)^2}$, and $l = \frac{\sigma \Delta t}{\rho c}$.
The stability condition used for the Eqs. (4.18)-(4.19) is

$$\Delta t < \frac{1}{2} \times \frac{(\Delta x)^2(\Delta y)^2}{\frac{k}{\rho c}[(\Delta x)^2 + (\Delta y)^2]}.$$

Here, $M_1 = 101$, $M_2 = 101$, $\Delta x = 0.01$, $\Delta y = 0.01$ and $\Delta t = 0.00002$ are chosen for simulation. Two different Δt are used to solve the Eqs. (4.16)-(4.17) and (4.18)-(4.19) separately. The details of the parameters used in the model are shown in Table 4.1 and the suitable values of the parameters are taken from the existing literature.

4.5 Results and Discussion

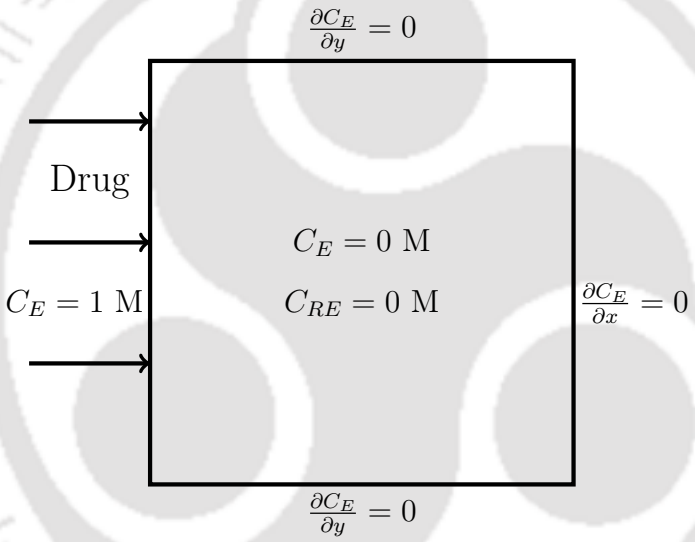

Figure 4.4: A schematic diagram of the model equations, which are presented in the Eqs. (4.7)-(4.9) for injecting drug into a biological tissue.

In the present study, the drug transport phenomenon in the diseased tissue is represented by a mathematical model. The main aim of this study is to focus on drug penetration through a targeted tissue when drug is injected from one side. The physical overview of the drug transport in this model is shown in as a diagram in Fig. 4.4. A qualitative analysis is performed to visualize the drug dynamics into the electroporated tissue through graphical representations in Figs. 4.5 - 4.15. The detailed discussion on the plotted graphs of drug concentrations for different values of drug permeability (P), diffusion coefficient (D) and pulse length (t_{ep}) is made.

Fig. 4.5 describes how the MTC (μ) changes with time after electroporation for different permeability and various pulse lengths. In Fig. 4.5a, it is noticed that μ increases with drug permeability. In Fig. 4.5b, it is also seen that the parameter μ increases with

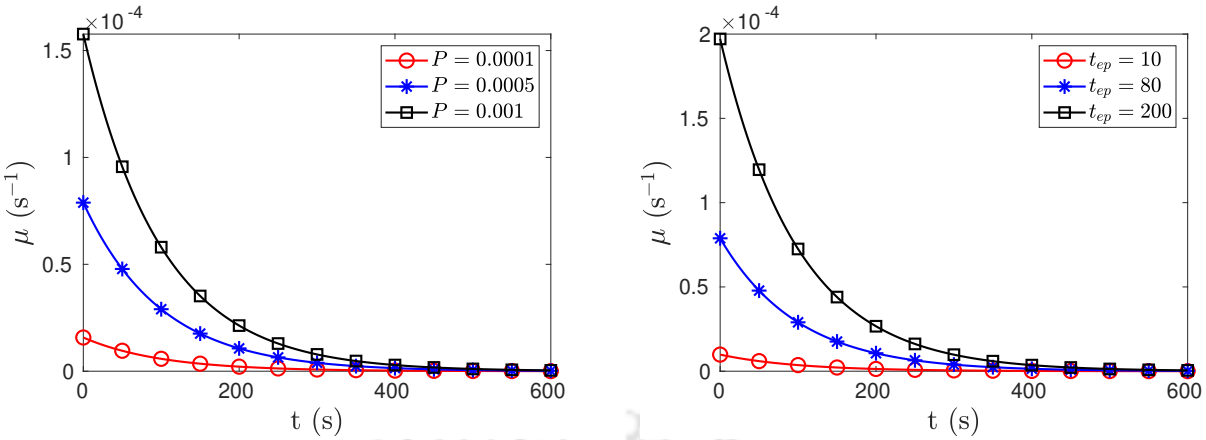

Figure 4.5: The changes of MTC with time after electroporation for different (a) permeability P (mm s^{-1}) and (b) pulse length t_{ep} (ms).

the pulse length because of the higher pore density for the application of longer pulses. The physical observation may be explained through the mathematical expression given by the Eq. (4.6). In both the graphs of Fig. 4.5, the MTC decreases with time due to membrane resealing. The increased MTC helps to increase the drug uptake rate into the cells from the extracellular region.

4.5.1 Drug transport phenomenon in the tissue

This section presents a full overview of the drug transport process in the targeted tissue when the drug is applied from the left side. The process includes continuous molecular diffusion in the homogeneous extracellular fluid medium, and drug uptake into the intracellular domain from the extracellular domain through the permeabilized cell membrane.

Fig. 4.6 shows the time dependent drug concentrations in extra- and intra-cellular spaces at the locations $x = 0.1$, $x = 0.5$ and $x = 0.9$. From Fig. 4.6a, it is observed that the drug concentration at $x = 0.1$ in the extracellular region increases within a short time. This is because the location is near to the drug source at the left boundary so the molecular diffusion to that point occurs quickly. On the other hand, the drug concentration in the intracellular region increases slowly at that time due to the low permeability of the cell membrane as fewer pores are formed immediately after the electroporation. It is also noticed that both the profiles overlap after some time, near about 150 s. Because, the membrane permeability increases due to sufficient number of pores formed by this time (near 150 s from the start of electroporation) and the dug uptake into the cells occurs faster. In Fig. 4.6b, it is shown that the drug concentrations (C_E, C_{RE}) at $x = 0.5$ for the entire time are relatively less than the same at $x = 0.1$. As the point $(0.5, 0.5)$ is in the middle and far from the drug source, less amount of drug reaches there. Another reason

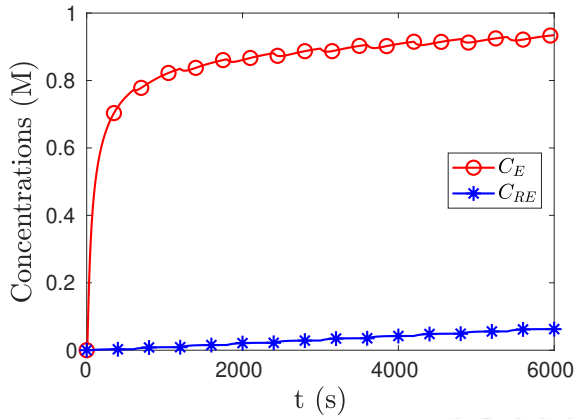

(a) $x = 0.1$ mm

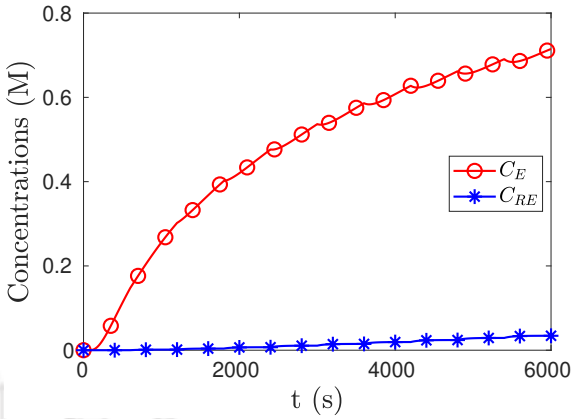

(b) $x = 0.5$ mm

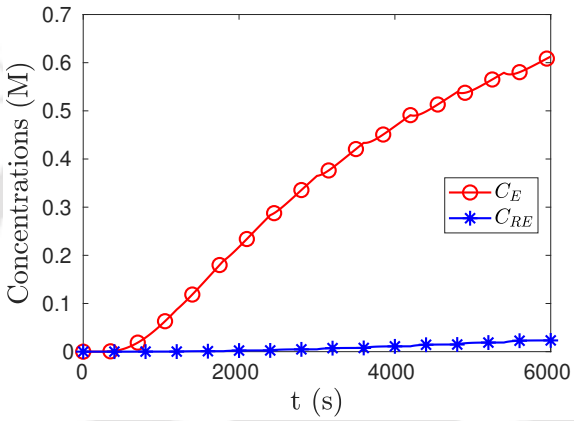

(c) $x = 0.9$ mm

Figure 4.6: The drug concentration (C_E, C_{RE}) profiles, which are changing with time, at three different locations parallel to x-axis along the line $y = 0.5$. Here, C_E, C_{RE} are calculated for $P = 0.0005$ mm s^{-1} and $D = 0.0001$ mm^2 s^{-1}.

is that the drug uptake in the cells near the boundary is higher. Similar observation is noticed through the Fig. 4.6c. As the point (0.9, 0.5) is far from the drug source, relatively less amount of drug reaches in the intracellular as well as extracellular region.

Comparison

To validate the present model, two comparisons are made. In first comparison, electroporation is not taken into account and results are compared with the experimental results of Wong's et al [87] and the theoretical results of Yadav and Dalal [88]. As no electroporation is considered, $\mu = 0$ is taken to solve the concentration equations in the present model and the comparison is shown in the Fig. 4.7. In the experiment [87], a test on nanoparticle penetration through a collagen gel (compared to tissue media) is performed. In FV-HMM model, the drug penetration through a tissue is studied and the heterogeneous multiscale method is used to solve the model. In all the three models, the drug penetration in the

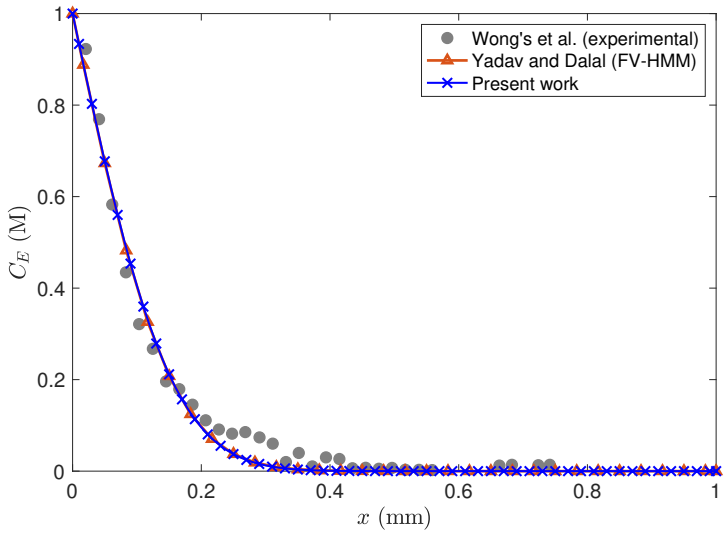

Figure 4.7: The present study is compared with the experimental work and the FV-HMM model.

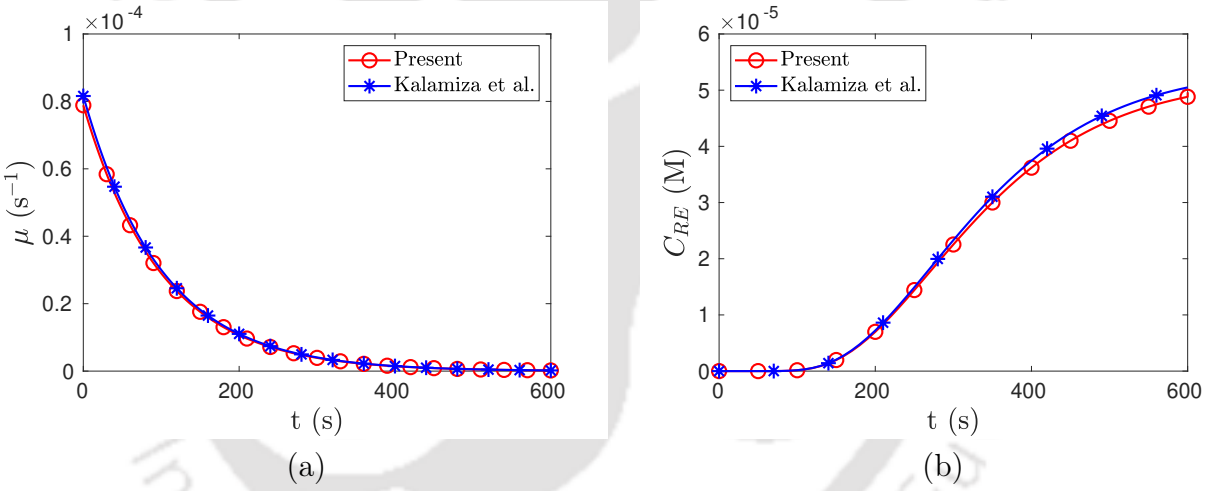

Figure 4.8: Comparison between the present results with the existing model. Here, the concentration (C_{RE}) are calculated at (0.5, 0.5) for $P = 0.0005$ mm s^{-1}, $D = 0.0001$ mm^2 s^{-1} and $t_{ep} = 80$ ms.

tissue is studied for a duration of 12 hours. The Fig. 4.7 shows that the drug penetration (present study) in the extracellular media along x-axis is very close to those in the other studies.

Another comparison is made when electroporation is incorporated i.e. $\mu \neq 0$. In this case, the present results are compared with the work of Kalamiza et al. [56]. The electroporation based MTC is taken from the model [56]. In order to compare the results, the MTC that includes the pore resealing effect can be written as [56],

$$\mu(t) = \frac{3Df_p}{d_m r_c} \cdot \exp\left(-\frac{t}{\tau}\right) = 8.16 \times 10^{-5} \cdot \exp\left(-\frac{t}{\tau}\right), \tag{4.20}$$

where $f_p = 3.4 \times 10^{-8}$ and $d_m = 5 \times 10^{-6}$ mm are considered.

The results for both MTCs (as in Eqs. (4.6) and (4.20)) are plotted in the Fig. 4.8. From the plots, it can be observed that there is a good agreement between the results.

Effects of drug permeability on drug concentrations

Fig. 4.9 illustrates the time-dependent drug transport at various locations throughout the tissue for different values of drug permeability. It is noticed from the Fig. 4.9a that at the initial stage, the extracellular concentrations increase rapidly as the point (0.1, 0.5) is close to the boundary where the drug is injected, so the drug diffusion to that point occurs quickly. Also, due to the same reason, the concentration profiles throughout the time are almost same for different permeability. But, in Figs. 4.9c & 4.9f, it is observed that the concentrations for higher values of P are lesser than the concentrations for smaller P. The reason is that the drug uptake into the cells is more for higher P, which is shown in Figs.4.9d & 4.9f. Hence, the drug permeability enhances the drug uptake rate into the cells. One important observation is that after the application of ten pulses, the amount of drug entered into the cells is much lesser compared to the amount of drug present in extracellular space. Slow mass transfer from extracellular to intracellular compartment is the possible reason.

Effects of diffusion coefficient on drug concentrations

Fig. 4.10 represents the time-dependent drug concentration (C_E, C_{RE}) profiles for different diffusion coefficients (D) in the tissue at a point (0.5, 0.5). It is observed from the graphs that the drug concentrations (C_E, C_{RE}) increase with the increase in D at all three locations. This is expected because, for a higher value of D, the drug particles move faster in the extracellular domain from the drug source and the drug uptake into cells is higher. As shown in Fig. 4.10a, the concentrations of drug (C_E) have a sudden increase as the drug diffusion to the location (0.5, 0.5) occurs faster. After some time, the drug concentrations (C_E) increase steadily due to the drug uptake by the cells, which is shown in the Fig. 4.10b. As a result of faster drug diffusion in the ECS, intracellular drug concentrations (C_{RE}) also increase with the increase in D that is noticed in Fig. 4.10b. There are some jumps in the profiles of C_{RE} because of repeated pulse application.

Effects of pulse length and pulse number on drug concentrations

Fig. 4.11 represents the drug concentration profiles in extracellular and intracellular compartments along the x-direction in the targeted tissue for different time duration of the applied pulses. Fig. 4.11a shows that the drug concentration in extracellular space decreases with the increase of pulse length. This is because the drug uptake into cells is

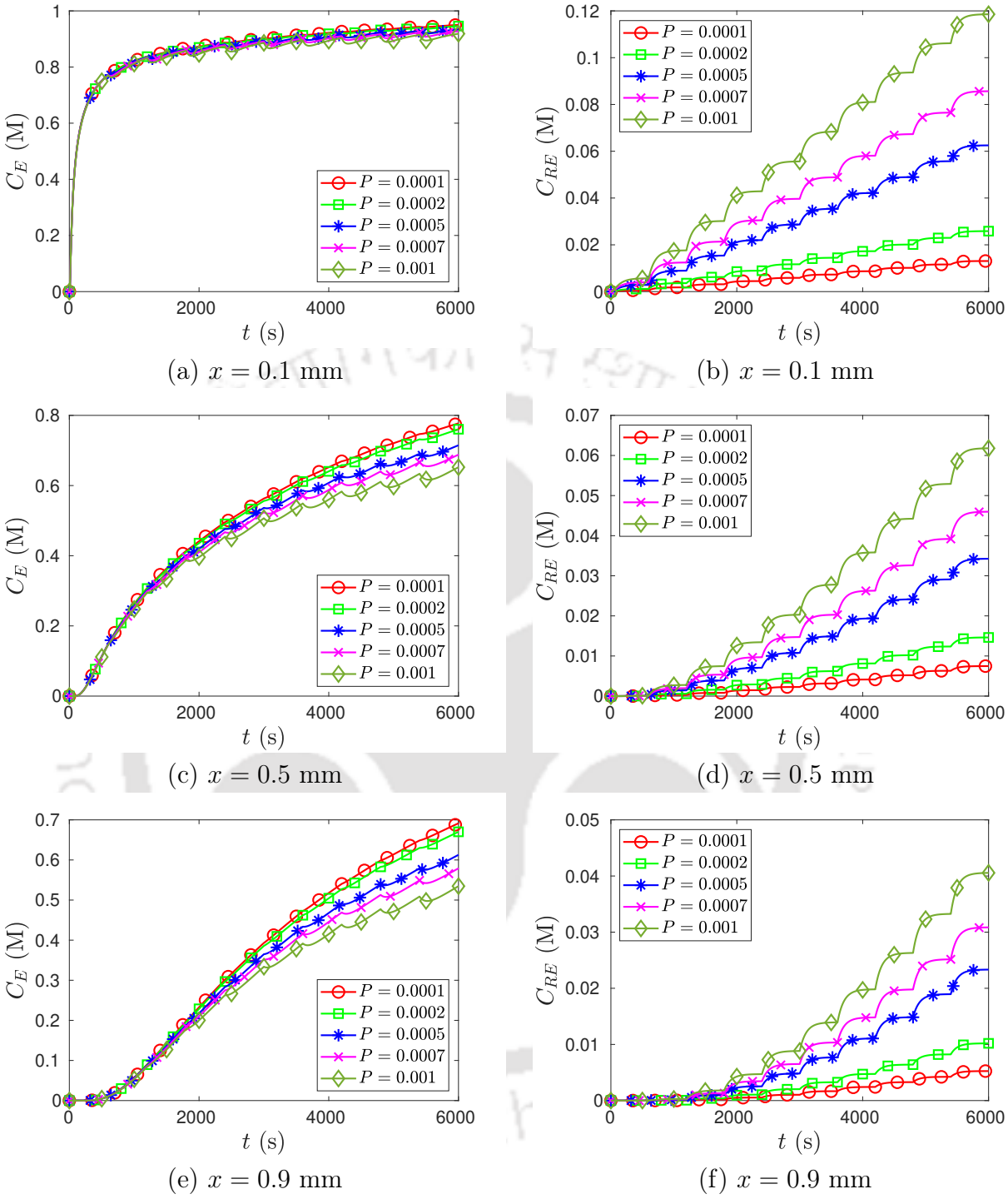

(a) $x = 0.1$ mm (b) $x = 0.1$ mm

(c) $x = 0.5$ mm (d) $x = 0.5$ mm

(e) $x = 0.9$ mm (f) $x = 0.9$ mm

Figure 4.9: Concentrations (C_E, C_{RE}) vs. time for $D = 0.0001$ mm^2 s^{-1} and different permeability (mm s^{-1}).

higher for the application of longer pulses (see Fig. 4.11b). Also, it is noticed from the Fig. 4.11b that the drug uptake into the cells as well as the drug penetration throughout the tissue increases for the application of long duration pulses. The reason is that the pore density as well as mass transfer rate is increased with the application of long duration

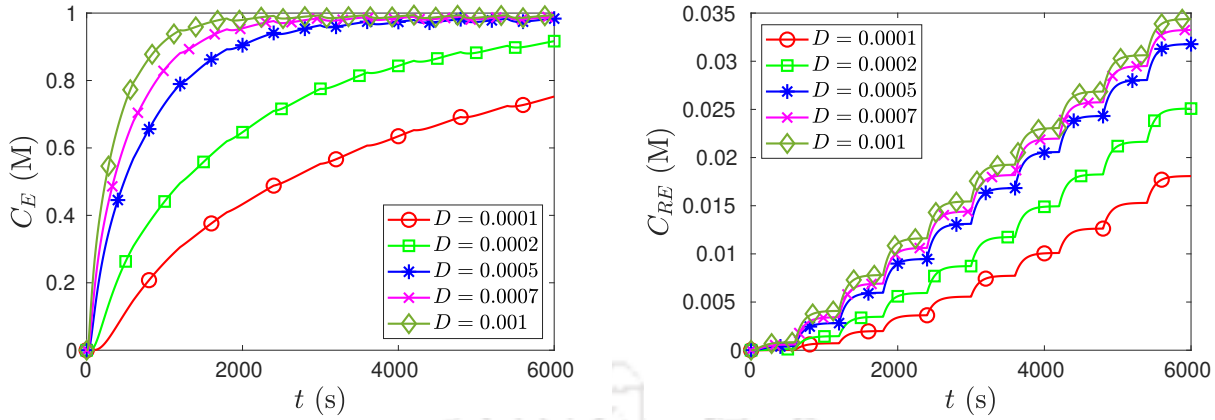

(a) (b)

Figure 4.10: Concentrations (C_E, C_{RE}) vs. time for $P = 0.0005$ mm s^{-1} and different D (mm^2 s^{-1}).

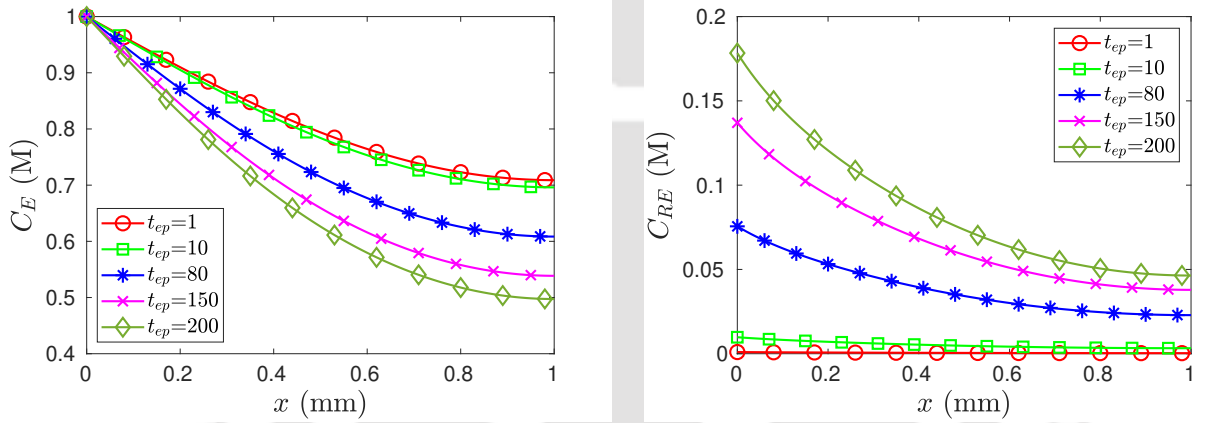

(a) (b)

Figure 4.11: The drug penetration along x-axis into the tissue after different pulse duration t_{ep} (ms). Concentrations (C_E, C_{RE}) are calculated for $D = 0.0001$ mm s^{-1} and $P = 0.0005$ mm^2 s^{-1}.

pulses, which is already observed through the Fig. 4.5b.

Fig. 4.12 shows the drug concentration profiles in extracellular and intracellular compartments along the x-direction in the tissue for different pulse numbers. It can be seen from both graphs that drug concentrations (C_E, C_{RE}) increase as PN increases. C_E increases as more drugs reach the ECS as a result of continuous diffusion for a long time. On the other hand, C_{RE} increases as a result of the periodic reopening of membrane pores by the use of a pulse repeatedly and due to the availability of more drugs within the ECS. Hence, a suitable number of a pulse that is applied periodically on the tissue can be determined as per the necessity of the amount of drug in the targeted cells.

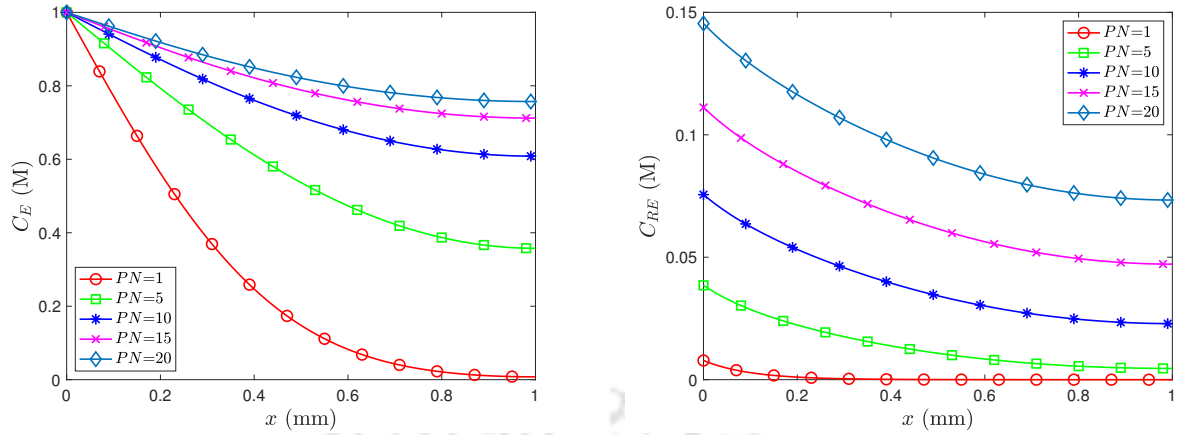

(a) (b)

Figure 4.12: The drug penetration along x-axis into the tissue after different pulse number PN of pulse length 80 ms. Concentrations (C_E, C_{RE}) are calculated for $D = 0.0001$ mm s^{-1} and $P = 0.0005$ mm^2 s^{-1}.

Visualization of drug penetration by the contour plots

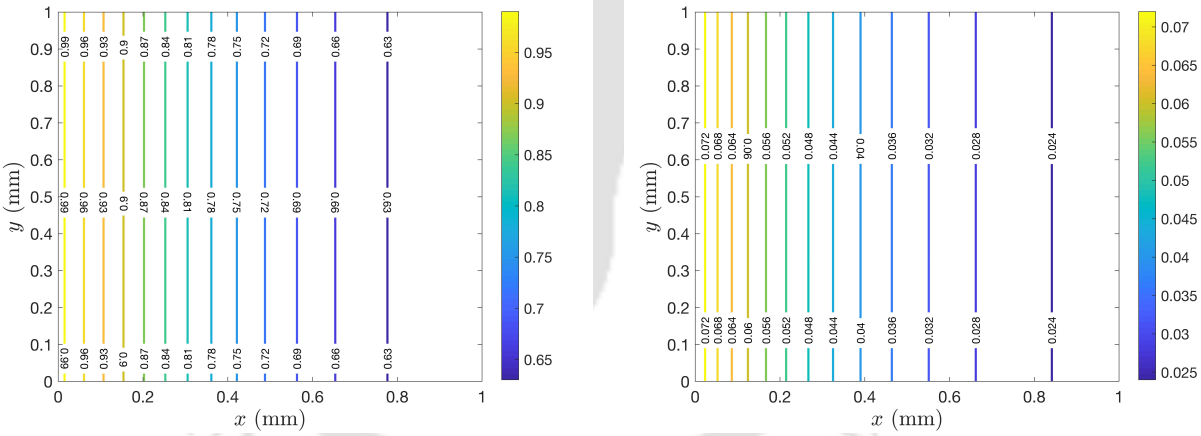

(a) C_E (b) C_{RE}

Figure 4.13: Contour plots of concentration distribution (iso-concentration lines) in the tissue. Here, C_E and C_{RE} are obtained for $P = 0.0005$ mm s^{-1}, $D = 0.0001$ mm^2 s^{-1}, $PN = 10$ and $t_{ep} = 80$ ms.

The drug penetration throughout the targeted tissue after electroporation with ten pulses is shown by the contour plots (Fig. 4.13). It is seen that after performing the electroporation of ten pulses with time gap of 600 s, a large amount of drug enters into the cells near the left boundary, whereas a lesser amount of drug reaches the cells near the right boundary. It takes different times for the drug to enter the cell at different locations in the tissue. These times are calculated numerically and given in the Table 4.2. Therefore, in this model's approach, a dose of drug with a concentration of more than

0.025 M can be administered into cells of a targeted tissue. This amount of drug could be a desired requirement for the treatment of the tissue. However, if more drug is required to treat a deceased tissue, it will be possible to increase the amount of drug into the cells by applying more pulses.

Table 4.2: Time taken to initiate drug into the cell at various locations are shown.

Location	Time (s)	C_{RE} (M)
(0.1, 0.5)	2.0×10^{-4}	1.614850×10^{-56}
(0.2, 0.5)	4.0×10^{-4}	1.653603×10^{-103}
(0.3, 0.5)	6.0×10^{-4}	1.693286×10^{-150}
(0.4, 0.5)	8.0×10^{-4}	1.733921×10^{-197}
(0.5, 0.5)	1.0×10^{-3}	1.775532×10^{-244}
(0.6, 0.5)	1.2×10^{-3}	1.818141×10^{-291}
(0.7, 0.5)	1.4×10^{-3}	1.861773×10^{-338}
(0.8, 0.5)	1.6×10^{-3}	1.906451×10^{-385}
(0.9, 0.5)	1.8×10^{-3}	1.952202×10^{-432}

4.5.2 Thermal effects in the tissue

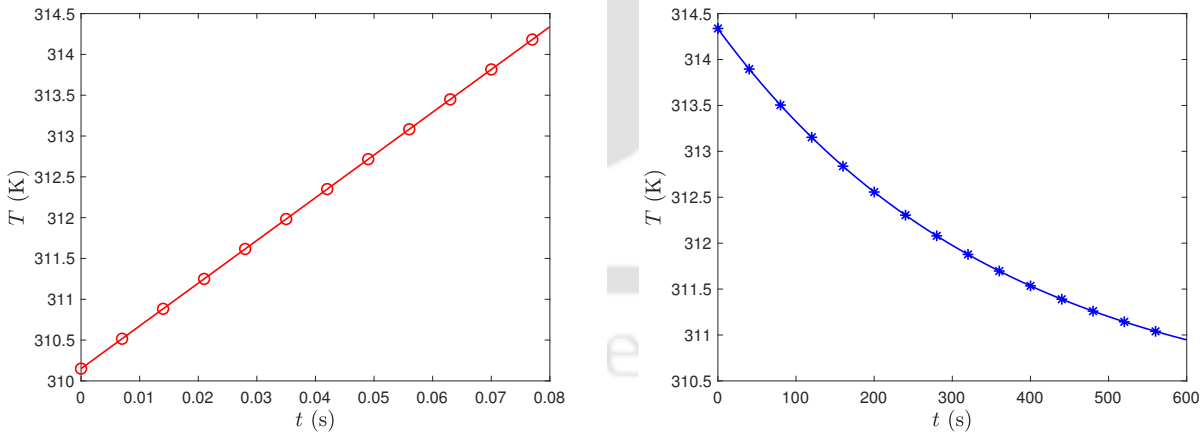

(a) During electroporation (b) After electroporation

Figure 4.14: The change of temperature T with time t at (0.5, 0.5).

Fig. 4.14a shows the change of temperature at the middle (0.5, 0.5) of the tissue during electroporation due to the application of one pulse of 80 ms. It is clearly observed that the temperature increases with the pulse time from the initial body (tissue) temperature 310.15 K due to Joule heating. However, Fig. 4.14b describes the temporal temperature

variations at (0.5, 0.5) after electroporation. From the figure, it is seen that the temperature gradually decreases with time from its peak value ($T_{ep} = 314.335$ K), and after a certain time around 600 s, it reaches the temperature (≈ 311 K) that is close to the body temperature T_b. This happens due to the continuous heat transfer from inside to the outside of the tissue.

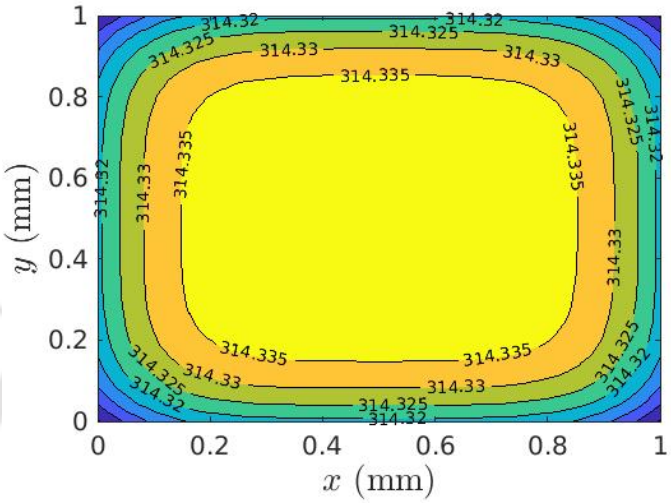

Figure 4.15: Temperature distribution over the tissue region after electroporation with one pulse.

Fig. 4.15 illustrates the temperature contours throughout the tissue region after the electroporation over a time duration of 80 ms. It is noticed that the maximum temperature is attained at the center, and the temperature becomes minimum at the corner points of the tissue region. The maximum value of the increased temperature is about 314.335 K, which is less than the possible temperature of cell damage (315.15 K = $42°C$) as reported in [31]. So, there is no chance of cell damage or cell death in the tissue due to application of the pulses. The main reason for slight increase in temperature due to electroporation is the application of low voltage pulse. One important observation is that in order to avoid any cell damage, the maximum pulse duration should be of 80 ms for the application of the electric field 28 V mm^{-1}. Hence, the electroporation configuration and model arrangement are options for successful drug delivery into the targeted tissue with reversible electroporation.

4.6 Conclusions

From this study, the following observations are made:

- The proposed mathematical model for drug delivery deals with an advanced electroporation technique. Low voltage multiple pulses are applied to introduce the drug

into the cells of a diseased tissue with no cell death.

- Since, the initial drug is injected from one side (left boundary) of the tissue, it takes a long time to spread the drug into the targeted tissue.
- The drug uptake into the cells increases with the pulse duration and the pulse number.
- It is observed that during electroporation, the tissue temperature increases from its initial body temperature (310.15 K) due to Joule heating.
- In this model, no cell damage takes place due to thermal effects as increased temperature is not that significant.
- The pulse length (80 ms) and the rest time between the pulses (600 s) are optimized to deliver sufficient drugs into the cells with no thermal damage.

The model is compared qualitatively with experimental and theoretical studies. The model could be useful in various clinical experiments and pharmaceutical sectors.

CHAPTER 5

POINT SOURCE DRUG AND THE DRUG LOSS FROM THE TISSUE BOUNDARY

In chapter 4, we have presented a model of drug delivery in which spatial changes of drug distribution in a tissue along with thermal effects due to applied pulses are studied. The proposed model in this chapter contains additional information, such as a variable σ that depends on E, the drug is injected as a point source, and the effects of drug loss at the tissue boundaries.

5.1 Introduction

Granot and Rubinsky [38] first attempted to develop a mathematical model for drug delivery in the tissue cells with reversible electroporation and proposed MTC in terms of pore density using the model [49]. A detailed relation between electroporation and the increment in the permeability that affects cellular drug uptake is theoretically described in a dual-porosity model by Kalamiza et al. [56]. The mass transport coefficient depending on membrane electropores is illustrated to solute transport into the tissue in their study. Argus et al. [1] developed a model where reversible and irreversible electroporations were considered for mass transport into different types of electroporated cells. The tissue electrical conductivity depending on electric field is studied in their work. Goldberg et al. [36] also used the pore creation model and proposed a multiphysics model for ion transport. In their model, they presented a mass transport equation using the Nernst-Planck equation for transporting different species into the cells.

There is no consideration about the effects of drug loss or drug elimination from the tissue in the above mentioned models. The method of drug injection as a point source is also not studied so far.

In the present study, a mathematical model for drug delivery is developed in which

bulk electroporation on tissue is taken into account. Only reversible electroporation has been emphasized in this model to cure whole infected tissue by delivering drug as a medicine. On this account, some low voltage multiple pulses are applied to succeed a sufficient amount of drugs into the targeted cells. A point source drug in terms of Dirac-delta function is introduced to represent initial drug distribution. The effects of drug loss from the tissue boundary through extracellular space on drug transport are studied thoroughly. In this study, suitable differential equations with appropriate initial and boundary conditions, which govern the biological circumstances, are presented. The main objective of the current study is to analyze the drug transport phenomena in the tissue by taking care of the effects of drug loss, which is imposed as boundary conditions.

5.2 Problem Formulation

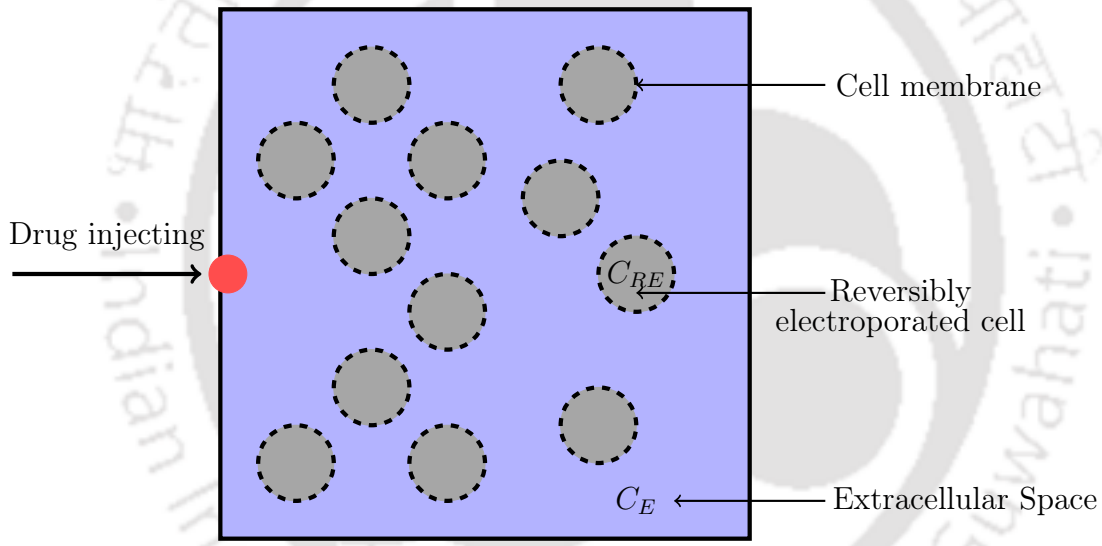

Figure 5.1: A schematic diagram of injecting drug into a biological tissue.

In this study, a biological tissue is considered and assumed to be cubical, having side length L. Structurally, the tissue is split into two parts: extracellular space and intracellular space. Both the spaces are separated by the porous cell membranes, which control the mass transport phenomenon from extracellular to intracellular domains. A schematic diagram as shown in Fig. 5.1 is provided to visualize the complete tissue structure as well as the drug injecting process into the tissue. Two electrodes are set at the upper and lower boundaries of the tissue for electroporation. The positive electrode is assigned with the potential ϕ_L, and the negative electrode is assigned with the potential ϕ_0 (as shown in Fig. 5.2). Due to the application of electric pulses, the transmembrane potential is increased, and the cell membrane gets permeabilized. As a result, nanometer-sized pores are formed in the cell membrane and the pore fraction coefficient (f_p) increases.

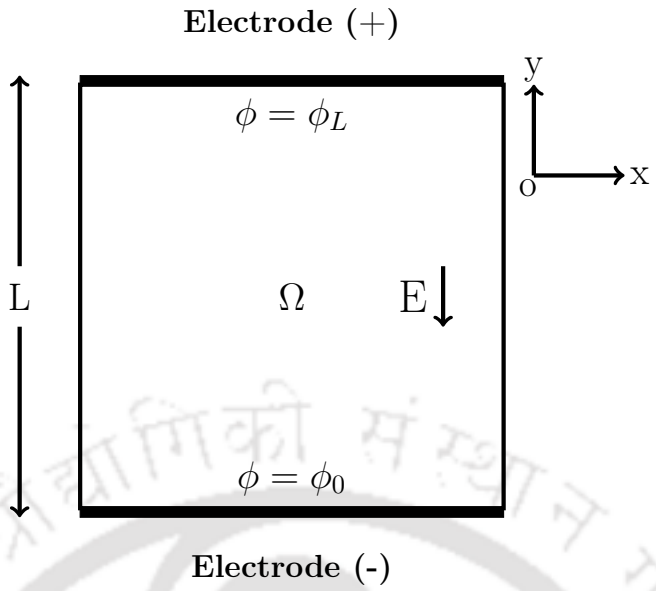

Figure 5.2: A schematic representation of bulk electroporation on the square tissue.

Repeated pulses are applied to the tissue over a specific time period with some time gap between the pulses. The pore resealing occurs in the rest time when a pulse is off. During this rest time, drug transport occurs under pore resealing effects. In the resealing period, the pore area decreases with time, and the drug transport rate gets slow. Multiple pulses are applied after completing the rest time of the previous pulse to enhance the mass transfer rate.

5.3 Model Development and Mathematical Equations

Because of the arrangement of two parallel electrodes, a uniform electric field and a non-uniform electric potential are generated. The potential (ϕ) distribution inside the tissue is obtained by solving the equation [9, 13, 77]

$$\vec{\nabla} \cdot (\sigma \cdot \vec{\nabla}\phi) = 0, \tag{5.1}$$

with boundary conditions: $\phi(y = 0) = \phi_0$ and $\phi(y = L) = \phi_L$, where σ is the tissue electrical conductivity.
The uniform electric field (E), through out the domain Ω is calculated by the magnitude of the gradient of the potential, mathematically expressed as

$$E = |\vec{\nabla}\phi| \tag{5.2}$$

5.3.1 Roles of tissue conductivity

The creation of pores in the cell membrane is one of the effective outcomes of electroporation. In macroscopic view, these pores have the effect of increasing the electrical conductivity. Therefore, the electrical conductivity increases as the electric field (E) increases. Previous studies have considered various functional dependencies of the electrical conductivity on the electric field magnitude [12, 51, 77]. From the experimental as well as computational study [77], it is known that during electroporation the electrical conductivity changes with the applied electric field and the relation is defined as,

$$\sigma(E) = \left[\frac{\sigma_{\max} - \sigma_{\min}}{1 + \gamma_1 \cdot \exp\left(-\frac{E-a}{b}\right)}\right] + \sigma_{\min}, \tag{5.3}$$

$$a = \frac{E_{\text{rev}} + E_{\text{irrev}}}{2} \text{ and } b = \frac{E_{\text{irrev}} - E_{\text{rev}}}{\gamma_2},$$

where E_{rev} and E_{irrev} are respective threshold values for reversible and irreversible electroporation, $\sigma_{\min}$ and $\sigma_{\max}$ are the minimum and the maximum tissue electrical conductivity respectively, γ_1 and γ_2 are the sigmoidal functional parameters.

5.3.2 Mass transfer coefficient calculation

The induced electric field is a cause for increasing transmembrane potential and as a result cell membrane get permeabilized. A symmetric sigmoid function, is developed in the model [1] to evaluate pore fraction coefficient (f_p) of the surviving cells (reversibly electroporated cells) which is defined as,

$$f_p = \left[1 + \exp\left(\frac{E_f - E}{b_f}\right)\right]^{-1}, \tag{5.4}$$

where E_f and b_f are the fitting parameters.
The mathematical formulation of the MTC (μ) is given as follows,

$$\mu(t) = \frac{P f_p}{r_c} e^{-\frac{t}{\tau}}, \tag{5.5}$$

where P is the drug permeability, r_c is the cell radius and τ is the resealing constant.

5.3.3 Drug transport phenomenon in the tissue

The drug concentrations in extracellular space and in reversibly electroporated cells are obtained by the mass transport equation as

$$\frac{\partial C_E}{\partial t} = \vec{\nabla}.\left(D\vec{\nabla}C_E\right) - \left(\frac{1-\varepsilon}{\varepsilon}\right)\mu(t) \times (C_E - C_{RE}), \tag{5.6}$$

$$\frac{\partial C_{RE}}{\partial t} = \mu(t) \times (C_E - C_{RE}), \tag{5.7}$$

where C_E and C_{RE} are the drug concentrations in extracellular space and reversible electroporated cells respectively; D is the effective diffusion coefficient of the drug in the extracellular space; ε is the porosity of the membrane pores. We solve the above equations considering initial and boundary conditions, which are as follows:

$$\left.\begin{aligned} &C_E(x,y,0) = C_1(x,y), && C_{RE}(x,y,0) = 0, \\ &\left(\frac{\partial C_E}{\partial x}\right)_{x=0} = \beta C_E, && \left(\frac{\partial C_E}{\partial x}\right)_{x=L} = \beta C_E, \\ &\left(\frac{\partial C_E}{\partial y}\right)_{y=0} = \beta C_E, && \left(\frac{\partial C_E}{\partial y}\right)_{y=L} = \beta C_E, \end{aligned}\right\} \tag{5.8}$$

where β represents the rate of mass loss from the tissue boundary which depends on the tissue's boundary properties. The initial drug that is injected through a particular point/location of the tissue boundary is mathematically defined as

$$C_1(x,y) = \begin{cases} n_d\delta(y-0.5), & x = 0 \\ 0, & \text{otherwise} \end{cases}$$

where n_d is the number of drug dose and $\delta(y)$ refers to the Dirac delta function. The delta function can be used in terms of normal distribution as

$$\delta_d(y) = \frac{1}{d\sqrt{\pi}}\exp\left(-\frac{y}{d}\right)^2, \quad 0 < d < 1. \tag{5.9}$$

5.4 Method of Solution

The governing equations (5.1) - (5.9) are solved numerically. Equations (5.1) - (5.3) are solved simultaneously to find optimum potential and electric field throughout the tissue region. In numerical computations, the calculation is started on taking $\sigma = \sigma_{\min}$ initially at t=0. A uniform electric field is induced in the tissue due to parallel electrode configuration at tissue boundaries. The field direction is from top to bottom, which is shown in the Fig. 5.2. We can determine the pore fraction coefficient from the expression

Table 5.1: Details of the parameters used in the simulation:

Symbol	Value	Description	Source
$\sigma_{\min}$	0.0 S m^{-1}	Minimum electrical conductivity	[1]
$\sigma_{\max}$	0.241 S m^{-1}	Maximum electrical conductivity	[1]
E_{rev}	46 V mm^{-1}	Threshold value for reversible electroporation	[1]
E_{irrev}	70 V mm^{-1}	Threshold value for irreversible electroporation	[1]
γ_1	8	Electrical conductivity parameter	[1]
γ_2	10	Electrical conductivity parameter	[1]
E_f	65.8 V mm^{-1}	Fitting parameter for MTC	[1]
b_f	7.5 V mm^{-1}	Fitting parameter for MTC	[1]
r_c	50 μm	Cell radius	[49]
D	10^{-3} mm^2 s^{-1}	Effective diffusion coefficient	
ε	0.18	Porosity of the membrane pores	[56]
P	5×10^{-4} mm s^{-1}	Permeability of drug	[38]
E	60 V mm^{-1}	Electrical field	
L	1 mm	Length of the rectangle	Fig. 5.2
ϕ_L	60 V	Potential on positive electrode	Fig. 5.2
ϕ_0	0 V	Potential on negative electrode	Fig. 5.2
PN	10	Pulse number	
t_{ep}	1 ms	Pulse length (ON TIME)	
t_M	100 s	Time for mass transfer (OFF TIME)	
n_d	100	Number of drug dose	
d	0.1	Constant in Dirac-delta function	Eq. (5.9)
β	0.1 mm^{-1}	Rate of mass loss at the boundary	

(5.4) using the optimized electric field. The mass transfer coefficient is now calculated from the relation (5.5). The coupled equations (5.6) - (5.9) are solved numerically using finite difference method. The details of the parameters used in the model are shown in Table 5.1. In discretization, we have used forward time centered space (FTCS) scheme to the equations (5.6) - (5.9) and discretized equations are as follows,

$$\begin{aligned}(C_E)_{i,j}^{n+1} =& a\,(C_E)_{i+1,j}^{n} + a\,(C_E)_{i-1,j}^{n} + b(t)\,(C_E)_{i,j}^{n} \\ &+ c\,(C_E)_{i,j+1}^{n} + c\,(C_E)_{i,j-1}^{n} + d(t)\,(C_{RE})_{i,j}^{n}\,, \qquad \begin{matrix} i = 1, 2, \cdots, M_1 \\ j = 1, 2, \cdots, M_2 \end{matrix}\end{aligned} \tag{5.10}$$

$$(C_{RE})_{i,j}^{n+1} = (C_{RE})_{i,j}^{n} + \mu(t)\Delta t\left[(C_E)_{i,j}^{n} - (C_{RE})_{i,j}^{n}\right], \qquad \begin{matrix} i = 1, 2, \cdots, M_1 \\ j = 1, 2, \cdots, M_2 \end{matrix} \tag{5.11}$$

where $a = \frac{D\Delta t}{(\Delta x)^2}$, $b(t) = 1 - \left[2D\left(\frac{1}{(\Delta x)^2} + \frac{1}{(\Delta y)^2}\right) + \frac{1-\varepsilon}{\varepsilon}\mu(t)\right]\Delta t$, $c = \frac{D\Delta t}{(\Delta y)^2}$, and $d(t) = \frac{1-\varepsilon}{\varepsilon}\mu(t)\Delta t$. Here, Δt is the time step size, Δx and Δy are the step sizes for space, M_1

and M_2 are the numbers of grid along x-axis and y-axis respectively.

Stability condition: To solve the equations (5.10) - (5.11) using FTCS scheme, the following stability condition is used.

$$\Delta t < \frac{1}{2} \times \frac{(\Delta x)^2(\Delta y)^2}{D[(\Delta x)^2 + (\Delta y)^2]}.$$

Here, $M_1 = 101$, $M_2 = 101$, $\Delta x = 0.01$, $\Delta y = 0.01$ and $\Delta t = 0.2$ are chosen for simulations.

5.5 Results and Discussion

In this study, a mathematical model and its numerical simulation are used to portray the drug transport phenomenon in diseased tissues. A qualitative analysis is conducted to visualize how the drug is transported into the electroporated tissue using graphical representations given in the Figs. 5.3 - 5.12. The results are discussed through the plotted graphs for different parameters like, rate of drug loss (β), drug permeability (P) and pulse number (PN).

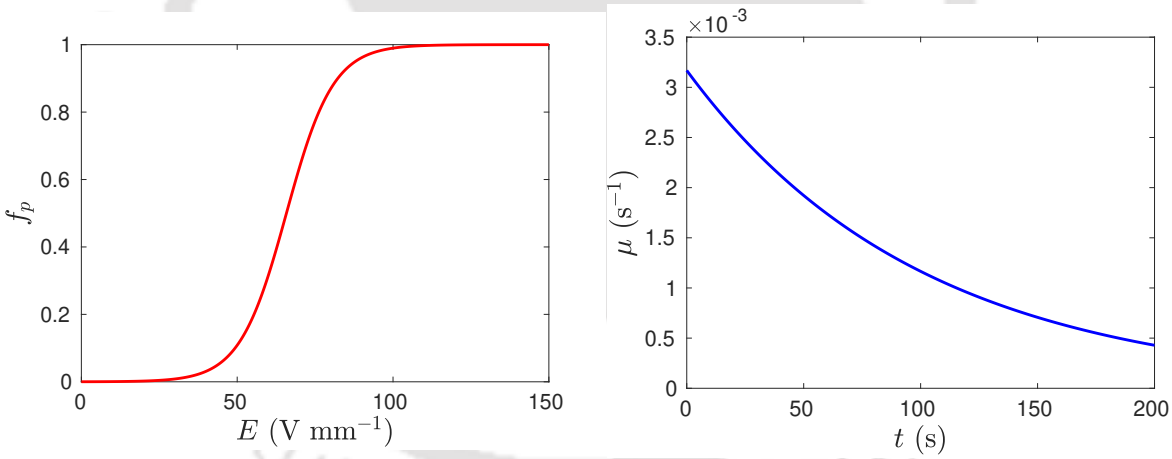

Figure 5.3: Represents (a) the changes of pore fraction coefficient (f_p) with the applied electric field and (b) the changes of MTC with time.

The drug transport from extracellular to intracellular space depends on the mass transfer rate through the cell membrane. This mass transfer rate depends on the pore fraction coefficient, which is an outcome of electroporation. The changes of f_p with the electric field are shown by the graph in Fig. 5.3a. It is observed that the pore fraction coefficient suddenly increases when the applied field crosses a certain limit (50 V mm^{-1}). The maximum value (= 1) of f_p is attained when the field is greater than 100 V mm^{-1}. In this model, The strength of the electric field is considered to be 60 V mm^{-1} to get a

higher value of f_p that enhances the mass transfer rate in the cell membrane. Also, this electric field does not cause irreversible electroporation as $E < E_{rev}$. Fig. 5.3b shows that the MTC decreases with time due to the effect of membrane resealing after completion of a pulse. If MTC decreases during mass transfer (OFF TIME), the drug uptake by the cells will be affected. Thus, in order to maintain a higher mass transfer rate, it is necessary to reopen the membrane pores by repeating pulses.

5.5.1 Drug transport phenomenon in the tissue

In this section, a complete overview about the drug transport from the point source to the tissue concerning the effects of drug losses from the boundaries of the tissue is discussed. The physical phenomenon of drug delivery with the prescribed boundary condition is highlighted through the picture given in the Fig. 5.4.

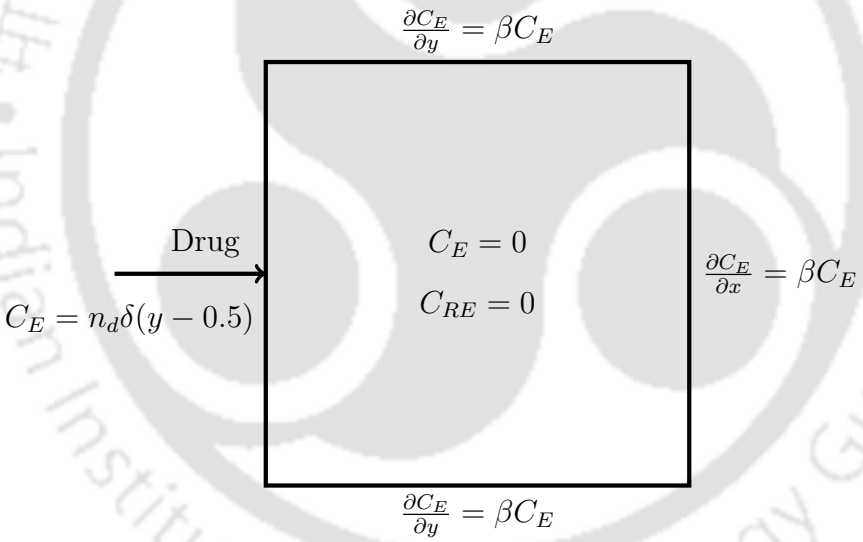

Figure 5.4: A schematic diagram of the model equations, which are presented in the Eqs. (5.6)-(5.9) for injecting drug into a biological tissue.

Fig. 5.5 represents the changes of drug concentration profiles in the ECS and ICS with time. In the figure, extracellular concentration initially increases sharply due to the diffusion of drug into the ECS from its source. Once the drugs start entering into the cells, the concentration decreases until it reaches an equilibrium state. On the other hand, intracellular concentration increases with time due to continuous drug intake into the cells. It is observed that both the profiles merge after a certain time due to drug saturation in the ECS and ICS.

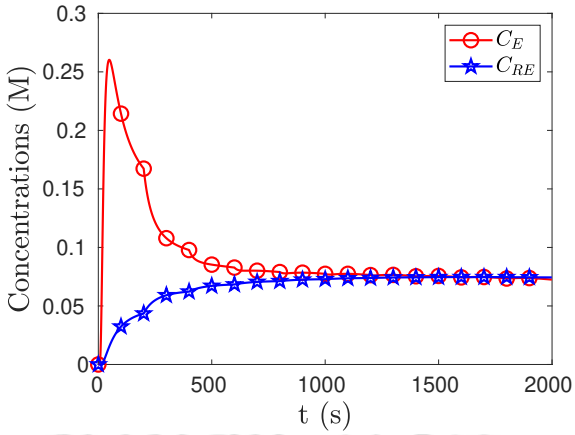

Figure 5.5: Temporal changes of drug concentrations (C_E, C_{RE}). Here, concentrations are obtained for $\beta = 0.1$ mm^{-1} at the point (0.5, 0.5).

Comparison

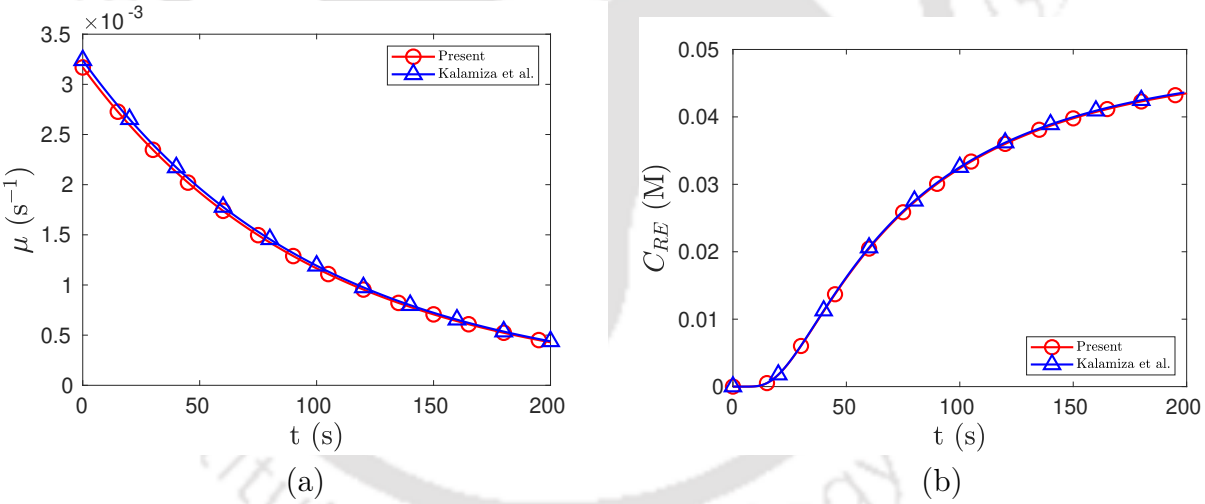

Figure 5.6: The results for MTC and intracellular drug concentrations are compared with the result of the existing model [56]. (a) To match MTC, $f_p = 2.7 \times 10^{-7}$ and $d_m = 5 \times 10^{-6}$ mm are taken. (b) The drug concentrations (C_{RE}) are calculated at (0.5, 0.5) for $P = 0.0005$ mm s^{-1}, $D = 0.001$ mm^2 s^{-1} and $PN = 1$.

In order to validate the present model, a comparison is made between the present results and the results of the model proposed by Kalamiza et al. [56]. The MTC that depends on membrane permeability is taken from the model [56]. There is no pore resealing term present in the MTC of the Kalamiza's model. For the sake of comparison with our results, the pore resealing term $\left(\exp\left(-\frac{t}{\tau}\right)\right)$ is included in the MTC $\left(\frac{3Df_p}{d_m r_c}\right)$ used by kalamiza et

al. [56] in their article, which can be expressed as,

$$\mu_k(t) = \frac{3Df_p}{d_m r_c} \cdot \exp\left(-\frac{t}{\tau}\right) = 0.0032 \cdot \exp\left(-\frac{t}{\tau}\right), \tag{5.12}$$

where $f_p = 2.7 \times 10^{-7}$ and $d_m = 5 \times 10^{-6}$ mm.

Fig. 5.6 presents the results for both MTCs given in the equations (5.5) and (5.12). It can be observed from the graphs that the results are in good agreement.

Effects of drug permeability on drug transport

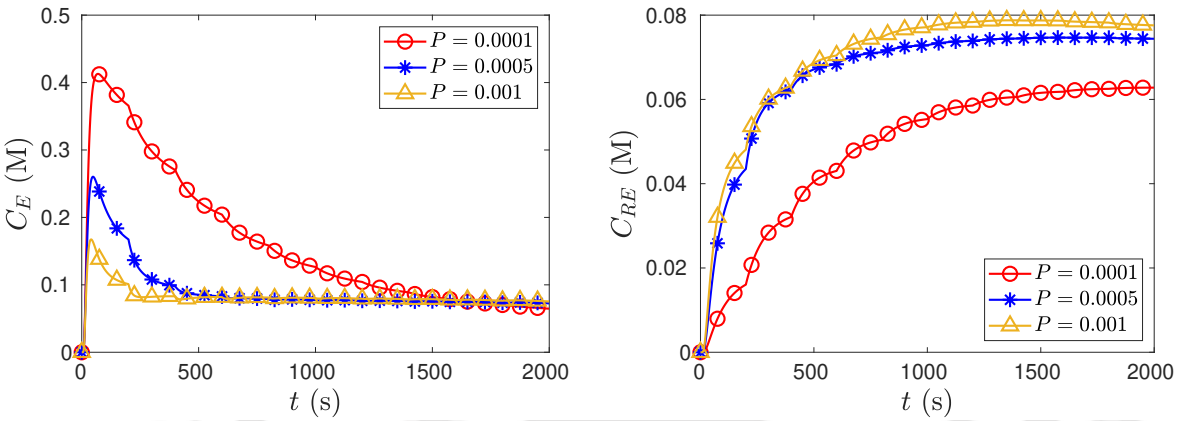

Figure 5.7: Time-dependent drug concentration profiles for different permeability of drug.

The drug transport from extracellular to intracellular space depends on MTC, which is a function of drug permeability (see eq. (5.5)). So, the drug permeability parameter plays an important role in the drug uptake into the cells. The permeability dependency on drug concentrations (C_E, C_{RE}) is described through the Fig. 5.7. It is noticed in the Fig. 5.7a that the drug concentration in the ECS decreases with time as there is a continuous drug uptake into the cells. Also, extracellular drug concentration decreases with the increase in drug permeability because intracellular drug uptake is more with the increase in permeability as shown in Fig. 5.7b.

Effects of drug loss on drug transport

The drug penetration throughout the extracellular media in the tissue for different rates of drug loss (β) at the tissue boundaries is described in Fig. 5.8. The results are plotted after performing 10 pulses of 1 ms with a rest time 200 s between two pulses. It is clearly noticed that the drug penetration in the tissue is affected with the increase of β. This is obvious as more drugs move outside from the tissue domain with the increase in β. It is

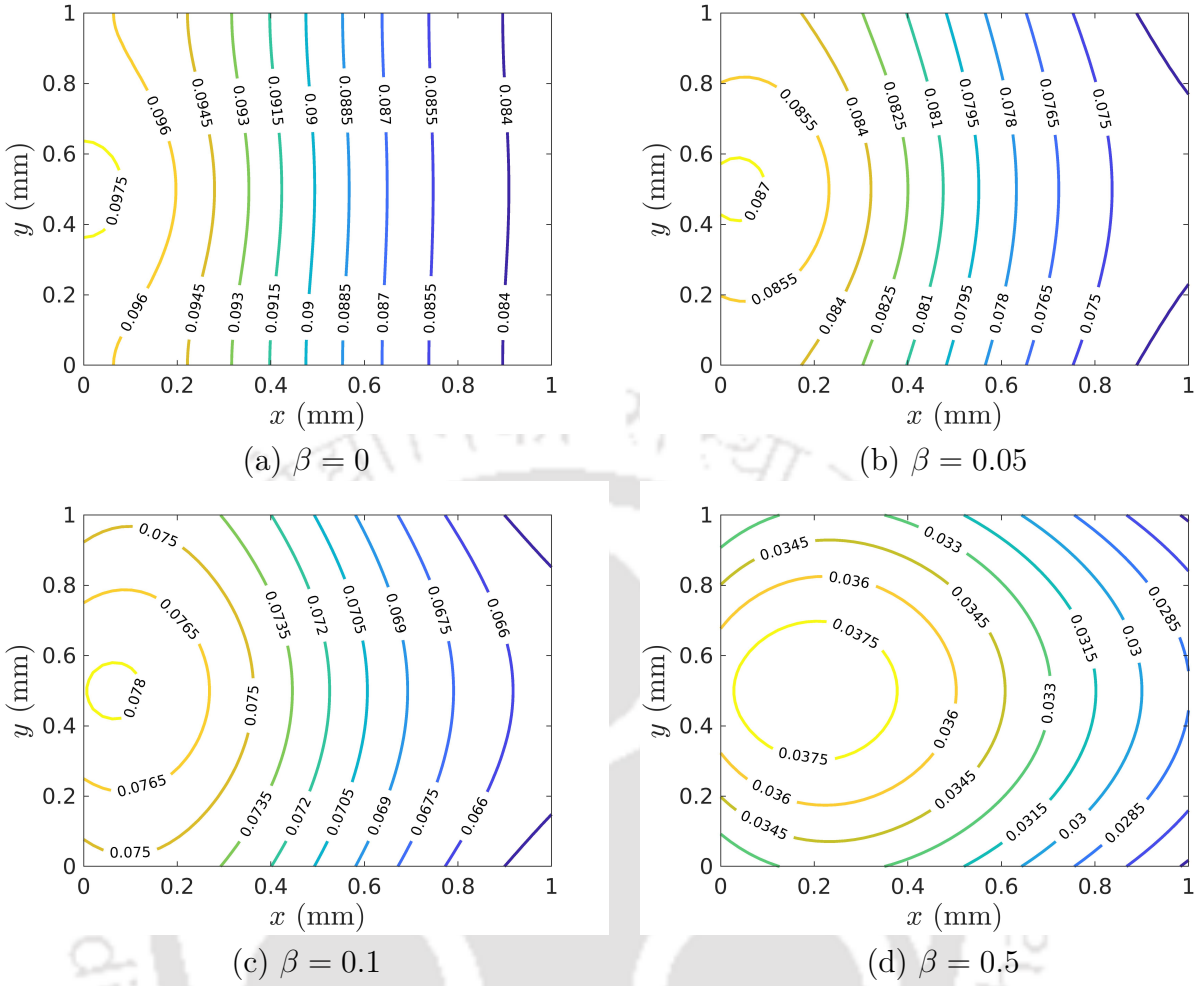

(a) $\beta = 0$ (b) $\beta = 0.05$

(c) $\beta = 0.1$ (d) $\beta = 0.5$

Figure 5.8: Drug distribution in the ECS after electroporation with 10 pulses of 1 ms for different values of β (mm $^{-1}$).

also observed in the Fig. 5.8d that the amount of drugs reach into the ECS is less for high value of β. However, higher amount of drugs enters into the ECS for lower value of β and maximum amount of drugs reaches for $\beta = 0$ (i.e., no drug loss from tissue boundaries) which is shown in the Fig. 5.8a.

Fig. 5.9 shows the spatial changes of cellular drug uptake in the tissue for different values of β. It is observed from the graphs that the drug uptake into the cells decreases with the increase in β. It may be due to the fact that fewer drugs reach in the ECS around cells for higher values of β, as observed in 5.8 so that less amount of drugs enters into the cells from ECS. Also, it is noticed from the contour plots that the amount of drugs intake into the cells decreases along x-axis from left to right as the drug source is located at the left boundary.

The temporal changes of drug concentrations in ECS and ICS for different values of the parameter β are illustrated by the Fig. 5.10. According to Fig. 5.10a, the extracellular

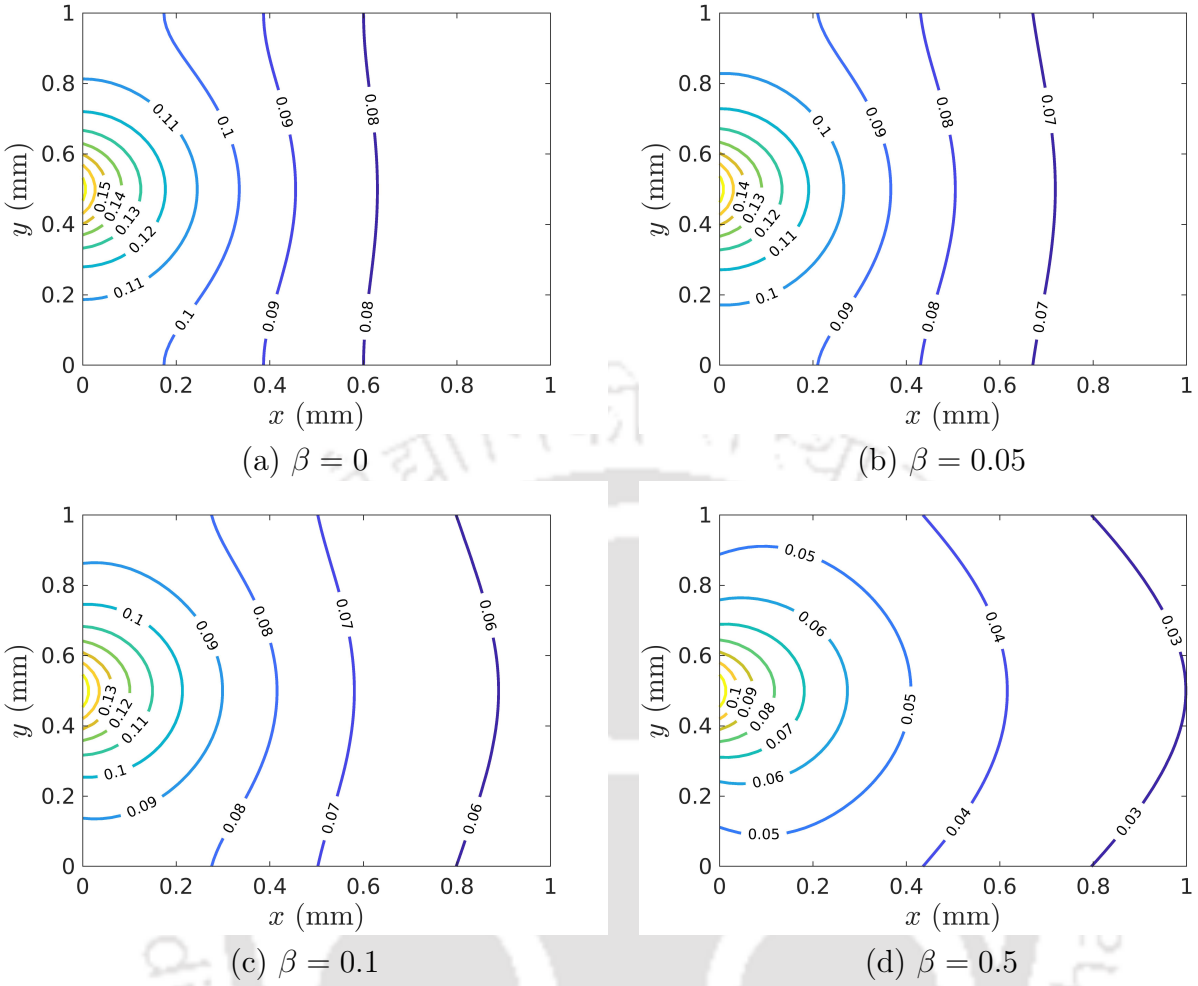

Figure 5.9: Drug distribution in the ICS after electroporation with 10 pulses of 1 ms for different values of β (mm^{-1}).

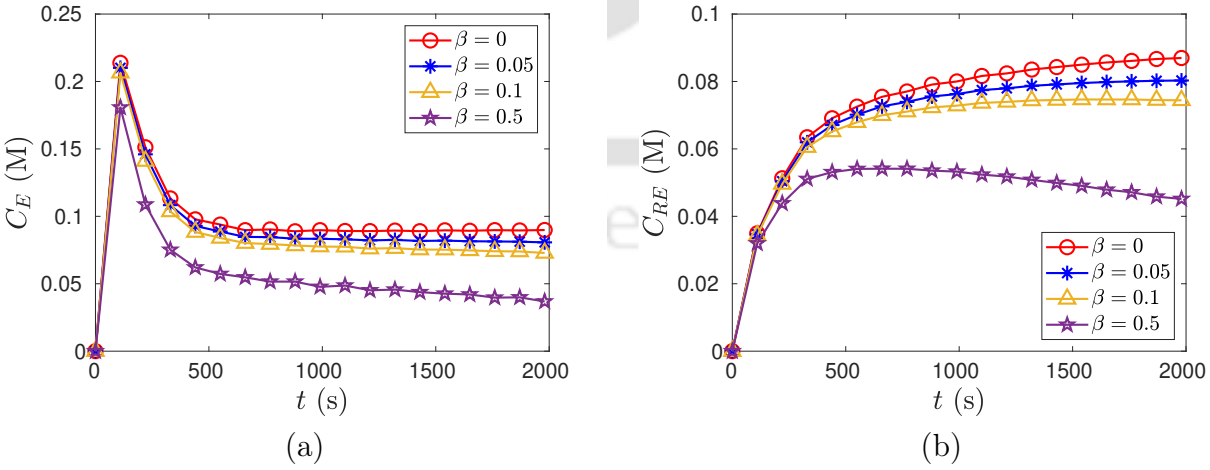

Figure 5.10: Time-dependent concentration profiles in (a) ECS and (b) ICS for different values of β (mm^{-1}).

drug concentration increases rapidly within the first pulse as a result of rapid drug diffusion in the ECS. It starts decreasing when the drug enters the cells and continues to do so until it reaches an equilibrium state. Fig. 5.10b shows that the intracellular drug profiles increase throughout the time for all values of β except $\beta = 0.5$. For the less values of β $(= 0, 0.05, 0.1)$, the concentration increases due to continuous drug intake into the cells with the application of repeated pulses and low rate of drug losses. For the higher value of β $(= 0.5)$, the cellular drug uptake increases initially but after a certain time ($\approx$ 500 s), it decreases due to huge drug losses.

Effects of pulse number on drug transport

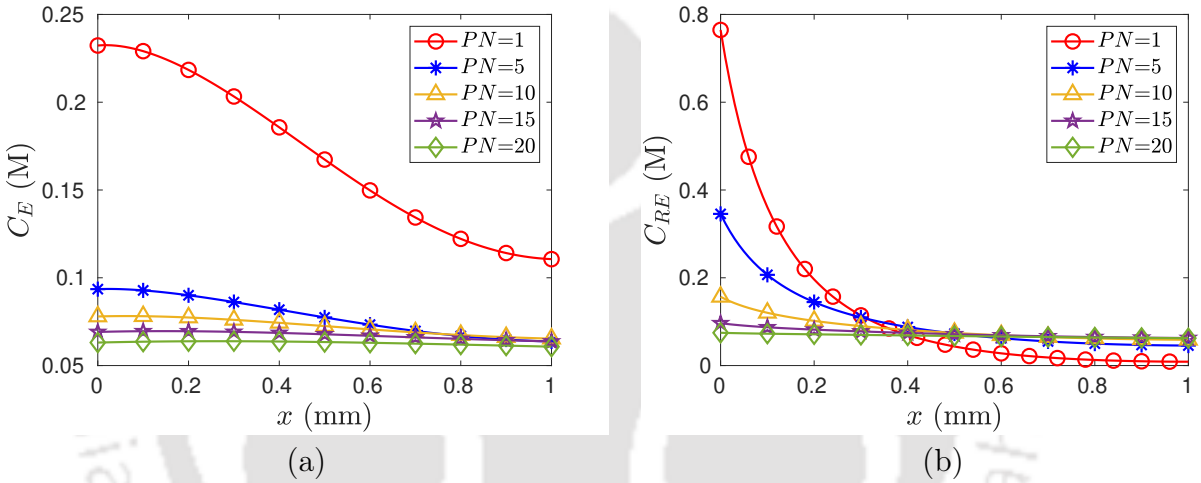

Figure 5.11: Concentration changes along x-axis in (a) ECS and (b) ICS at $y = 0.5$ for $\beta = 0.1$ mm^{-1} and different pulse numbers.

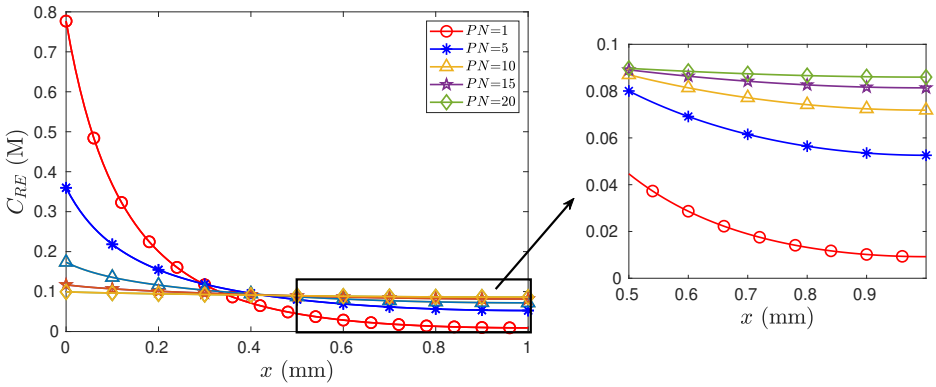

Figure 5.12: Concentration changes along x-axis in ICS at $y = 0.5$ for $\beta = 0$ mm^{-1} and different pulse numbers.

In this model, multiple pulses are applied to enhance the drug transport rate into the cells. If a single pulse is applied and mass transport occurs for a long duration, the mass transfer rate slows down due to pore resealing effects. Fig. 5.11 describes the changes of drug concentrations in ECS and ICS with the variation of the pulse number. It is seen from Fig. 5.11a that the extracellular concentration decreases with the increase in pulse number. The possible reasons are: (i) the increment of drug intake into the cells with the increase in pulse number; (ii) the drug loss from the tissue boundaries (as $\beta = 0.1$). In Fig. 5.11b, it is noticed that the intracellular drug concentration decreases with pulse number in the region $0 \leq x < 0.4$ and increases in the region $0.4 \leq x \leq 1$ of the tissue. This opposite behavior before and after $x = 0.4$ is noticed due to continuous drug diffusion from left to right and ongoing drug introduction into the cells in the domain $0.4 \leq x \leq 1$. Fig. 5.12 is plotted when there is no drug loss (i.e, $\beta = 0$) to show the actual effects of pulse number. One observation is made from the figure that multiple pulses are required for the uniform drug distribution into the targeted cells of the tissue. It is concluded from the above discussion that the drug concentrations in both the regions ECS and ICS reach a stable state after the application of a certain number of pulses ($PN = 20$, in this case). Hence, for this model, the maximum number of pulses is 20, which is enough to inject a sufficient quantity of drug into the cells uniformly.

5.6 Conclusions

The present study proposes an improved mathematical model for drug delivery in which a point source drug is introduced at the tissue boundary. The effects of drug loss from the boundary of the targeted tissue is also emphasized through this model. The following significant observations are made from this study:

- The prescribed model is capable of describing a complete overview of drug transport phenomena in the targeted tissue with reversible electroporation.
- In the electroporation based drug delivery, the Dirac-delta function is used to represent the point source drug more appropriately.
- The model deals with Neumann boundary condition to incorporate the drug elimination process from the tissue.
- The drug loss from the tissue boundaries is an important factor in drug transport. The model captures the mechanism of drug dose.
- It is observed that the drug uptake into the cells increases with applications of multiple pulses.

- It is also seen that the cellular drug uptake is improved for smaller values of β.
- The drug uptake into the cell becomes slow, even if multiple pulses are applied, due to huge drug loss at the tissue boundaries.
- Uniform drug distribution into the cells is done successfully. So, the model configuration is a successful tool to treat the whole targeted tissue by introducing drug as a medicine.

The proposed model could be helpful in pharmaceutical industry and medical sciences.

CHAPTER 6

DRUG METABOLISM AFTER ENTERING INTO THE CELLS

In chapter 5, we have solved a model that deals with reversible electroporation, point source drug and the effects of drug loss. In this chapter, we have developed a mathematical model which is an extension of the previous model (chapter 5) with the inclusion of cellular drug metabolism effect.

6.1 Introduction

Physiologically, drug metabolism is a biotransformation process in which pharmaceutical substances get transformed in the body. The liver is mostly responsible for drug metabolism processes because it contains enzymes that facilitate the reactions. Metabolism occurs in the body to change the chemical structure of the substance, allowing it to be excreted more easily. During drug metabolism, various reactions take place, such as oxidation, reduction, hydrolysis, hydration, conjugation, condensation, and isomerization. Generally, a drug becomes inactivated once it gets metabolized. On the other hand, some metabolized drugs might be pharmacologically active and affect the body. However, the active metabolite form of drugs makes the medicine effectives. In addition, mathematical modeling of drug metabolism and transport in the tissue is crucial for the pharmaceutical industry since it provides an improved platform for drug development and in vivo experiments [83].

In this study, we focus the process of drug metabolism in the cells during mass transport. To deal with that effects, one reaction term is added in the mass transport equation for intracellular space. The combined effects of both the reactions, such as boundary drug loss in extracellular space and drug metabolism in intracellular space, are studied in this model. The modified mass transport equations for finding drug concentrations in extra-

cellular and intracellular spaces are solved. A detailed discussion is made to examine the effects of the electric field, drug permeability, metabolism parameters, and pulse number on mass transport.

6.2 Problem Formulation

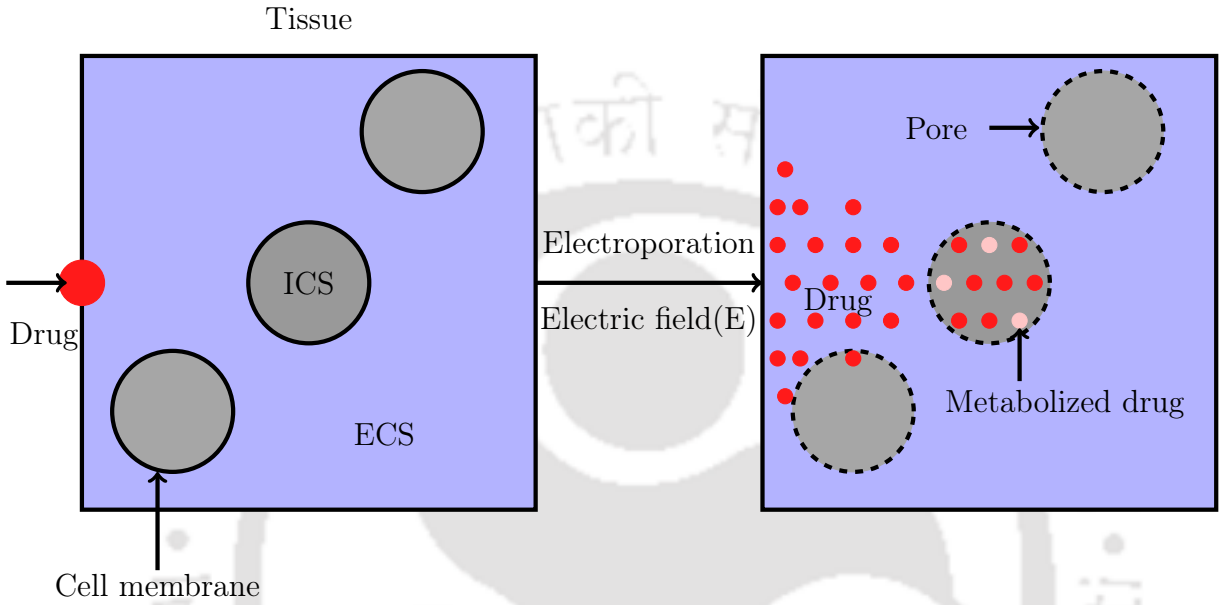

Figure 6.1: Schematic diagram of drug injecting and drug metabolism processes in a biological tissue.

The model considers a biological tissue that contains diseased cells and requires treatment. The tissue region is assumed to be cubical in structure and in 2D view it appears square. There are two structural parts of a tissue: extracellular space and intracellular space. The cell membrane separates both spaces, restricting the mass transport from the extracellular into the intracellular compartment. Both the spaces are separated by the porous cell membranes, which control the mass transport phenomenon. The Fig. 6.1 depicts an overview of the entire tissue structure and how the drug is injected into the tissue cells. Electric fields are applied on the tissue to permeabilize cell membranes.

Fig. 6.2 is a diagram of the electroporation configuration for this model. Electroporation is performed by placing electrodes at the upper and lower edges of the tissue. In this experiment, the positive and negative electrodes have potentials of ϕ_L and ϕ_0, respectively. Electric pulses increase the transmembrane potential, causing the cell membrane to become permeable. As a result, formation of nanometer-sized pores in the cell membrane takes place and there is an increase in the pore fraction coefficient (f_p). Repeated pulses are applied to the tissue over a specific period of time with a temporal gap between them. The mass transport occurs in the rest time when the pulse is off. The pore resealing also

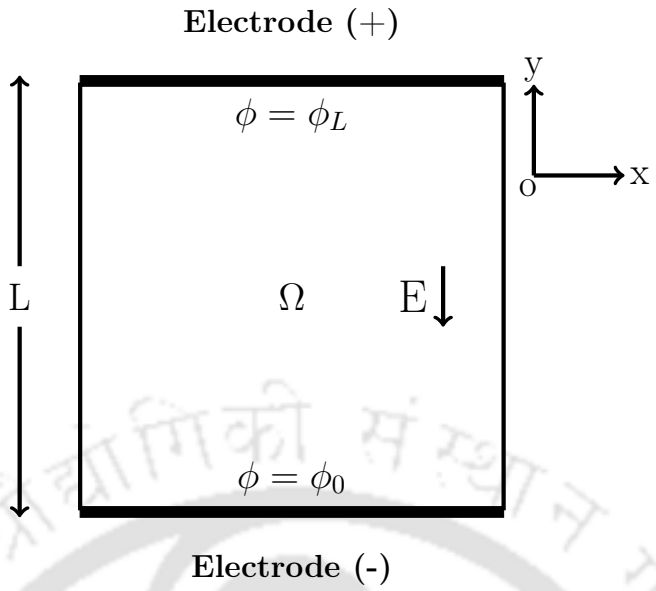

Figure 6.2: A schematic representation of electroporation of a tissue.

occurs during this rest time. Drug transport slows down during the resealing period due to a decrease in pore area. Multiple pulses are applied to reopen the pores.

Drug particles diffuse from its source in the extracellular space and enter the cells through the membranes when pore formation occurs. After reaching the cells, some drugs metabolize and become another form of drug (see Fig. 6.1). As a result of drug metabolism, the amount of pure drugs given initially is reduced in the cell. This study examines the effects of metabolism on drug transport in details using mathematical modeling. The governing equations for describing the physical circumstances are provided below.

6.3 Model Development and Mathematical Equations

The arrangement of two parallel electrodes produces a uniform electric field in the tissue domain. The potential (ϕ) distribution within the tissue can be calculated by the given equation [9, 13, 77]

$$\vec{\nabla} \cdot (\sigma \cdot \vec{\nabla}\phi) = 0, \tag{6.1}$$

with boundary conditions: $\phi(y = 0) = \phi_0$ and $\phi(y = L) = \phi_L$, where σ is the tissue electrical conductivity.
The uniform electric field (E) is obtained by

$$E = |\vec{\nabla}\phi| \tag{6.2}$$

6.3.1 Relation between σ and E

One of the purposes of electroporation is the creation of pores in the cell membrane. In addition to the effects of pore formation, the deformation of the cell membrane affects the extracellular conductivity. There are many studies [12,51,77] that have examined the functional dependence of electrical conductivity on electric field. According to the experimental and computational study, electrical conductivity changes during electroporation and is dependent on the applied electric field, which is expressed as,

$$\sigma(E) = \left[\frac{\sigma_{\max} - \sigma_{\min}}{1 + \gamma_1 \cdot \exp\left(-\frac{E-a}{b}\right)}\right] + \sigma_{\min}, \tag{6.3}$$

$$a = \frac{E_{\text{rev}} + E_{\text{irrev}}}{2} \text{ and } b = \frac{E_{\text{irrev}} - E_{\text{rev}}}{\gamma_2},$$

where E_{rev} and E_{irrev} are respective threshold values for reversible and irreversible electroporation, $\sigma_{\min}$ and $\sigma_{\max}$ are the minimum and the maximum tissue electrical conductivity respectively, γ_1 and γ_2 are the sigmoidal functional parameters.

6.3.2 MTC calculation

The induced electric field causes the transmembrane potential to increase, resulting in the permeabilization of the cell membrane. Membrane permeability increases due to electroporation and pore formation, and this is determined by the pore fraction coefficient of the cells that are reversibly electroporated. Argus et al. [1] introduced a symmetric sigmoid function in their model to evaluate the pore fraction coefficient (f_p), which is defined as,

$$f_p = \left[1 + \exp\left(\frac{E_f - E}{b_f}\right)\right]^{-1}, \tag{6.4}$$

where E_f and b_f are the fitting parameters.

The permeability of drug plays an important role in the mass transport through the cell membrane. Therefore, the mass transfer rate in the cell membrane depends on f_p that is caused by the membrane permeabilization and drug permeability, which depends on the nature of the drug. During rest time in the process of drug transport, the mass transfer rate decreases due to resealing effects. Hence, combining all of those factors, the mass transfer coefficient (MTC) can be formulated mathematically as,

$$\mu(t) = \frac{P f_p}{r_c} e^{-\frac{t}{\tau}}, \tag{6.5}$$

where P is the drug permeability, r_c is the cell radius and τ is the resealing constant.

6.3.3 Drug transport phenomenon in the tissue

Using the mass transport equation, the concentrations of drugs in the extracellular space and in the cells (reversibly electroporated) are calculated as,

$$\frac{\partial C_E}{\partial t} = \vec{\nabla}.\left(D\vec{\nabla}C_E\right) - \left(\frac{1-\varepsilon}{\varepsilon}\right)\mu(t) \times (C_E - C_{RE}), \tag{6.6}$$

$$\frac{\partial C_{RE}}{\partial t} = \mu(t) \times (C_E - C_{RE}) - S_M \tag{6.7}$$

with the following initial and boundary conditions:

$$\left.\begin{aligned} &C_E(x,y,0) = C_1(x,y), && C_{RE}(x,y,0) = 0, \\ &\left(\frac{\partial C_E}{\partial x}\right)_{x=0} = \beta C_E, && \left(\frac{\partial C_E}{\partial x}\right)_{x=L} = \beta C_E, \\ &\left(\frac{\partial C_E}{\partial y}\right)_{y=0} = \beta C_E, && \left(\frac{\partial C_E}{\partial y}\right)_{y=L} = \beta C_E, \end{aligned}\right\} \tag{6.8}$$

The source term that represents the drug metabolism effects [54] is expressed as

$$S_M = \frac{V_{\max} C_{RE}}{C_{RE} + K_m}, \tag{6.9}$$

where C_E and C_{RE} are the drug concentrations in extracellular space and reversible electroporated cells respectively; D is the effective diffusion coefficient of the drug in the extracellular space; ε is the porosity of the membrane pores; $V_{\max}$ is the maximum metabolic rate; K_m is the intracellular drug concentration where metabolism rate is half of $V_{\max}$; β represents the rate of mass (drugs) loss from the tissue boundary and depends on the tissue's boundary properties.

The drug injection through a particular point/location of the tissue boundary is mathematically defined as

$$C_1(x,y) = \begin{cases} n_d\delta(y-0.5), & x = 0 \\ 0, & \text{otherwise} \end{cases}$$

$\delta(y)$ is the Dirac delta function, which can be symbolically expressed by

$$\delta_d(y) = \frac{1}{d\sqrt{\pi}} \exp\left(-\frac{y}{d}\right)^2, \quad 0 < d < 1. \tag{6.10}$$

Table 6.1: The parameter's detail used for simulation of the model:

Symbol	Value	Description	Source
$\sigma_{\min}$	0.0 S m^{-1}	Minimum electrical conductivity	[1]
$\sigma_{\max}$	0.241 S m^{-1}	Maximum electrical conductivity	[1]
E_{rev}	46 V mm^{-1}	Threshold value for reversible electroporation	[1]
E_{irrev}	70 V mm^{-1}	Threshold value for irreversible electroporation	[1]
γ_1	8	Electrical conductivity parameter	[1]
γ_2	10	Electrical conductivity parameter	[1]
E_f	65.8 V mm^{-1}	Fitting parameter for MTC	[1]
b_f	7.5 V mm^{-1}	Fitting parameter for MTC	[1]
r_c	50 μm	Cell radius	[49]
D	10^{-3} mm^2 s^{-1}	Effective diffusion coefficient	
ε	0.18	Porosity of the membrane pores	[56]
P	5×10^{-4} mm s^{-1}	Permeability of drug	[38]
E	60 V mm^{-1}	Electrical field	
L	1 mm	Length of the rectangle	Fig. 6.2
ϕ_L	60 V	Potential on positive electrode	Fig. 6.2
ϕ_0	0 V	Potential on negative electrode	Fig. 6.2
PN	10	Pulse number	
t_{ep}	1 ms	Pulse length (ON TIME)	
t_M	100 s	Time for mass transfer (OFF TIME)	
n_d	100	Number of dose	
d	10	Constant in Dirac-delta function	
β	0.1 mm^{-1}	Rate of mass loss at the boundary	
$V_{\max}$	10^{-6} M s^{-1}	Maximum metabolic rate	[10]
K_m	10^{-4} M	Drug concentration where metabolism rate is $\frac{V_{max}}{2}$	[10]

6.4 Method of Solution

The governing equations (6.1)-(6.10) prescribed in this model are solve numerically. To obtain complete solutions, the following steps are needed to follow:

- Step 1: Equations (6.1)-(6.3) are solved to find electric field according to the electrode arrangement described in Fig. 6.2.
- Step 2: Using this electric field, the pore fraction rate coefficient is obtained by the equation (6.4).
- Step 3: The MTC is calculated by Eq. (6.5).
- Step 4: The equations (6.6)-(6.10) are solved numerically using finite difference method.
- The details of the parameters used in this model are given in the Table 6.1.

The equations (6.6) - (6.9) are discretized using the forward time centered space (FTCS) scheme. The discretized equations are as follows,

$$\begin{aligned}(C_E)_{i,j}^{n+1} =& a\,(C_E)_{i+1,j}^{n} + a\,(C_E)_{i-1,j}^{n} + b(t)\,(C_E)_{i,j}^{n} \\ &+ c\,(C_E)_{i,j+1}^{n} + c\,(C_E)_{i,j-1}^{n} + d(t)\,(C_{RE})_{i,j}^{n},\end{aligned} \tag{6.11}$$

$$(C_{RE})_{i,j}^{n+1} = (C_{RE})_{i,j}^{n} + \mu(t)\Delta t\left[(C_E)_{i,j}^{n} - (C_{RE})_{i,j}^{n}\right] - \frac{V_{\max}\,(C_{RE})_{i,j}^{n}}{(C_{RE})_{i,j}^{n} + K_m}, \tag{6.12}$$

where

$$\begin{aligned} &i = 1, 2, \cdots, M_1 \\ &j = 1, 2, \cdots, M_2 \\ &a = \frac{D\Delta t}{(\Delta x)^2}, \\ &b(t) = 1 - \left[2D\left(\frac{1}{(\Delta x)^2} + \frac{1}{(\Delta y)^2}\right) + \frac{1-\varepsilon}{\varepsilon}\mu(t)\right]\Delta t, \\ &c = \frac{D\Delta t}{(\Delta y)^2}, \\ &d(t) = \frac{1-\varepsilon}{\varepsilon}\mu(t)\Delta t. \end{aligned}$$

Here, Δt is the time step size, Δx and Δy are the step sizes for space, M_1 and M_2 are the numbers of grids along x-axis and y-axis respectively. In order to satisfy the stability condition described in chapter 5, $M_1 = 101$, $M_2 = 101$, $\Delta x = 0.01$, $\Delta y = 0.01$, and $\Delta t = 0.2$ are used for computations.

6.5 Results and Discussion

Using mathematical modeling and numerical simulation, the present study describes the drug transport phenomenon in diseased tissues. This study primarily focuses on the results for the combined effects of drug metabolism and drug elimination from the tissue. The graphical representations in Figs. 6.3 - 6.7 are provided to analyze mass transport behavior into the electroporated tissue qualitatively. The following sections provide further details about the results for different drug permeabilities, metabolic rate, and pulse numbers.

6.5.1 Drug transport in the tissue

The drug concentrations profiles, in different compartments of the tissue, that change with time, are shown in Fig. 6.3. In Fig. 6.3a shows that the extracellular drug concentration

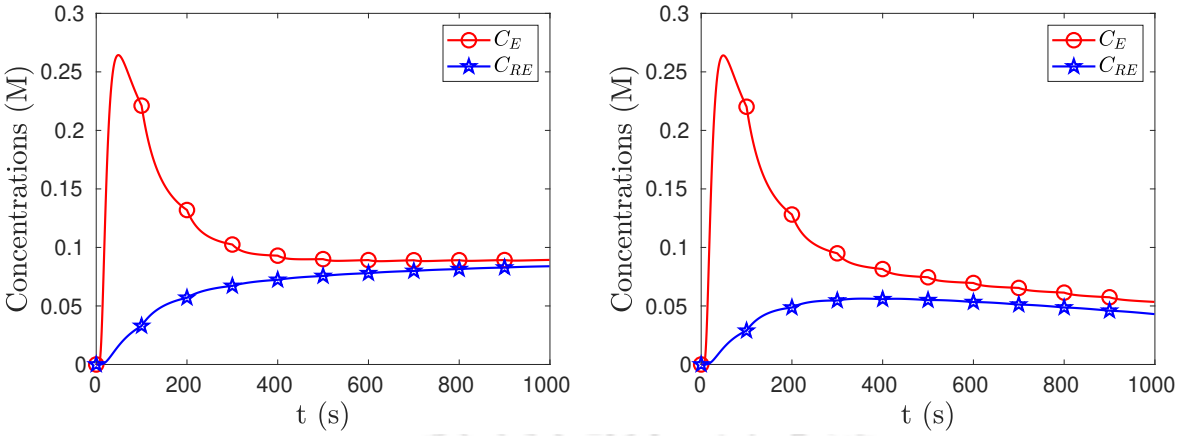

(a) Without metabolism ($V_{\max} = 0$ M s^{-1}) (b) With metabolism ($V_{\max} = 10^{-6}$ M s^{-1})

Figure 6.3: Intracellular drug concentration vs time at (0.5, 0.5).

decreases from its peak value and cellular drug concentration increases with time in the absence of drug metabolism. After some time (400 s), both profiles are approaching to each other to merge together due to dug saturation. On the other hand, in Fig. 6.3b the drug concentrations initially increase and after some time decrease asymptotically. Profiles do not tend to merge due to drug metabolism in the cell. Since some drugs are metabolized after reaching the cell, intracellular drugs decrease continuously. Due to concentration gradient, drug diffusion from extracellular to intracellular domains occurs, and therefore, the extracellular concentration continues to decrease over the rest of the time.

6.5.2 Effects of E on drug transport

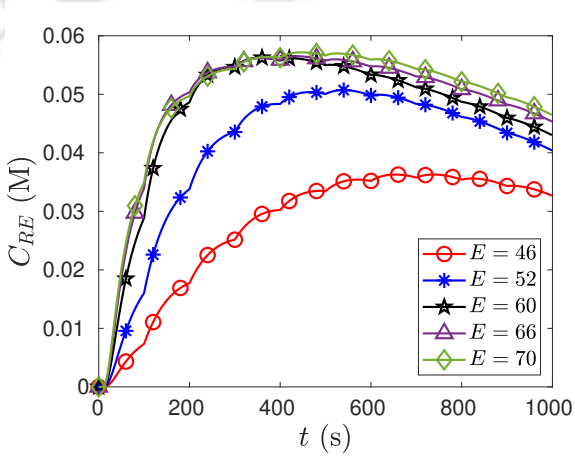

Figure 6.4: Drug concentration vs time for different values of E (mm s^{-1}).

Several experiments are conducted with this model using various electric fields to

understand the role of the pulse strength on drug uptake and the corresponding results are shown in Fig. 6.4. Suitable fields are chosen in the range of $46 - 70$ V mm^{-1} for reversible electroporation. The plotted graphs show that intracellular drug uptake increases with the strength of pulses. Further, it is observed that $E = 60$ is enough to maximize drug uptake, and that uptake is similar for higher electric fields ($E = 66, 70$). It is insignificant to use stronger fields than 60. For the purposes, the electric field $E = 60$ is therefore considered throughout this study.

6.5.3 Drug metabolism in the cells

To clearly observe the effects of drug metabolism in cellular drug uptake, the roles of metabolism parameter $V_{\max}$ is thoroughly investigated in this study. The detailed analysis is provided in the next section.

Effects of $V_{\max}$

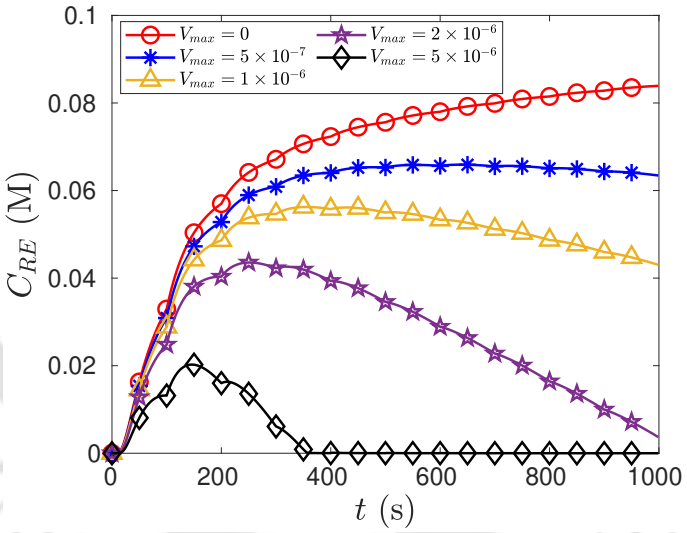

Figure 6.5: Intracellular drug concentration vs time for different values of $V_{\max}$ (M s^{-1}).

One of the important parameters for drug metabolism inside a cell is the maximum metabolic rate ($V_{\max}$), which is present in the reaction term given in Eq. (6.9). In order to observe the effects of $V_{\max}$ on drug uptake, the model is solved for different values of $V_{\max}$ and the results are graphically presented in Fig. 6.5. The figure shows that intracellular drug concentration reduces with higher metabolism rate. It is observed that the metabolism effect on drug uptake is not much significant when $V_{max} < 10^{-6}$. However, the metabolism effect is higher for $V_{max} \geq 2 \times 10^{-6}$, and as a result the intracellular drug concentration is rapidly reduced. If $V_{\max} \geq 2 \times 10^{-6}$, the drug concentration in the cell increases initially with time, then decreases as time progress, and finally it reaches to

zero. Accordingly, all drugs that reach into the cell are metabolized within the process for these values of $V_{\max}(\geq 2 \times 10^{-6})$. So, on completion of drug transport, every cell contains only drugs metabolites.

6.5.4 Effects of P on drug transport

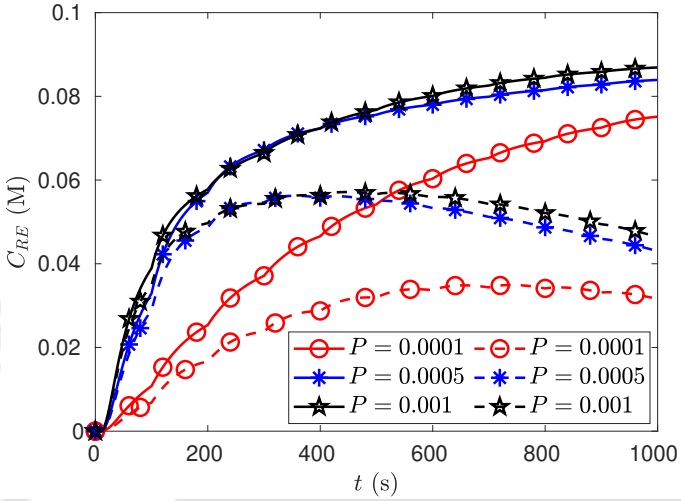

Figure 6.6: Intracellular drug concentration vs time for different values of P (mm^2 s^{-1}). Solid lines '-' indicate the results without metabolism and dashed lines '- -' indicate the results with metabolism.

Drugs can be classified as either highly permeable, low permeable, or impermeable depending on their permeability. Various tests on drug permeability are conducted to identify the proper class of drugs that can be easily injected into the cell. Fig. 6.6 illustrates the results for different drug permeabilities with and without drug metabolism effects. It is seen that the intracellular concentration increases with the increase in drug permeability. It is also seen that the drug concentration reduces when metabolism is considered. In addition, the amount of pure drugs (that initially injected) within the cells become less due to metabolic changes.

6.5.5 Effects of PN on drug transport

In this study, multiple pulses are applied over a specific period of time to maintain a higher mass transfer rate in the cell membrane, which allows for faster drug uptake into the cell. The model equations are solved for various pulse numbers (PN) in order to analyze the role of repeat pulses. Fig. 6.7 represents the effects of pulse number in drug delivery into the cells. In Fig. 6.7a when metabolism is not considered, the drug uptake decreases with PN in the tissue region $0 \leq x < 0.4$ and increases slightly in the region $0.4 \leq x < 1$. It is because the cells closer to the drug source absorb the drug more quickly,

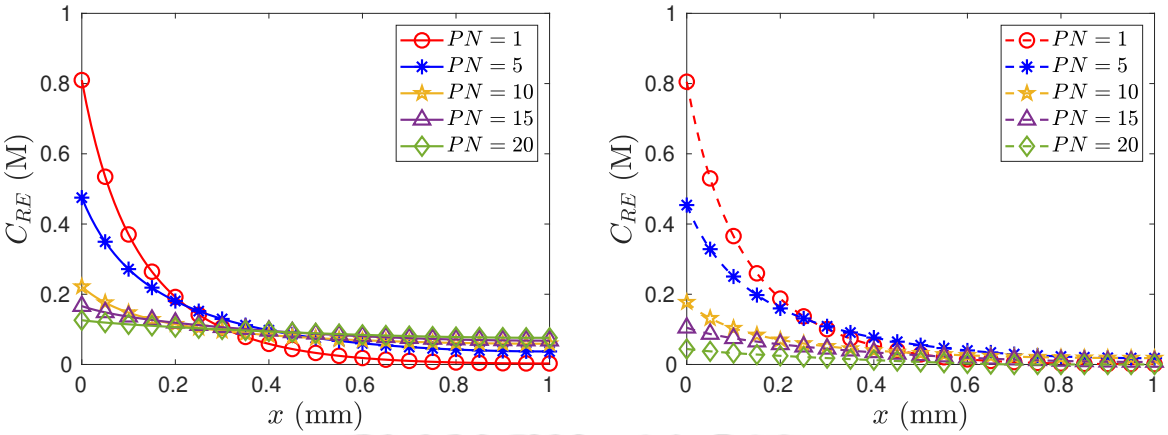

(a) Without metabolism ($V_{max} = 0$ M s^{-1}) (b) With metabolism ($V_{max} = 10^{-6}$ M s^{-1})

Figure 6.7: Intracellular drug concentration vs time for and different PN.

whereas cells away from the drug source need more number of pulses to reach the same level of drug absorption. Furthermore, it is observed that uniform drug uptake occurs into all cells of the tissue with the increase in PN. If metabolism effects are taken into account, the drug uptake into the cells decreases with PN throughout the tissue domain, which is shown in Fig. 6.7b. This happens due to the combined effects of drug loss from the tissue boundaries and drug metabolism in the cells.

6.6 Conclusions

This study proposes an improved mathematical model for drug delivery that focuses on the drug metabolism process. The model considers only reversible electroporation to treat all cells by delivering drug. Proper electrode configuration is made in order to permeabilize all the cells of the targeted tissue. The model equations are solved numerically using FDM and the grid independent results are provided.

This study found the following important outcomes:

- This model is more realistic in the area of electroporation-based drug delivery since it incorporates the important process of drug metabolism.
- The combined effect of drug loss from the extracellular space and drug metabolism in the cells on mass transport is investigated for the first time.
- To maximize the drug absorption by the targeted cells, the appropriate electric field and types of drugs are found.
- The application of multiple pulses is needed for uniform drug distribution into the cells and enhancement of the mass transport rate.

- Due to metabolism, some metabolites of drugs are formed in the cells and the amount of pure drugs gets reduced.
- It is shown that all drugs in the cells are metabolized within the process of mass transport (1000 s) if $V_{max} > 2 \times 10^{-6}$.

CHAPTER 7

CONCLUSIONS AND FUTURE SCOPE

7.1 Conclusions

A key aspect of electroporation is that a wide range of molecules, ions, drugs, proteins, DNA etc. can be directly inserted into living cells. It has already been tested clinically for head and neck cancers with negligible side effects using electrochemotherapy, which utilizes electroporation to increase the bioavailability of anti-cancer drugs in tumour cells. As experimental findings most of the time fail to completely describe the characterization of such drug delivery processes, so it is important to improve the existing mathematical models.

The present dissertation provides some mathematical models for drug delivery using electroporation. The models deal with the drug transport through extracellular space into the electroporated cells of a biological tissue. The principal observations that are found from the proposed models in this thesis are summarized below.

The study provides a comprehensive overview of drug transport phenomena into the targeted cells through the use of tissue electroporation, as it captures the complete picture from membrane permeabilization to drug metabolism. The proposed models considers reversible as well as irreversible electroporation, and membrane resealing. Through a comparative investigation, it is observed that drugs can be injected during and after the pulse application. The model equations are solved numerically or analytically, depending on their complexities. Analytical solutions for drug concentrations in different compartments are provided. Through graphical depictions, quantitative analysis illustrates biological and physical phenomena in more details. Physiological characterization of a tissue correlates well with each and every visualization observed in the graphical representations. The results of this study agree well with the theoretical and experimental results of the existing research.

This research develops a mathematical model that focuses on the penetration of drugs into a single cell. It is observed that the drug entry into the cell through the different locations of the cell membrane is not similar due to the nonhomogeneous membrane permeabilization and pore formation. In order to compute the mass transport across the cell membrane, the permeable interface method is used in the numerical simulation. The appropriate electric field and class of drugs are determined for faster drug entry into the target cell. The model can be used to treat cancer and tumour cells.

Thermal changes in the tissue due to Joule heating caused by the application of pulses are studied. During electroporation, tissue temperature is found to rise with time from the initial body temperature (310.15 K) and attains its maximum value (314.335 K) at the end of a pulse (80 ms). Once the pulse stops, the tissue temperature begins to decrease, and during the rest period when mass transfer takes place, the tissue temperature returns to its normal level. There is no cell damage as the maximum increased temperature (314.335 K) is less than the possible temperature (315.15 K) of cell damage. Both temporal and spatial changes in drug concentration are explained through graphical representations.

Based on the membrane permeabilization and pore formation, mass transfer coefficient (as a function of pore density) is developed and used in mass transport equations to calculate drug concentrations in various compartments. The effects of different parameters, such as electric field, drug permeability, effective diffusion coefficient, pulse length and number of pulses on drug concentrations are discussed. A sensitivity analysis of some important parameters is performed. It is found that concentrations of drugs (C_E, C_{RE}, C_{IRE}) are most sensitive to P, whereas they are least sensitive to V_{ep}.

The concept of a point source drug as a dose of medicine is introduced in this model. The process of drug elimination from tissue is also studied once the drug reaches the extracellular space. The loss of drugs from the tissue in the process of elimination affects the drug uptake into the cells. To analyze the combined effects of drug elimination and drug metabolism, an improved model for drug delivery in a diseased tissue is also proposed. In this study, one of the most important findings is that intracellular drugs are completely metabolized during the drug transport process.

Furthermore, the models are validated by comparing the results of the present works with the results available in the existing literature. Thus, the current mathematical models described in this thesis may act as optimization tools to improve the drug delivery process through electroporation. This research work will open up many possibilities regarding combined use of electroporation with other efficient drug delivery methods, like iontophoresis to yield more useful data that improves electroporation. The proposed mathematical models can be used in order to improve drug delivery in tissues through the electroporation approach. This research work could be helpful in various clinical studies once experimental validations are performed.

7.2 Future Scope

The latest model of our study takes into account the metabolism process for a better outcome. In order to directly relate to the real physical situation, mathematical models for drug delivery can be improved by including many other processes. The following are some future directions of the current study.

- Future models for electroporation-based drug delivery into diseased cells may include
  (i) the effects of drug absorption and drug clearance,
  (ii) nonhomogeneous tissue media and nonuniform electric fields.
- Experimental research (*in vitro* and *in vivo*) on the proposed models can be conducted to utilize the results in real life applications.
- The single cell model can be generalized including the effects of irreversible electroporation that may be useful in the treatment of cancer and tumour cells.
- In this study, we have noticed that there is a significant increment in the tissue temperature due to electroporation. The effects of temperature on electrical conductivity can be incorporated into future models.
- The multiscale approach can be used for solving mass transport equations to find drug concentrations in different domains.

BIBLIOGRAPHY

[1] F. Argus, B. Boyd, and S. M. Becker. Electroporation of tissue and cells: A three-equation model of drug delivery. *Computers in Biology and Medicine*, 84:226–234, 2017.

[2] S. Becker. Modeling transdermal delivery by electroporation: The thermodynamic approach. In *Handbook of Electroporation*, pages 1–17. Springer International Publishing, 2016.

[3] S. Becker, B. Zorec, D. Miklavčič, and N. Pavšelj. Transdermal transport pathway creation: electroporation pulse order. *Mathematical Biosciences*, 257:60–68, 2014.

[4] M. Belehradek, C. Domenge, B. Luboinski, S. Orlowski, J. Belehradek Jr, and L. M. Mir. Electrochemotherapy, a new antitumor treatment. first clinical phase i-ii trial. *Cancer*, 72(12):3694–3700, 1993.

[5] J. E. Bestman, R. C. Ewald, S. L. Chiu, and H. T. Cline. In vivo single cell electroporation for transfer of dna and macromolecules. *Nature Protocols*, 1(3):1268–1272, 2006.

[6] I. H. Blank. Penetration of low-molecular-weight alcohols into skin. i. effect of concentration of alcohol and type of vehicle. *Journal of Investigative Dermatology*, 43(5):415–420, 1964.

[7] A. Bolhassani, E. Mohit, N. Ghasemi, M. Salehi, M. Taghikhani, and S. Rafati. Enhancement of potent immune responses to HPV16 E7 antigen by using different vaccine modalities. *B. M. C. Proceedings*, 5:P19, 2011.

[8] J. A. Bouwstra, P. L. Honeywell-Nguyen, G. S. Gooris, and M. Ponec. Structure of the skin barrier and its modulation by vesicular formulations. *Progress in Lipid Research*, 42(1):1–36, 2003.

[9] B. Boyd and S. Becker. Macroscopic modeling of in vivo drug transport in electroporated tissue. *Journal of Biomechanical Engineering*, 138(3):031008–11, 2016.

[10] H. S. Brown, M. Griffin, and J. B. Houston. Evaluation of cryopreserved human hepatocytes as an alternative in vitro system to microsomes for the prediction of metabolic clearance. *Drug Metabolism and Disposition*, 35(2):293–301, 2007.

[11] D. Chang. *Guide to electroporation and electrofusion*. Academic Press, 1991.

[12] S. Čorović, I. Lacković, P. Sustaric, T. Sustar, T. Rodic, and D. Miklavčič. Modeling of electric field distribution in tissues during electroporation. *Biomedical Engineering Online*, 12(1):1–27, 2013.

[13] S. Čorović, L. M. Mir, and D. Miklavčič. In vivo muscle electroporation threshold determination: Realistic numerical models and in vivo experiments. *The Journal of Membrane Biology*, 245(9):509–520, Sep 2012.

[14] H. G. L. Coster. A quantitative analysis of the voltage-current relationships of fixed charge membranes and the associated property of "punch-through". *Biophysical Journal*, 5(5):669–686, 1965.

[15] H. G. L. Coster. Discovery of "punch-through" or membrane electrical breakdown and electroporation. *European Biophysics Journal*, 39(1):185–189, 2009.

[16] H. G. L. Coster and U. Zimmermann. Dielectric breakdowm in the membranes of valonia utricularis. the role of energy dissipation. *Biochimica et Biophysica Acta (BBA) - Biomembranes*, 382(3):410–418, 1975.

[17] H. G. L. Coster and U. Zimmermann. Direct demonstration of dielectric breakdown in the membranes of valonia utricularis. *Zeitschrift für Naturforschung C*, 30(1-2):77–79, 1975.

[18] H. G. L. Coster and U. Zimmermann. The mechanism of electrical breakdown in the membranes of valonia utricularis. *The Journal of Membrane Biology*, 22:73–90, 1975.

[19] R. V. Davalos, L. M. Mir, and B. Rubinsky. Tissue ablation with irreversible electroporation. *Annals of Biomedical Engineering*, 33(223), 2005.

[20] R. V. Davalos, B. Rubinsky, and L. M. Mir. Theoretical analysis of the thermal effects during in vivo tissue electroporation. *Bioelectrochemistry*, 61(1):99–107, 2003.

[21] K. A. DeBruin and W. Krassowska. Electroporation and shock-induced transmembrane potential in a cardiac fiber during defibrillation strength shocks. *Annals of Biomedical Engineering*, 26(4):584–596, Jul 1998.

[22] K. A. DeBruin and W. Krassowska. Modeling electroporation in a single cell. i. effects of field strength and rest potential. *Biophysical Journal*, 77(3):1213–1224, 1999.

[23] K. A. DeBruin and W. Krassowska. Modeling electroporation in a single cell. ii. effects of ionic concentrations. *Biophysical Journal*, 77(3):1225–1233, 1999.

[24] A. R. Denet, R. Vanbever, and V. Préat. Skin electroporation for transdermal and topical delivery. *Advanced Drug Delivery Reviews*, 56(5):659–674, 2004.

[25] J. Dermol-Černe and D. Miklavčič. From cell to tissue properties – modeling skin electroporation with pore and local transport region formation. *IEEE Transactions on Biomedical Engineering*, 65(2):458–468, 2017.

[26] J. Dermol-Černe, E. Pirc, and D. Miklavčič. Mechanistic view of skin electroporation – models and dosimetry for successful applications: an expert review. *Expert Opinion on Drug Delivery*, 17(5):689–704, 2020.

[27] J. Dermol-Černe, J. Vidmar, J. Ščančar, K. Uršič, G. Serša, and D. Miklavčič. Connecting the in vitro and in vivo experiments in electrochemotherapy - a feasibility study modeling cisplatin transport in mouse melanoma using the dual-porosity model. *Journal of Controlled Release*, 286:33–45, 2018.

[28] C. S. Djuzenova, U. Zimmermann, H. Frank, V. L. Sukhorukov, E. Richter, and G. Fuhr. Effect of medium conductivity and composition on the uptake of propidium iodide into electropermeabilized myeloma cells. *Biochimica et Biophysica Acta (BBA)-Biomembranes*, 1284(2):143–152, 1996.

[29] J. J. Escobar-Chávez, D. Bonilla-Martínez, M. A. Villegas-González, and A. L. Revilla-Vázquez. Electroporation as an efficient physical enhancer for skin drug delivery. *The Journal of Clinical Pharmacology*, 49(11):1262–1283, 2009.

[30] K. R. Foster and H. R. Schwan. Dielectric properties of tissues and biological materials: a critical review. *Critical Reviews in Biomedical Engineering*, 17:25–104, 1989.

[31] P. A. Garcia, R. V. Davalos, and D. Miklavčič. A numerical investigation of the electric and thermal cell kill distributions in electroporation-based therapies in tissue. *PLOS ONE*, 9(8):1–12, 2014.

[32] B. Gauger and F. W. Bentrup. A study of dielectric membrane breakdown in the fucus egg. *The Journal of Membrane Biology*, 48:249–264, 1979.

[33] J. Gehl, T. H. Sorensen, K. Nielsen, P. Raskmark, S. L. Nielsen, T. Skovsgaard, and L. M. Mir. In vivo electroporation of skeletal muscle: threshold, efficacy and relation to electric field distribution. *Biochimica et Biophysica Acta*, 1428,:233–240, 1999.

[34] R. W. Glaser, S. L. Leikin, L. V. Chernomordik, V. F. Pastushenko, and A. I. Sokirko. Reversible electrical breakdown of lipid bilayers: formation and evolution of pores. *Biochimica et Biophysica Acta (BBA) - Biomembranes*, 940(2):275–287, 1988.

[35] E. Goldberg, A. Soba, D. Gandía, M. L. Fernández, and C. Suárez. Coupled mathematical modeling of cisplatin electroporation. *Bioelectrochemistry*, 140:107788, 2021.

[36] E. Goldberg, C. Suárez, M. Alfonso, J. Marchese, A. Soba, and G. Marshall. Cell membrane electroporation modeling: A multiphysics approach. *Bioelectrochemistry*, 124:28–39, 2018.

[37] A. J. Gormley, N. Larson, A. Banisadr, R. Robinson, N. Frazier, A. Ray, and H. Ghandehari. Plasmonic photothermal therapy increases the tumor mass penetration of hpma copolymers. *Journal of Controlled Release*, 166(2):130–138, 2013.

[38] Y. Granot and B. Rubinsky. Mass transfer model for drug delivery in tissue cells with reversible electroporation. *International Journal of Heat and Mass Transfer*, 51(23):5610–5616, 2008.

[39] W. H. Helfand and D. L. Cowen. Evolution of pharmaceutical oral dosage forms. *Pharmacy in History*, 25(1):3–18, 1983.

[40] L. Houghton. Science photo library, 327-329 harrow road, london w9 3rb, united kingdom.

[41] J. Hrabe, S. Hrabětová, and K. Segeth. A model of effective diffusion and tortuosity in the extracellular space of the brain. *Biophysical journal*, 87(3):1606–1617, 2004.

[42] P. Jani, G. W. Halbert, J. Langridge, and A. T. Florence. Nanoparticle uptake by the rat gastrointestinal mucosa: quantitation and particle size dependency. *Journal of Pharmacy and Pharmacology*, 42(12):821–826, 1990.

[43] C. Jiang, R. Davalos, and J. Bischof. A review of basic to clinical studies of irreversible electroporation therapy. *IEEE Transactions on Biomedical Engineering*, 62(1):4–20, 2015.

[44] K. A. Jinturkar, M. N. Rathi, and A. Misra. Gene delivery using physical methods. In *Challenges in delivery of therapeutic genomics and proteomics*, pages 83–126. Elsevier, 2011.

[45] K. J. Kinosita and T. Y. Tsong. Hemolysis of human erythrocytes by a transient electric field. *Proceedings of the National Academy of Sciences*, 74:1923–1927, 1977.

[46] T. Kotnik and D. Miklavčič. Analytical description of transmembrane voltage induced by electric fields on spheroidal cells. *Biophysical Journal*, 79(2):670–679, 2000.

[47] T. Kotnik, L. Rems, M. Tarek, and D. Miklavčič. Membrane electroporation and electropermeabilization: Mechanisms and models. *Annual Review of Biophysics*, 48(1):63–91, 2019.

[48] W. Krassowska. Effects of electroporation on transmembrane potential induced by defibrillation shocks. *Pacing and Clinical Electrophysiology*, 18(9):1644–1660, 1995.

[49] W. Krassowska and P. D. Filev. Modeling electroporation in a single cell. *Biophysical Journal*, 92(2):404–417, 2007.

[50] J. Kreuter and P. P. Speiser. In vitro studies of poly (methyl methacrylate) adjuvants. *Journal of Pharmaceutical Sciences*, 65(11):1624–1627, 1976.

[51] I. Lacković, R. Magjarević, and D. Miklavčič. Incorporating electroporation-related conductivity changes into models for the calculation of the electric field distribution in tissue. In *XII Mediterranean Conference on Medical and Biological Engineering and Computing 2010*, pages 695–698, Berlin, Heidelberg, 2010. Springer Berlin Heidelberg.

[52] T. Lammers, P. Peschke, R. Kühnlein, V. Subr, K. Ulbrich, J. Debus, P. Huber, W. Hennink, and G. Storm. Effect of radiotherapy and hyperthermia on the tumor accumulation of hpma copolymer-based drug delivery systems. *Journal of Controlled Release*, 117(3):333–341, 2007.

[53] P. I. Lee and J.-X. Li. Evolution of oral controlled release dosage forms. *Oral Controlled Release Formulation Design and Drug Delivery*, pages 21–31, 2010.

[54] J. A. Leedale, J. A. Kyffin, A. L. Harding, H. E. Colley, C. Murdoch, P. Sharma, D. P. Williams, S. D. Webb, and R. N. Bearon. Multiscale modelling of drug transport and metabolism in liver spheroids. *Interface Focus*, 10(2):20190041, 2020.

[55] L. Li, T. L. M. ten Hagen, M. Bolkestein, A. Gasselhuber, J. Yatvin, G. C. van Rhoon, A. M. Eggermont, D. Haemmerich, and G. A. Koning. Improved intratumoral nanoparticle extravasation and penetration by mild hyperthermia. *Journal of Controlled Release*, 167(2):130–137, 2013.

[56] S. Mahnič-Kalamiza, D. Miklavčič, and E. Vorobiev. Dual-porosity model of solute diffusion in biological tissue modified by electroporation. *Biochimica et Biophysica Acta (BBA) - Biomembranes*, 1838(7):1950–1966, 2014.

[57] S. Mahnič-Kalamiza, E. Vorobiev, and D. Miklavčič. Electroporation in food processing and biorefinery. *The Journal of Membrane Biology*, 247:1279–1304, 2014.

[58] D. Miklavčič, G. Serša, E. Brecelj, J. Gehl, D. Soden, G. Bianchi, P. Ruggieri, C. R. Rossi, L. G. Campana, and T. Jarm. Electrochemotherapy: technological advancements for efficient electroporation-based treatment of internal tumors. *Medical & Biological Engineering & Computing*, 50(12):1213–25, 2012.

[59] S. Miyauchi, S. Takeuchi, and T. Kajishima. A numerical method for mass transfer by a thin moving membrane with selective permeabilities. *Journal of Computational Physics*, 284:490–504, 2015.

[60] T. B. Napotnik, M. Reberšek, P. T. Vernier, B. Mali, and D. Miklavčič. Effects of high voltage nanosecond electric pulses on eukaryotic cells (in vitro): A systematic review. *Bioelectrochemistry*, 110:1–12, 2016.

[61] J. C. Neu and W. Krassowska. Asymptotic model of electroporation. *Physical review E*, 59(3):3471, 1999.

[62] E. Neumann, C. A. Jordan, and A. E. Sowers. *Electroporation and Electrofusion in Cell Biology*. Springer International Publishing, Cham, 1989.

[63] E. Neumann, R. M. Schaefer, Y. Wang, and P. H. Hofschneider. Gene transfer into mouse lyoma cells by electroporation in high electric fields. *The EMBO Journal*, 1(7):841–845, 1982.

[64] K. Park. Questions on the role of the epr effect in tumor targeting. *Journal of Controlled Release*, 172(1):391–391, 2013.

[65] M. Pavlin, S. M. Kandu, M. Rebersek, G. Pucihar, F. X. Hart, R. Mag-jareviccacute, and D. Miklavčič. Effect of cell electroporation on the conductivity of a cell suspension. *Biophysical Journal*, 88(6):4378–4390, 2005.

[66] M. Pavlin and D. Miklavčič. Effective conductivity of a suspension of permeabilized cells: A theoretical analysis. *Biophysical Journal*, 85(2):719–729, 2003.

[67] M. Pavlin and D. Miklavčič. Theoretical and experimental analysis of conductivity, ion diffusion and molecular transport during cell electroporation—relation between short-lived and long-lived pores. *Bioelectrochemistry*, 74(1):38–46, 2008.

[68] N. Pavselj, Z. Bregar, D. Cukjati, D. Batiuskaite, L. M. Mir, and D. Miklavčič. The course of tissue permeabilization studied on a mathematical model of a subcutaneous tumor in small animals. *IEEE Transactions on Biomedical Engineering*, 52(8):1373–1381, 2005.

[69] U. Pliquett. Joule heating during solid tissue electroporation. *Medical and Biological Engineering and Computing*, 41:215–219, 2003.

[70] U. F. Pliquett and C. A. Gusbeth. Perturbation of human skin due to application of high voltage. *Bioelectrochemistry*, 51(1):41–51, 2000.

[71] M. R. Prausnitz. Do high-voltage pulses cause changes in skin structure? *Journal of Controlled Release*, 40(3):321–326, 1996.

[72] G. Pucihar, J. Krmelj, M. Reberšek, T. B. Napotnik, and D. Miklavčič. Equivalent pulse parameters for electroporation. *IEEE Transactions on Biomedical Engineering*, 58(11):3279–3288, 2011.

[73] C. Rosazza, S. H. Meglic, A. Zumbusch, M. P. Rols, and D. Miklavčič. Gene electrotransfer: A mechanistic perspective. *Current Gene Therapy*, 16(2):98–129., 2016.

[74] B. Rubinsky. Irreversible electroporation in medicine. *Technology in Cancer Research & Treatment*, 6(4):255–259, 2007.

[75] S. Satkauskas, M. Bureau, M. Puc, A. Mahfoudi, D. Scherman, D. Miklavčič, and M. L. Mir. Mechnisms of in vivo dna electrotransfer: Respective contributions of cell electropermeabilization and dna electrophoresis. *Molecular Therapy*, 5:133–140, 2002.

[76] G. Saulis. Pore disappearance in a cell after electroporation: theoretical simulation and comparison with experiments. *Biophysical Journal*, 73:1299–1309, 1997.

[77] D. Sel, D. Cukjati, D. Batiuskaite, T. Slivnik, L. M. Mir, and D. Miklavčič. Sequential finite element model of tissue electropermeabilization. *IEEE Transactions on Biomedical Engineering*, 52(5):816–827, 2005.

[78] A. Sen, M. E. Daly, and S. W. Hui. Transdermal insulin delivery using lipid enhanced electroporation. *Biochimica et Biophysica Acta (BBA)-Biomembranes*, 1564(1):5–8, 2002.

[79] K. C. Smith, J. C. Neu, and W. Krassowska. Model of creation and evolution of stable electropores for dna delivery. *Biophysical Journal*, 86(5):2813–2826, 2004.

[80] M. A. Swartz and M. E. Fleury. Interstitial flow and its effects in soft tissues. *Annual Review of Biomedical Engineering*, 9:229–256, 2007.

[81] J. Teissie, M. Golzio, and M. Rols. Mechanisms of cell membrane electropermeabilization: a minireview of our present (lack of?) knowledge. *Biochimica et Biophysica Acta (BBA)-General Subjects*, 1724(3):270–280, 2005.

[82] R. Vanbever, U. F. Pliquett, V. Preat, and J. C. Weaver. Comparison of the effects of short, high-voltage and long, medium-voltage pulses on skin electrical and transport properties. *Journal of Controlled Release*, 60(1):35–47, 1999.

[83] S. Visser, D. De Alwis, T. Kerbusch, J. Stone, and S. Allerheiligen. Implementation of quantitative and systems pharmacology in large pharma. *CPT: Pharmacometrics & Systems Pharmacology*, 3(10):1–10, 2014.

[84] M. Wang, O. Orwar, and S. G. Weber. Single cell transfection by electroporation using an electrolyte/plasmid-filled capillary. *Analytical Chemistry*, 81(10):4060–4067, 2009.

[85] J. C. Weaver. Electroporation of biological membranes from multicellular to nano scales. *IEEE Transactions on Dielectrics and Electrical Insulation*, 10:754–768, 2003.

[86] G. Widera, M. Austin, D. Rabussay, C. Goldbeck, S. W. Barnett, M. Chen, L. Leung, G. R. Otten, K. Thudium, M. J. Selby, and J. B. Ulmer. Increased dna vaccine delivery and immunogenicity by electroporation *in vivo*. *Journal of Immunology*, 164 (9):4635–4640, 2000.

[87] C. Wong, T. Stylianopoulos, J. Cui, J. Martin, V. P. Chauhan, W. Jiang, Z. Popović, R. K. Jain, M. G. Bawendi, and D. Fukumura. Multistage nanoparticle delivery system for deep penetration into tumor tissue. *Proceedings of the National Academy of Sciences*, 108(6):2426–2431, 2011.

[88] K. Yadav and D. Dalal. The heterogeneous multiscale method to study particle size and partitioning effects in drug delivery. *Computers & Mathematics with Applications*, 92:134–148, 2021.

[89] U. Zimmermann, G. Pilwat, and F. Riemann. Dielectric breakdown of cell membranes. *Biophysical Journal*, 14(11):881–899, 1974.

[90] B. Zorec, S. Becker, M. Rebersek, D. Miklavčič, and N. Pavselj. Skin electroporation for transdermal drug delivery: The influence of the order of different square wave electric pulses. *International Journal of Pharmaceutics*, 457(1):214–223, 2013.

BIODATA

Current Status

Senior research fellow of Department of Mathematics, Indian Institute of Technology Guwahati, Guwahati 781039, India.

Education

- 2011 – 2013: **Master of Science** (Mathematics)
  Visva-Bharati University, Santiniketan, West Bengal, India.
- 2008 – 2011: **Bachelor of Science** (Honours in Mathematics)
  Ramananda College, The University of Burdwan, West Bengal, India.

List of Published and Communicated Articles

- Nilay Mondal, Koyel Chakravarty and D. C. Dalal, **Mathematical modelling of drug delivery in tissue cells using electroporation**, *AIP Conference Proceedings*, 1975(1), 030017, 2018.
- Nilay Mondal, Koyel Chakravarty and D. C. Dalal, **A mathematical model of drug dynamics in an electroporated tissue**, *Mathematical Biosciences and Engineering*, 18(6), 8641-8660, 2021.
- Nilay Mondal and D. C. Dalal, **Modelling of reversible tissue electroporation and its thermal effects in drug delivery** (Communicated).
- Nilay Mondal and D. C. Dalal, **A model for reversible electroporation to deliver drugs into diseased tissues** (Communicated).
- Nilay Mondal and D. C. Dalal, **A study of metabolism after delivering drug into the cells using reversible tissue electroporation** (Communicated).

- Nilay Mondal, K. S. Yadav and D. C. Dalal, **Enhanced drug uptake on application of electroporation in a single-cell model** (Communicated).

Conferences & Workshops Attended

- GIAN course on Reservoir Simulation: Mathematical Techniques in Oil and Gas Recovery, July 18-29, 2016, Center for Education Technology, IIT Guwahati, Guwahati, Assam, India.
- Workshop on Mathematical Modeling and Its Applications, August 19-20, 2016, Department of Mathematics, NIT Meghalaya, Shillong, Meghalaya, India.
- 5th International Conference on Complex Dynamical Systems and Applications (CDSA-2017), December 4-6, 2017, IIT Guwahati, Guwahati, Assam, India.
- International Conference on Frontier in Industrial and Applied Mathematics (FIAM-2018), April 26-27, 2018, NIT Hamirpur, Hamirpur, Himachal Pradesh, India.
- International Conference on Advances in Differential Equations and Numerical Analysis (ADENA-2020), October 12-15, 2020, Department of Mathematics, IIT Guwahati, Guwahati, Assam, India.